THE TIME-TEMPERATURE BEHAVIOR OF GRAPHITE EPOXY LAMINATES.

YEOW, YEN THYE

DEGREE DATE: 1978

Date: 9/9/95 Time: 3:30:59PM

Page: 1 Document Name: untitled

DTIC DOES NOT HAVE THIS ITEM

__ 1 - AD NUMBER: D428357
__ 6 - UNCLASSIFIED TITLE: THE TIME-TEMPERATURE BEHAVIOR OF GRAPHITE
__ EPOXY LAMINATES.
__10 - PERSONAL AUTHORS: YEOW, Y. T. ;
__11 - REPORT DATE: , 1978
__12 - PAGINATION: 153P
__20 - REPORT CLASSIFICATION: UNCLASSIFIED
__21 - SUPPLEMENTARY NOTE: DISSERTATION SUBMITTED TO VIRGINIA
__ POLYTECHNIC INSTITUTE AND STATE UNIVERSITY IN PARTIAL FULFILLMENT
__ OF REQUIREMENTS FOR PHD. SEE ALSO PL-29676.
__22 - LIMITATIONS (ALPHA): APPROVED FOR PUBLIC RELEASE; DISTRIBUTION
__ UNLIMITED. AVAILABILITY: UNIVERSITY MICROFILMS INTERNATIONAL, 300 N.
ZEEB RD, ANN ARBOR, MI, 48106, NO. 7818563.
__33 - LIMITATION CODES: 1 24

DISCLAIMER NOTICE

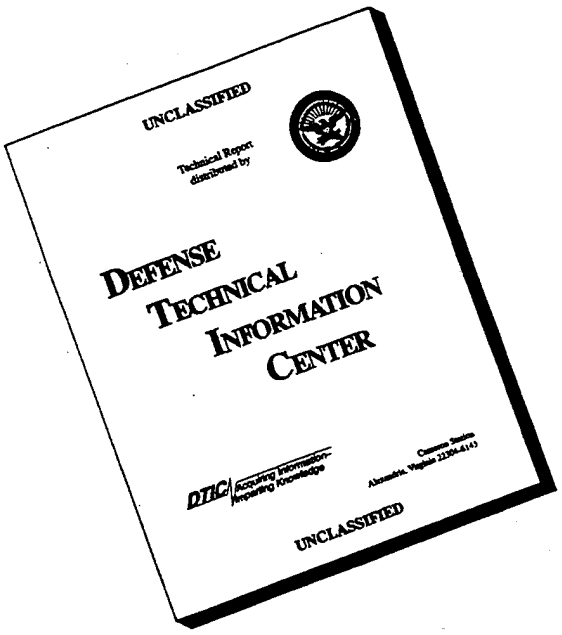

THIS DOCUMENT IS BEST QUALITY AVAILABLE. THE COPY FURNISHED TO DTIC CONTAINED A SIGNIFICANT NUMBER OF PAGES WHICH DO NOT REPRODUCE LEGIBLY.

INFORMATION TO USERS

This material was produced from a microfilm copy of the original document. While the most advanced technological means to photograph and reproduce this document have been used, the quality is heavily dependent upon the quality of the original submitted.

The following explanation of techniques is provided to help you understand markings or patterns which may appear on this reproduction.

1. The sign or "target" for pages apparently lacking from the document photographed is "Missing Page(s)". If it was possible to obtain the missing page(s) or section, they are spliced into the film along with adjacent pages. This may have necessitated cutting thru an image and duplicating adjacent pages to insure you complete continuity.

2. When an image on the film is obliterated with a large round black mark, it is an indication that the photographer suspected that the copy may have moved during exposure and thus cause a blurred image. You will find a good image of the page in the adjacent frame.

3. When a map, drawing or chart, etc., was part of the material being photographed the photographer followed a definite method in "sectioning" the material. It is customary to begin photoing at the upper left hand corner of a large sheet and to continue photoing from left to right in equal sections with a small overlap. If necessary, sectioning is continued again — beginning below the first row and continuing on until complete.

4. The majority of users indicate that the textual content is of greatest value, however, a somewhat higher quality reproduction could be made from "photographs" if essential to the understanding of the dissertation. Silver prints of "photographs" may be ordered at additional charge by writing the Order Department, giving the catalog number, title, author and specific pages you wish reproduced.

5. PLEASE NOTE: Some pages may have indistinct print. Filmed as received.

Xerox University Microfilms
300 North Zeeb Road
Ann Arbor, Michigan 48106

THE TIME-TEMPERATURE BEHAVIOR OF GRAPHITE EPOXY LAMINATES

by

Yew Thye Yeow

Dissertation submitted to the Graduate Faculty of the

Virginia Polytechnic Institute and State University

in partial fulfillment of the requirements for the degree of

DOCTOR OF PHILOSOPHY

in

Engineering Mechanics

APPROVED:

H. F. Brinson, Chairman

R. P. McNitt

K. L. Reifsnider

D. H. Morris

M. R. Louthan

May 1978

Blacksburg, Virginia

ACKNOWLEDGEMENTS

The author wishes to express his sincere appreciation to Professor H. F. Brinson, his advisor and project director, for his advice and guidance during the entire endeavor of the author's graduate studies. In addition, the author wishes to express:

- his thanks to his committee members for their well-posed comments and criticisms.
- his gratefulness to his monitors D. P. Williams of NASA Headquarters, Washington, D.C., and H. G. Nelson of the Materials and Physical Sciences Branch, NASA-Ames Research Center, Moffet Field, CA 94035 for financing this challenging project.
- his appreciation to Bob Davis, Ken McCauley and Archie Montgomery for their assistance in the experimental work.
- his thanks to Mrs. Peggy Epperly for the excellent typing throughout the course of the investigation.

and lastly but not least, the encouragement and flexibilities of his parents are well-appreciated.

TABLE OF CONTENTS

LIST OF ILLUSTRATIONS

LIST OF TABLES

NOMENCLATURE

$\bar{\alpha}_{ij}$	Thermal coefficient of expansion with respect to the global coordinates
α_{ij}	Thermal coefficient of expansion with respect to the local coordinates
$2a$	Total crack length
$2a_o$	Total inherent flaw crack length
a_1	Characteristic length for point stress criterion
a_T	Shift factor, function of temperature
$2b$	Total crack length
$\bar{\beta}_{ij}$	Thermal stress characteristics with respect to the global coordinates
β_{ij}	Thermal stress characteristics with respect to the local coordinates
C_1, C_2	Material constants for the WLF equation
$\bar{C}_{ij}(\zeta - \zeta')$	Relaxation moduli with respect to the global coordinates
$C_{ij}(\zeta - \zeta')$	Relaxation moduli with respect to the local coordinates
ζ	Reduced time, defined as $\int_{-\infty}^{t} \frac{dt}{a_T}$
ζ'	Reduced time, defined as $\int_{-\infty}^{t} \frac{dt}{a_T}$
$C_{ij}(\sigma_i)$	Local stiffness as a function of stress, σ_i
$\bar{C}_{ij}(\sigma_i)$	Global stiffness as a function of stress, σ_i
d_o	Characteristic length for the average stress criterion
dN	Load increment

$d\varepsilon^{\circ}$	Laminate strain increment
$d\varepsilon_i$	Lamina strain increment
$d\sigma_i$	Lamina stress increment
ΔH_a	Apparent activation energy
Δt	Time increment
ΔT	Temperature change
ξ	Normalized crack length and is equal to $\frac{a}{a + d_o}$
ξ'	Normalized crack length and is equal to $\frac{a}{a + a_1}$
ε_{ij}	Strains expressed in the local coordinates
$\bar{\varepsilon}_{ij}$	Strains expressed in the global coordinates
E_{11}	Modulus in the direction of the fibers
E_{22}	Modulus in the direction transverse to the fibers
E_{xx}	Axial modulus of off-axis laminate
$F(a/w)$	Finite width correction factor
G_{12}	Intralamina shear modulus
$H(\zeta)$	Step function; = 0 for $\zeta < 0$ and = 1 for $\zeta > 0$
K_{IC}	Mode I critical stress intensity factor
K_{II}	Mode II stress intensity factor
K_Q	Fracture toughness
L	Total laminate thickness
Ln	Natural logarithm
N_i	Applied loads
ρ	Density at temperature, T
ρ_o	Density at temperature, T_o
R	Universal gas constant

S	Quasi-elastic shear strength
$\bar{S}_{ij}(\zeta - \zeta')$	Creep compliance with respect to global coordinates
$S_{ij}(\zeta)$	Creep compliance with respect to local coordinates
$\bar{\sigma}_{ij}$	Stresses with respect to the global coordinates
σ_{ij}	Stresses with respect to the local coordinates
$\sigma_c{}^f$	Finite width notched strength
σ_o	Quasi-elastic ultimate strength of unnotched laminate
σ_c	Critical remote stress normal to the crack
τ	Reference time
t	Time
t_k	Lamina thickness
T	Temperature
T_g	Primary glass transition temperature (180°C)
$T_g{}^s$	Secondary glass transition temperature (60°C)
T_o, T_o'	Reference temperatures
$[TM]$	Transformation matrix
$[T^k]$	Transformation matrix for the k^{th} lamina
ν_{12}	Major Poisson's ratio
ν_{21}	Minor Poisson's ratio
X	Quasi-elastic strength in the fiber direction
$X_{mm}(t)$	Principal creep strengths; m = 1,2,6
x-y	Global Cartesian coordinate system
Y	Quasi-elastic strength transverse to the fiber direction
1-2	Local of material Cartesian coordinate system with 1 in the direction of the fibers and 2 is in the direction transverse to the fibers

I. INTRODUCTION

The use of composite materials in structural design has been practiced since the early stages of the human civilization. It is only lately that a very major effort has been made in improving and comprehending the response and behavior of this class of "tailorable" materials. Depending on one's needs, modern composites may consist of a number of different types of constituents. The particular class of modern composites which is of interest here is the one consisting of continuous fibers embedded in a polymeric matrix or binder. Structures made from these types of constituents will exhibit some form of time-dependent behavior [1] as one phase (the matrix) is time-dependent and the other (the fiber) may or may not be time-dependent, depending on the type of fiber used [2]. For example, automobile tires reinforced with polyester cord will correspond to the former and epoxy based composites reinforced with graphite fibers is representative of the latter. In addition, irrespective of the type of reinforcement, the interface between the fiber and matrix is time-dependent [3]. For definitive purposes, only epoxy based continuous fiber reinforced composites are investigated here; namely, graphite/epoxy laminates. Unless otherwise stated, this class of composites is the one addressed throughout this manuscript.

When considering the time-dependent behavior of a composite material, there are at least four accelerating factors (temperature, stress, vibration and moisture) [4] that will affect the viscoelastic

behavior of a material. The type of time analogy (superposition) selected is solely determined by the detrimental effects of the individual accelerator on a structure. In reality, all four accelerators are generally present in most structures. Simulation of experiments containing all four accelerating factors and boundary value definition of these experiments are indeed complex. Consequently, investigations pertaining to such real-time simulation have not heretofore been accomplished. However, individual time analogies have been reported [5-10]. Unfortunately, the majority of these limited investigations are neither detailed nor complete enough to be comprehensively applied to two-phase composite systems in general. The primary goal of this investigation is to address these latter issues as outlined in greater detail subsequently.

The objective of the present investigation is to provide an in-depth study on the time-temperature behavior of epoxy based continuous and elastic fiber reinforced composite materials and explore the possibilities of using the time-temperature analogy as an accelerated characterization method to predict long-term behavior. Both analytical and experimental time-temperature procedures will be presented. The reason for considering only one time analogy is primarily due to the constraints imposed by time limitations which would rule out such a diverse investigation as multi-parametric predictions. However, it is felt that by using the present limited study other environmental parameters can be appropriately and confidently incorporated in future multi-parametric investigations as time permits. The reason for selecting the time-temperature analogy is that among the four analogies,

this is the most common and also the most detrimental environmental parameter. In addition, this parameter is one to which epoxy based composite structures are always subjected.

Preliminary investigations on the time-temperature behavior of graphite/epoxy laminates indicated that the investigation could essentially be separated into two parts; i.e., room-temperature and elevated temperature responses. At elevated temperatures, especially at or above the glass-transition temperature (T_g), major time-dependent behavior was observed. At room-temperature, only very minor viscoelastic effects were observed. Thus, based on the following reasons, the material can be assumed to be time dependent at room temperature;

a) In the analyses of Sandhu [11], Sendeckyj et al. [12] and others [13], where only quasi-elastic behavior is assumed, good correlations between analysis and experiments were obtained.

b) The strain rate test data of Daniel et al. [14], as well as VPI data, revealed only minor viscoelastic behavior. However, the results were inconclusive due to the scatter in the data.

c) The creep test data presented herein shows only a very slight creep behavior for off-axis tensile tests.

For these reasons, the behavior at room temperature can be considered as a special case in our time-temperature investigation. For the sake of completeness, validation of test methods used in this investigation and to provide a better insight to the present and future time-dependent investigations, this special case is summarized and

substantiated by the analytical and experimental results given in Appendices A and B, where a synopsis of the unnotched behavior is presented in Appendix A and a synopsis of the notched behavior is presented in Appendix B.

The format adopted in this manuscript is to first present the analytical methodology (Chapter II). In this chapter, the reduction of the anisotropic time-temperature constitutive stress-strain relations to a simpler form, a discussion on the time-temperature superposition principle and the creep strength prediction methodology are presented. The following chapter (Chapter III) presents the experimental procedure including our observations of and rationale for the test methods used. In Chapter IV, data reduction and predictions of the unidirectional master curves obtained from short term tests are discussed. In addition, the procedure used in the creep to rupture predictions is also discussed. The analytical and experimental results are compared and discussed in Chapter V. Finally, in Chapter VI a summary of the investigation, as well as conclusions and possible avenues of future research in this area of composite materials, is discussed.

II. ANALYTICAL METHODOLOGY

The viscoelastic structural response of a thermorheologically simple material (TSM) is affected by temperature mainly through thermal expansion and changes in relaxation and retardation times (sometimes known as rheological coefficients) [15,16]. Thermodynamically, the linear viscoelastic relations between stresses and strains for an anisotropic TSM can be written compactly by means of the Boltzmann superposition integral [17] as

$$\bar{\sigma}_{ij} = \int_{-\infty}^{t} \bar{C}_{ijk\ell}(\zeta - \zeta') \frac{\partial \bar{\varepsilon}_{k\ell}}{\partial \zeta'} d\zeta' - \int_{-\infty}^{t} \bar{\beta}_{ij}(\zeta - \zeta') \frac{\partial \Delta T}{\partial \zeta'} d\zeta' \qquad (1)$$

and in the inverse form as

$$\bar{\varepsilon}_{ij} = \int_{-\infty}^{t} \bar{S}_{ijk\ell}(\zeta - \zeta') \frac{\partial \bar{\sigma}_{k}}{\partial \zeta} d\zeta - \int_{-\infty}^{t} \bar{\alpha}_{ij}(\zeta - \zeta') \frac{\partial \Delta T}{\partial \zeta'} d\zeta' \qquad (2)$$

where $\bar{\sigma}_{ij}$ and $\bar{\varepsilon}_{ij}$ = stress and strain, respectively, with respect to time.

$\bar{C}_{ijk\ell}(\zeta - \zeta')$ and $\bar{S}_{ijk\ell}(\zeta - \zeta')$ = relaxation moduli and creep compliances, respectively.

$\bar{\beta}_{ij}(\zeta - \zeta')$ and $\bar{\alpha}_{ij}(\zeta - \zeta')$ = thermal stress and strain characteristics of the material, respectively.

ΔT = change in temperature, T.

$\zeta = \int_{-\infty}^{t} \frac{dt}{a_T}$ = reduced time

$\zeta' = \int_{-\infty}^{\tau} \frac{dt}{a_T}$ = reduced time

$a_T = a_T(T)$ = shift factor

and $i,j,k,l = 1,2,3,\ldots,6$

The first and second integral on the right hand side of equations (1) and (2) represents the response due to mechanical and thermal loads, respectively, and the lower limit ($-\infty$) is used to account for the loading history of the material. Consequently, equations (1) and (2) are sometimes known as the "Hereditary Integrals."

Under isothermal conditions, equations (1) and (2), reduce to

$$\bar{\sigma}_{ij} = \int_{-\infty}^{t} \bar{C}_{ijk\ell}(\zeta - \zeta') \frac{\partial \bar{\varepsilon}_{k\ell}}{\partial \zeta'} d\zeta' \tag{3}$$

and

$$\bar{\varepsilon}_{ij} = \int_{-\infty}^{t} \bar{S}_{ijk\ell}(\zeta - \zeta') \frac{\partial \bar{\sigma}_{k\ell}}{\partial \zeta'} d\zeta' \tag{4}$$

respectively. The significance of the material properties in equations (3) and (4) is revealed when step-function loads are applied. Mathematically, the step-function stresses can be represented as

$$\bar{\sigma}_{k\ell} = H(\zeta)\bar{\sigma}'_{k\ell} \tag{5}$$

where $\bar{\sigma}'_{k\ell}$ are constants and

$$H(\zeta) = \begin{cases} 0 \text{ for } \zeta < 0 \\ 1 \text{ for } \zeta > 0 \end{cases} \tag{6}$$

Substituting equations (5) and (6) into equation (4), which represents a creep test, and for virgin materials, the resulting equation can be expressed as

$$\bar{\varepsilon}_{ij} = \bar{S}_{ijk\ell}(\zeta)\bar{\sigma}'_{k\ell} \tag{7}$$

The inverse of equation (7), relaxation test, is

$$\bar{\sigma}_{ij} = \bar{C}_{ijk\ell}(\zeta)\bar{\varepsilon}'_{k\ell} \tag{8}$$

where $\bar{\varepsilon}'_{k\ell}$ are constants. In terms of the real-time parameter, t, equations (7) and (8) can be expressed as

$$\bar{\varepsilon}_{ij} = \bar{S}_{ijk\ell}(t)\bar{\sigma}'_{k\ell} \tag{9}$$

and

$$\bar{\sigma}_{ij} = \bar{C}_{ijk\ell}(t)\bar{\varepsilon}'_{k\ell} \tag{10}$$

respectively. At this stage, either equations (7) and (8) or equations (9) and (10) are sufficient to represent the most anisotropic time-dependent response of a TSM subjected to the step-function loads described earlier. For monolithic materials such as unidirectional composite laminates, the thirty-six material constants of equations (7) to (10) can be reduced to four when material and geometric symmetries and a plane state of stress are assumed. Thus, equation (9) can be expressed as

$$\begin{Bmatrix} \bar{\varepsilon}_{11} \\ \bar{\varepsilon}_{22} \\ \gamma_{12} \end{Bmatrix} = \begin{bmatrix} \bar{S}_{11}(t) & \bar{S}_{12}(t) & \bar{S}_{16}(t) \\ \bar{S}_{12}(t) & \bar{S}_{22}(t) & \bar{S}_{26}(t) \\ \bar{S}_{16}(t) & \bar{S}_{26}(t) & \bar{S}_{66}(t) \end{bmatrix} \begin{Bmatrix} \bar{\sigma}'_{11} \\ \bar{\sigma}'_{22} \\ \bar{\sigma}'_{12} \end{Bmatrix} \tag{11}$$

where $\bar{\gamma}_{12} = 2\bar{\varepsilon}_{12}$. Or simply as

$$\{\bar{\varepsilon}\} = [\bar{S}(t)]\{\bar{\sigma}'\} \tag{12}$$

and the inverse of equation (12) is

$$\{\bar{\sigma}\} = [\bar{C}(t)]\{\bar{\varepsilon}'\} \tag{13}$$

It should be mentioned that equations (12) and (13) are expressed in terms of the global coordinate system. If the local and global coordinate systems coincide then the values of the coupling terms ($\bar{S}_{16}(t)$, $\bar{S}_{26}(t)$, $\bar{C}_{16}(t)$ and $\bar{C}_{26}(t)$) are zero. Tensorally, the local and global coordinate systems are related by a transformation matrix, [TM], which is expressed as

$$[TM] = \begin{bmatrix} \cos^2\theta & \sin^2\theta & -2\cos\theta\sin\theta \\ \sin^2\theta & \cos^2\theta & 2\cos\theta\sin\theta \\ \sin\theta\cos\theta & -\sin\theta\cos\theta & \cos^2\theta - \sin^2\theta \end{bmatrix} \tag{14}$$

where θ is the angle between the local (1-2 coordinates) and the global (x-y coordinates) axes, as shown in Figure 1. The relationship between the compliance expressed in terms of the local coordinates, [S(t)], and the compliance expressed in terms of the global coordinates, $[\bar{S}(t)]$, is found to be

$$[\bar{S}(t)] = [TM]^{-1}\,[S(t)][TM] \tag{15}$$

where

$$[S(t)] = \begin{bmatrix} S_{11}(t) & S_{12}(t) & 0 \\ S_{12}(t) & S_{22}(t) & 0 \\ 0 & 0 & S_{66}(t) \end{bmatrix} \tag{16}$$

where $S_{11}(t)$ and $S_{22}(t)$ are the compliances along and transverse to the fibers, respectively, $S_{12}(t) = \nu_{12}(t)S_{11}(t)$, $\nu_{12}(t)$ is the major Poisson's ratio, and $S_{66}(t)$ is the intralamina shear compliance. Thus, knowing these four time-dependent constants, the creep properties of any arbitrary unidirectional laminate can be obtained from equation (15).

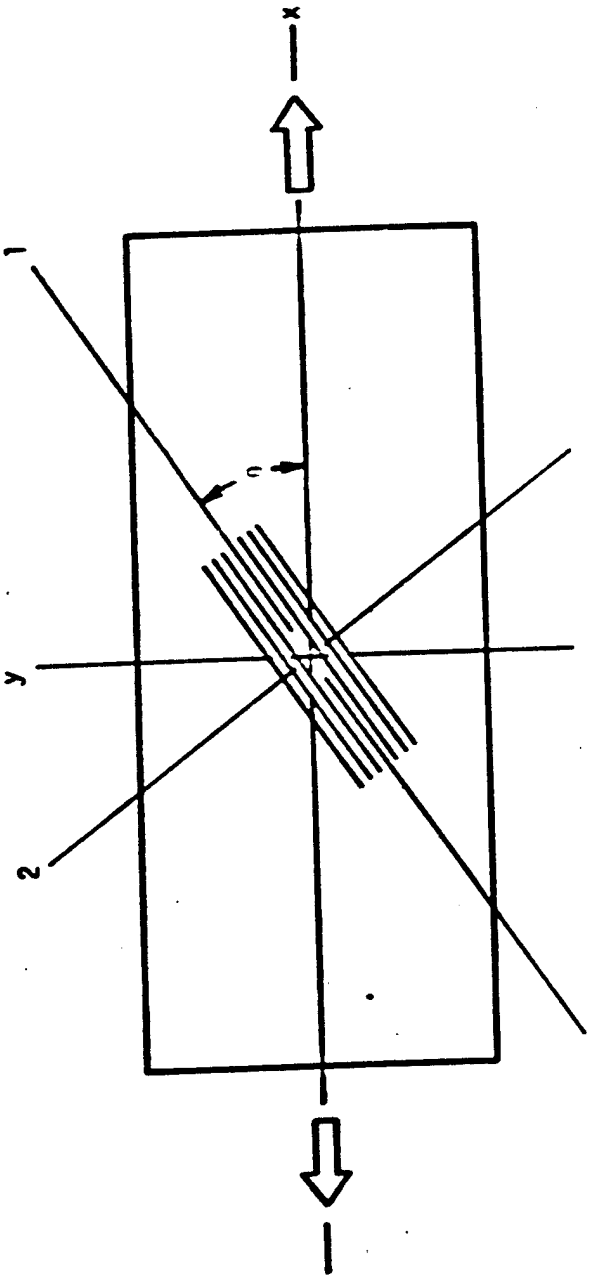

Figure 1. Coordinate System Used for General Lamina or Ply and for Off-Axis Tests.

Among the nine terms of the $[\bar{S}(t)]$ matrix, the first diagonal term ($\bar{S}_{11}(t)$, axial compliance) is perhaps the most important. By substituting equations (14) and (16) into equation (15), the resulting axial compliance term is expressed as

$$\bar{S}_{11}(t) = S_{xx}(t) = S_{11}(t)\,\mathrm{Cos}^4\theta + (S_{66}(t) + 2S_{12}(t))\,\mathrm{Cos}^2\theta\,\mathrm{Sin}^2\theta + S_{22}(t)\,\mathrm{Sin}^4\theta \tag{17}$$

Equation (17) is the time-dependent analogue of the elastic orthotropic transformation equation. In terms of stresses and strains, the principal material compliances of equation (17) are expressed as

$$S_{11}(t) = \frac{\varepsilon_{11}(t)}{\sigma_{11}^{i}} \tag{18a}$$

$$S_{22}(t) = \frac{\varepsilon_{22}(t)}{\sigma_{22}^{i}} \tag{18b}$$

$$S_{66}(t) = \frac{\gamma_{12}(t)}{\tau_{12}^{i}} \tag{18c}$$

and

$$S_{12}(t) = \frac{\varepsilon_{22}(t)}{\sigma_{11}^{i}} \tag{18d}$$

Experimentally, the stresses and strains of equations (18a) and (18d) are obtained from a $[0°]_s$ uniaxial test, those of equation (18b) are obtained from a $[90°]_s$ uniaxial test, and those of equation (18c) can be obtained from a $[10°]_s$ uniaxial test or other shear testing as described in Appendix A.

By the same procedure, the other five elements of the symmetric $[\bar{S}(t)]$ matrix can be obtained. Thus, by the application of appropriate assumptions and tensoral arguments, one can obtain the required

constitutive equations for unidirectional composites. However, physically the time-temperature verification and data reduction of the constitutive equation is no trivial matter. For continuity sake, this aspect will be placed in perspective and appropriately discussed in the data reduction section of this manuscript.

Time-Temperature-Superposition Principle (TTSP)

Basically, the TTSP or method of reduced variables [18,19] is a method by which long-term time-dependence can be determined by short-term response taken at various elevated temperatures. It is based on the relation

$$E_{ij}(t',T_o) = \frac{\rho_o T_o}{\rho T} E_{ij}(t,T) \tag{19}$$

where $E_{ij}(t,T)$ and $E_{ij}(t',T_o)$ are the moduli at temperature T and reference temperature T_o, respectively, ρ and ρ_o are the densities at temperature T and the reference temperature, T_o, respectively. For solids the ratio ρ_o/ρ is very small and is often neglected. The time parameters t' and t are related by the shift factor, a_T, and is defined by the relation

$$t = \int_o^{t'} \frac{dt}{a_T} \tag{20}$$

It must be mentioned that equation (19) as written is only valid for relaxation moduli. For composites, the axial creep compliance relationship can be expressed as

$$S_{xx}(t',T_o) = \frac{T}{T_o} S_{xx}(t,T) \tag{21}$$

or in the reciprocal form as

$$\frac{1}{S_{xx}(t',T_o)} = \frac{T_o}{T\, S_{xx}(t,T)} \qquad (22)$$

Due to the very small change in densities with respect to temperature, the density ratio is neglected in equations (21) and (22).

The implication of equations (19) and (22) is that the TTSP will enable one to reduce the complex time-temperature dependence of a viscoelastic material over several temperatures to a single time dependence at a certain reference temperature and a separate temperature dependence. The latter dependence is represented by the variation of the shift factors with respect to the isothermal ambient temperature. Physically, it would mean that by conducting short-term tests at different ambient temperatures, the long-term response of the viscoelastic material is represented by a composite curve constructed by shifting all of the short-term curves to obtain a master curve. This master curve is obtained by the horizontal shifting of the reduced viscoelastic functions with respect to a reference temperature along the logarithmic time axis.

As such, the role of the shift factor is of great importance when the TTSP is invoked. Generally, for ambient temperatures below the glass transition temperature (T_g), the shift factors are related to the ambient temperature by an apparent activation energy (ΔH_a) defined as: [18]

$$\Delta H_a = R \frac{d(\text{Ln } a_T)}{d(1/T)} \qquad (23)$$

where R is the universal gas constant, Ln is the natural logarithm and the other parameters are as previously defined. If Ln a_T is directly proportional to 1/T, equation (23) can be further simplified to an Arrhenius type equation, that is,

$$\Delta H_a = 2.303R \, \text{Log}_{10} \, a_T \left[\frac{1}{T} - \frac{1}{T_g}\right] \tag{24}$$

The implication of equation (24) is that the activation energy is constant for ambient temperatures below the T_g. If the ambient temperature is at or above the T_g then the shift factor is related to the ambient temperature by an empirical equation known as the William-Landel-Ferry (WLF) equation [18-20]. The WLF expression is given as

$$\text{Log}_{10} \, a_T = \frac{C_1[T - T_g]}{C_2 + [T - T_g]} \tag{25}$$

where C_1 and C_2 are material constants.

Generally, the applicability of the TTSP needs no verification. However, due to morphological changes associated with changes in temperature, load and duration of the test [21,22], poor correlations between the deformation predicted by TTSP and experiment may occur. Often, these deviations are minimized by shifting the deformation versus log time curves vertically, in addition to the horizontal shifts [23-26]. When the latter procedure is applied to the construction of the master curve, the material is generally considered to be thermorheologically complex (TCM). The only verification of the applicability of the TTSP to any particular material is made by performing long-term experiments.

Time-Dependent Strength Prediction

The two previous sections of this chapter were devoted mainly to the short- and long-term time-temperature behavior of unnotched composite materials. To completely characterize the time-temperature stress-strain behavior of a material requires that a criterion be used to define time-dependent failure or more specifically time-dependent separation or rupture. Analytically, failure criterion or criteria must be invoked if this aspect of the material behavior is to be considered.

To date, a large number of time-independent failure criteria for anisotropic materials have been proposed [27] but to the author's knowledge, no time-dependent anisotropic failure criteria have been proposed. An alternative would be to apply the correspondence principal [28] to the time independent criteria and derive its time-dependent analogue. However, such a procedure would require the mathematical functional representation of the time-dependent material properties. A variety of empirical and numerical techniques for acquiring the viscoelastic functions have been proposed [29-30]. Depending on the material behavior and the degree of sophistication of the mathematical representation, the failure criterion derived in this manner may or may not be appropriate [31].

In addition to the complexities discussed above, the results of Grinman and Gol'dman [32] showed that the isothermal failure behavior of isotropic high density polyethylene varies from a quasi-brittle (at medium and high stress-levels) to a brittle (at low stress-levels)

fracture. The implication is that the shape of the failure surface varies with time, that is, from a criterion with dependent failure modes (short-term) to a criterion with independent failure modes (long-term). Consequently, Grinman and Gol'dman used two different criteria to correlate their creep to rupture experimental results with analysis. In addition, these authors assumed that the principal strengths are functions of time and isochronal principal strengths are used for their predictions.

In view of the limitations in using the correspondence principal to derive time-dependent failure criterion and the failure mode variation with time, discussed above, the philosophy adopted here in predicting delayed creep failure is to utilize short-term test results to predict long-term failure. The rationale and procedure used in the predictions will be discussed in subsequent paragraphs.

Consider a creep to rupture test. Assuming that the time-temperature variations of the principal creep compliance master curves are identical to the variations of their respective principal strengths, the following relation between strengths and compliances is postulated, that is,

$$\frac{X_{mm}(t,T)}{X_{mm}(ta_T,T')} = \frac{S_{mm}(t,T)}{S_{mm}(ta_T,T')} \tag{26}$$

where $X_{mm}(t,T)$ = creep strength at T°C

$X_{mm}(ta_T,T')$ = creep strength at T'°C

m = 1,2,6 (summation not implied)

and

T°C > T'°C

It should be mentioned that the assumptions used, $X_{mm} = X_{mm}(t)$ and the identical variation of the principal strengths and compliances, are similar to those used in reference [32] and [33], respectively. The implication of equation (26) is that if the principal compliances obey the TTSP (that is, if master curves of the principal material compliances can be obtained) then the time-dependent failure envelopes will possess the same shape as the master curves. Perhaps more importantly, equation (26) assumes identical shift factors for creep strengths and compliances, respectively. The physical interpretation of equation (26) is that if one principal creep strength is known, the other principal creep strengths (within the time-temperature range of its respective compliance master curve) can be calculated.

Once the three principal strength master curves at a particular temperature are known, the application of the three time-dependent strengths to failure prediction of different plane states of stress is performed by using isochronal principal strengths in conjunction with a time-independent failure criterion derived from a tensoral point of view. Based on the brief but concise survey and evaluation of time-independent failure criteria in Appendix A, the criterion chosen here is the one proposed by Puppo and Evensen [34]. Besides the advantages discussed in Appendix A, the preference of this criterion over the others is primarily based on convenience. That is, the variation of the failure surface with time can be appropriately accounted for by the interaction factor and its exponent. The criterion proposed by Puppo and Evensen for a plane state of stress is expressed as

$$\left[\frac{\sigma_{11}}{X_{11}}\right]^2 - \gamma\left[\frac{X_{11}}{X_{22}}\right]\left[\frac{\sigma_{11}}{X_{11}}\right]\left[\frac{\sigma_{22}}{X_{22}}\right] + \gamma\left[\frac{\sigma_{22}}{X_{22}}\right]^2 + \left[\frac{\tau_{12}}{X_{66}}\right]^2 = 1 \qquad (27a)$$

$$\gamma\left[\frac{\sigma_{11}}{X_{11}}\right]^2 - \gamma\left[\frac{X_{22}}{X_{11}}\right]\left[\frac{\sigma_{11}}{X_{11}}\right]\left[\frac{\sigma_{22}}{X_{22}}\right] + \left[\frac{\sigma_{22}}{X_{22}}\right]^2 + \left[\frac{\tau_{12}}{X_{66}}\right]^2 = 1 \qquad (27b)$$

where $\gamma = \left[\frac{3X_{66}^2}{X_{11}X_{22}}\right]^n$ and n is a material parameter. If isochronal strengths are used then

$$X_{11} = X_{11}(t)$$

and

$$X_{22} = X_{22}(t)$$

$$X_{66} = X_{66}(t)$$

Again, the strengths in equations (27a) and (27b) are along the material axes. For a prescribed plane state of stress due to creep loading, the applied stresses are constant but the principal strengths are time-dependent. As time progresses, the principal time-dependent strengths decrease. Failure is said to occur when the sum of the terms on the left hand side of equation (27a) or (27b) equals to unity.

Thus, from the Boltzman superposition integral expressed in equation (2), it is shown how one could utilize the TTSP and isochronal strengths to predict the time-temperature behavior of a unidirectional composite laminate subjected to creep loading. The validity of the assumptions made, can only be verified by experiments. Only one composite system is chosen to verify the methodology described above. It is felt that if the experimental results do indeed correlate with

the analytical representation then the methodology can be extended to other composite systems.

III. EXPERIMENTAL CONSIDERATIONS AND OBSERVATIONS

As mentioned earlier, graphite/epoxy composite laminates were used in the experimental program. This particular composite system was selected because of the stability of the graphite fibers under different thermal conditions, that is, they do not change morphologically as is seen in some glass fibers. Except for the AS-3501 graphite/epoxy laminates used in some of the tests in Appendices A and B, all the experimental results presented here were obtained from T300/934 graphite/epoxy laminates. The fiber volume ratio of all cured panels were approximately 60% to 65%.

Since only the time-temperature analogy is considered here, the effects of the other three accelerating factors (moisture, vibration and stress) were eliminated or minimized in the experiments as follows:

The first factor, moisture, was eliminated by heating the specimens in an oven at 120°C for a few hours, weighing the specimens individually and repeating the procedure until the weight of the specimens stabilizes. Generally, the stabilization of the specimen's weight was observed after the second thermal cycle. These "dry" specimens were stored in a desiccator until tested.

The second factor, vibration, was avoided by performing relaxation or creep tests. Due to testing requirements, creep testing was preferred because it was easier to maintain constant stress than constant strain. Also, creep represents a stress state that results in a catastrophic failure mode more often than relaxation.

Finally, the third factor, stress, was minimized by operating at stress-levels such that linear behavior would occur. For example, consider the plot of the creep stress-level versus 15-minute creep strain of Figure 2. The initiation of the non-linear behavior likely occurred at approximately the point where the stress-strain plot begins to deviate from the straight line passing through the lower stress-level points. As expected, the non-linearity always initiated at a higher stress-level as the isothermal ambient temperature was lowered. By operating at stress-levels much lower than the non-linear initiation stress-level of the respective laminate, the material behavior could be assumed to be linear viscoelastic.

Another precautionary measure suggested by Shapery [26] was also adopted in the investigation. That is, under mechanical creep loading, if the initial jump in strain, ε_0, was equivalent to that when the specimen was unloaded the material behavior was assumed to be linear, as illustrated in Figure 3.

To insure that meaningful data were acquired (that is, the creep response measured was primarily due to the specimen and not due to the adhesive used to bond the end-tabs to the specimen or a combination of both responses), the gripping of the specimen onto the testing machine was not done with conventional wedge grips. Instead, a modified version of the gripping system suggested by Chamis and Sinclair [35] was used. The modification made here was the introduction of a pin through the mid-section of each clamped section of the specimen. The advantages gained from this gripping system were: The in-plane bending of the tensile specimen, discussed by Pagano and Halpin [36], and

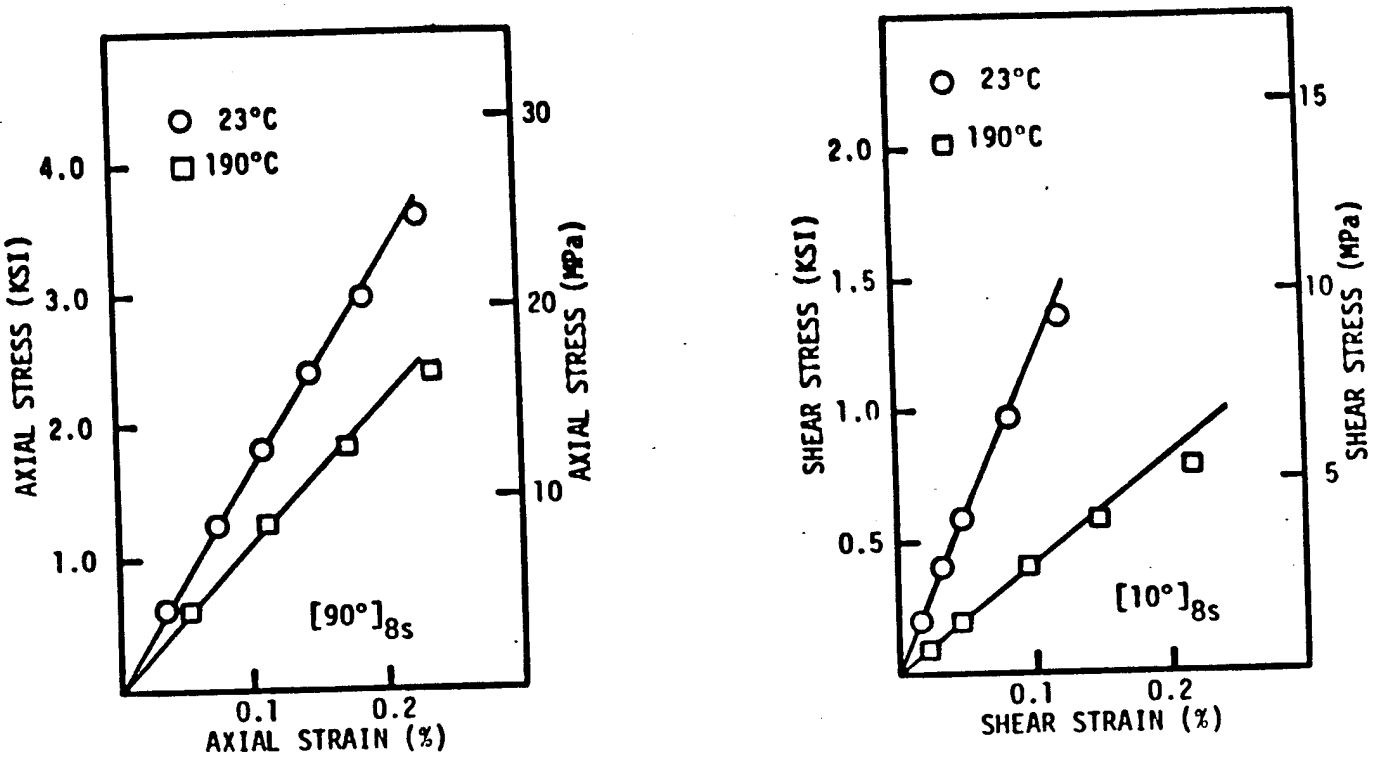

Figure 2. Linearity Check (Stress-Strain Curves After 15 Min. Creep) for T300/934 Graphite/Epoxy Laminate.

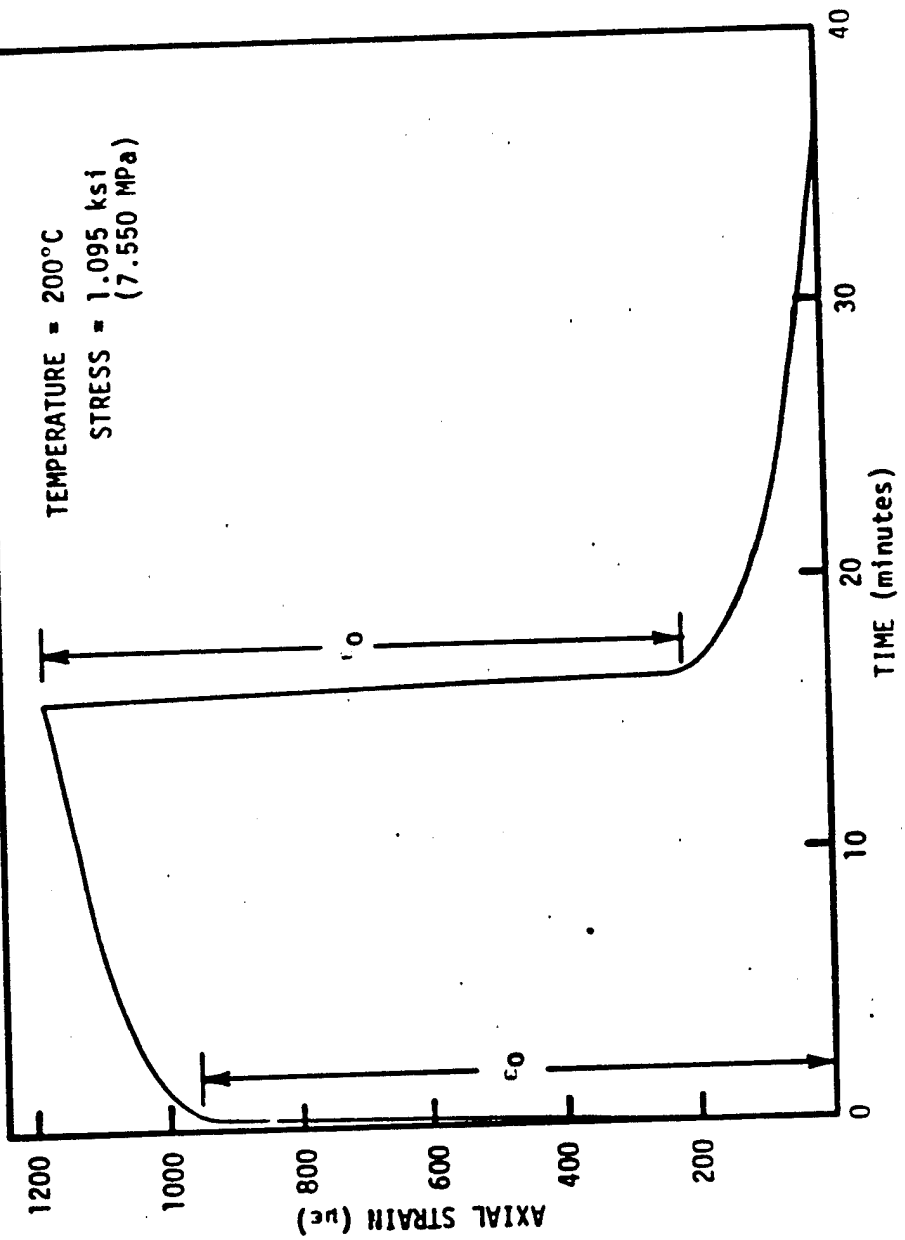

Figure 3. Creep and Creep Recovery of $[90°]_{8s}$ T300/934 Graphite/Epoxy Laminate.

slippage in the gripped sections were eliminated. It should be noted that slippage may not create as large an error in the creep tests as in relaxation tests but could still lead to a very severe consequence if not considered.

In addition to the above considerations, specimens need to be conditioned thermally and mechanically [37], prior to data acquisition. This requirement is due to the fact that epoxy based composite materials are normally cured at a temperature below their vitrification temperature. Consequently, the properties of such materials may vary if the material were cycled mechanically and/or thermally [38]. Such behavior may be observed in some photoelastic material where the stress-optic constants vary with thermal cycles. Based on these findings, some of the laminates used here were thermally and mechanically conditioned.

After five thermal cycles, both the mechanical and thermal properties were essentially the same for the fifth cycle as the first. Figure 4 shows the expansional behavior of the $[90°]_{8s}$ laminate for the first three thermal cycles. Three distinct values of the coefficients of thermal expansion in the 90° (transverse to the fibers) and 45° directions were observed. The averaged thermal strains were measured by two rectangular rosettes mounted on each side of the specimen and in-situ temperature compensated by two identical rosettes mounted on a material (known as "Flat Glass" by Corning Glass of Blacksburg) with a thermal coefficient of expansion of approximately 0.5 $\mu\varepsilon/°C$. The trilinear thermal behavior of the material occurred in the three temperature ranges indicated in Figure 4. Subsequently, two distinct

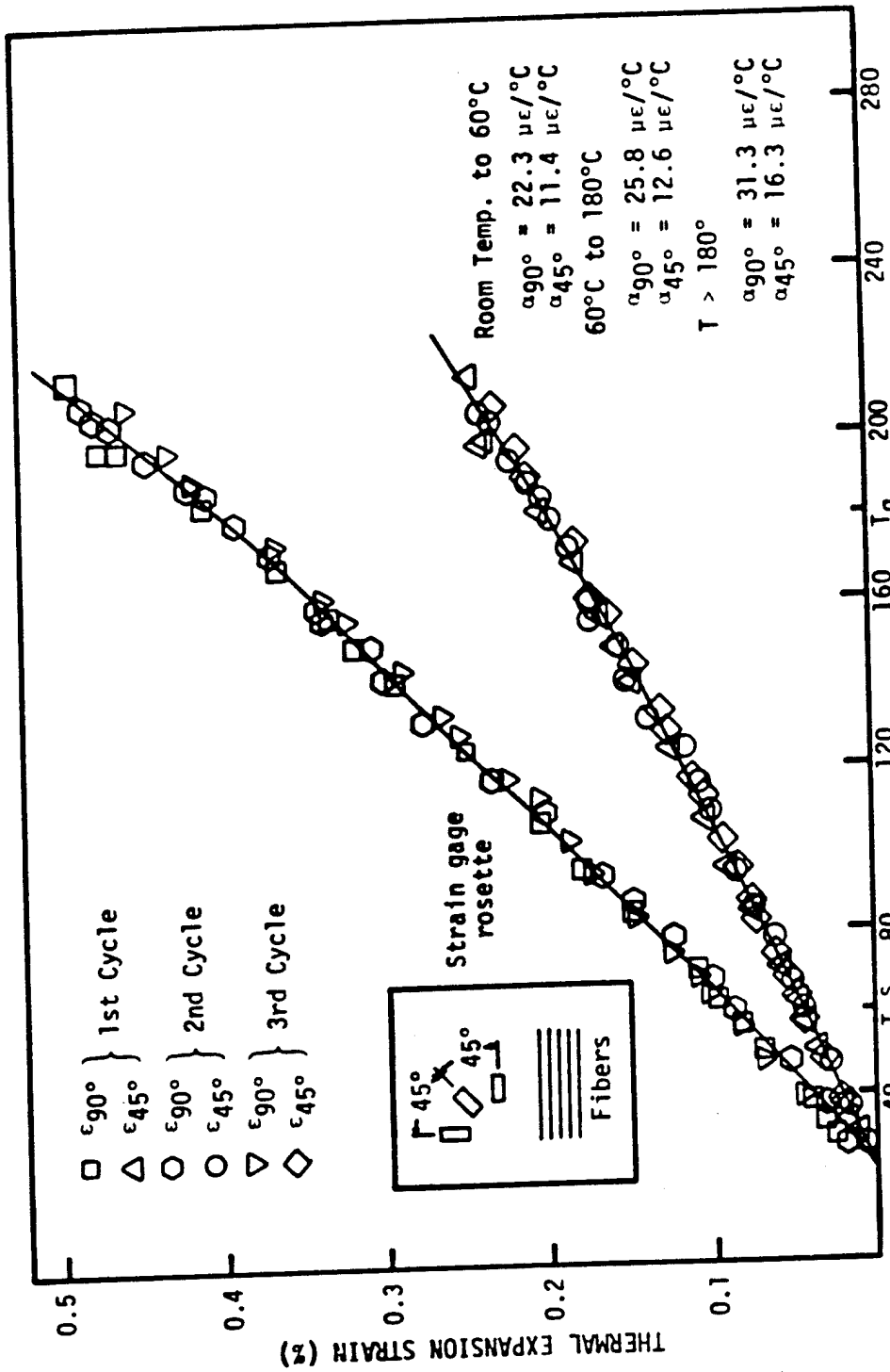

Figure 4. Thermal Expansion of $[90°]_{8s}$ T300/934 Graphite/Epoxy Laminate with Glass-Transition Temperatures Indicated.

glass transition temperatures were ascertained from this study; the secondary glass transition temperature at 60°C and the primary glass transition temperature at 180°C.

Upon completion of the thermal cycles, the specimens were mechanically conditioned by subjecting the specimens to creep loads of approximately 50% of the room-temperature ultimate load. After 15 minutes, the specimens were unloaded and allowed to recover to approximately zero strain. The process was repeated five times and the specimens were further subjected to fifty low frequency cyclic loads. At the end of the thermal and mechanical cycles, the properties of the specimens were essentially the same as they were in the virgin state. This tended to indicate that thermal and mechanical cycling were unnecessary for our material and that the specimens could be used repeatedly for at least the number of thermal and mechanical cycles mentioned.

After establishing the essential experimental procedure, 16-minute uniaxial creep tests followed by recovery to approximately zero strain were performed on the $[0°]_{8s}$, $[10°]_{8s}$, $[15°]_{8s}$, $[30°]_{8s}$, $[45°]_{8s}$, $[60°]_{8s}$, $[75°]_{8s}$ and $[90°]_{8s}$ tensile specimens, at different isothermal temperature levels. The reason for choosing a time of 16 minutes was due to the experimental procedure adopted. That is, data were acquired 1 minute after the initiation of the load and at 3-minute intervals thereafter. A typical creep-recovery curve is as shown in Figure 3. The $[10°]_{8s}$ laminate was used to obtain the time-dependent intralamina shear stress-strain response as discussed in Appendix A.

Upon completion of the short-term tests, 25-hour continuous creep tests were performed on the same specimens at 180°C. Complete recovery

of these medium-term tests were not obtained because of the length of time required by the recovery process. The purpose for this series of tests was to validate the TTSP as discussed earlier.

Finally, new specimens were used to ascertain the time frame of the creep to rupture (delayed failure) tests. At least two specimens of identical orientation but subjected to different stress-levels were used. In all the creep to rupture tests, the ambient temperature was maintained at 180°C. It should be mentioned that delayed failures were not observed at all the prescribed stress-levels of the respective laminates. The specimens that did not fail in 72 hours were replaced by another identical specimen, subjected to higher stress-levels.

In all the creep tests, only the $[0°]_{8s}$ specimen displayed no creep behavior. At elevated temperatures up to 210°C, the mechanical properties were essentially the same as the room-temperature values. In addition, the major Poisson's ratio (ν_{12}, obtained from this laminate) is found to be time-independent. This observation clearly substantiates one of the earlier assumptions; that is, the fiber was fundamentally elastic.

IV. DATA REDUCTION

EXPERIMENTAL MASTER CURVE DETERMINATION

The data reduction of the short-term creep compliances was performed by measuring the isochronal strains from 1 minute to 16 minutes at 3-minute increments and dividing the six measured strains by the applied stress at a particular temperature level. This procedure was repeated for all temperature levels. The compliances were in turn multiplied by the factor T/T_o where T is the absolute temperature at which the test was performed and $T_o = T_g = 453°K$. The values obtained in this manner are frequently referred to as reduced values and form the basis of the TTSP as discussed in Chapter II. The primary glass transition temperature was taken as the reference temperature mainly for two reasons: First, this temperature is unique for each polymeric material and, second, such a selection simplifies the task of verifying the Arrhenius and WLF equations discussed in Chapter II. By plotting these reduced compliances versus $\log_{10}$(time) and joining the shifted isothermal reduced values by a smooth curve, segments of a long continuous curve can be visualized. Examples of such plots are shown in Figures 5 to 13, except that the reciprocal of the reduced compliances are used instead of moduli. The purpose of this procedure will be discussed in the next chapter.

By shifting horizontally the reduced curves obtained at temperatures above the T_g to the right and the ones obtained at temperatures below the T_g to the left, a smooth continuous master curve is obtained.

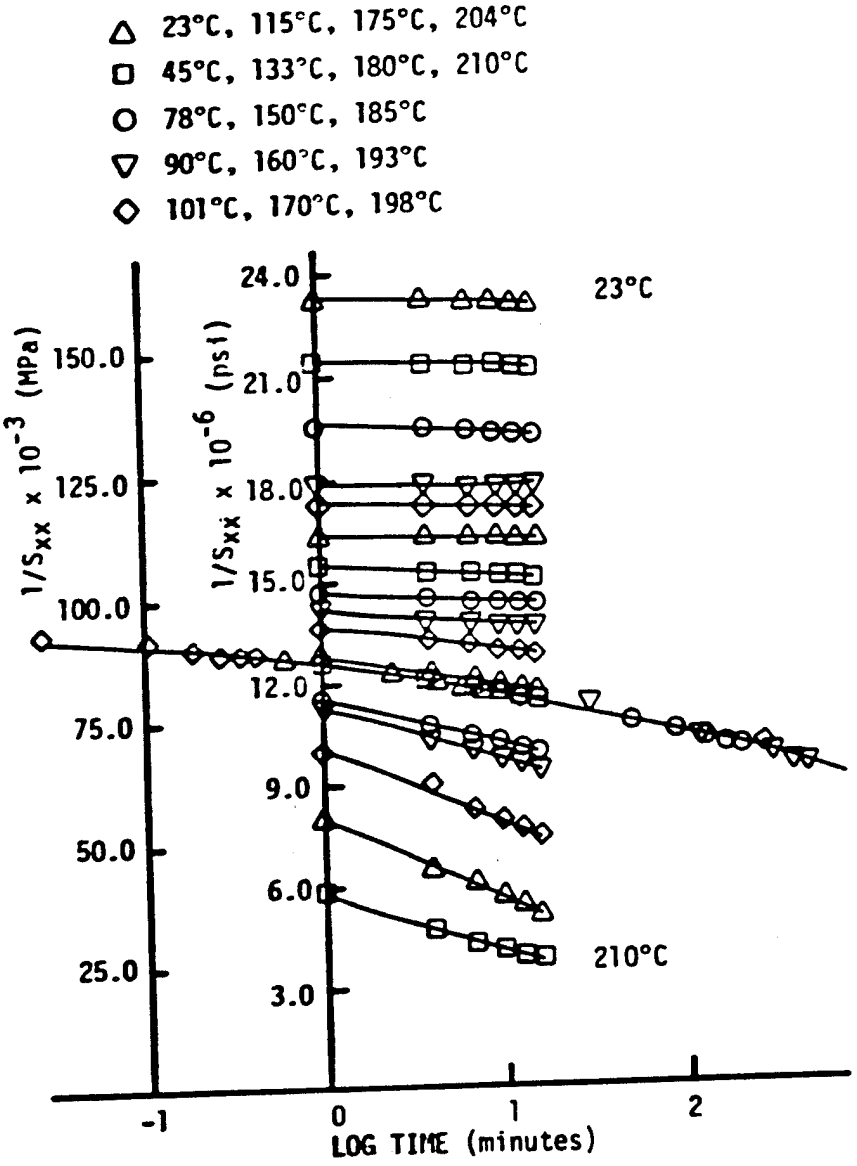

Figure 5. Reduced Reciprocal of Compliance, $1/S_{xx}$, and Portion of 180°C Master Curve for $[10°]_{8s}$ T300/934 Graphite/ Epoxy Laminate.

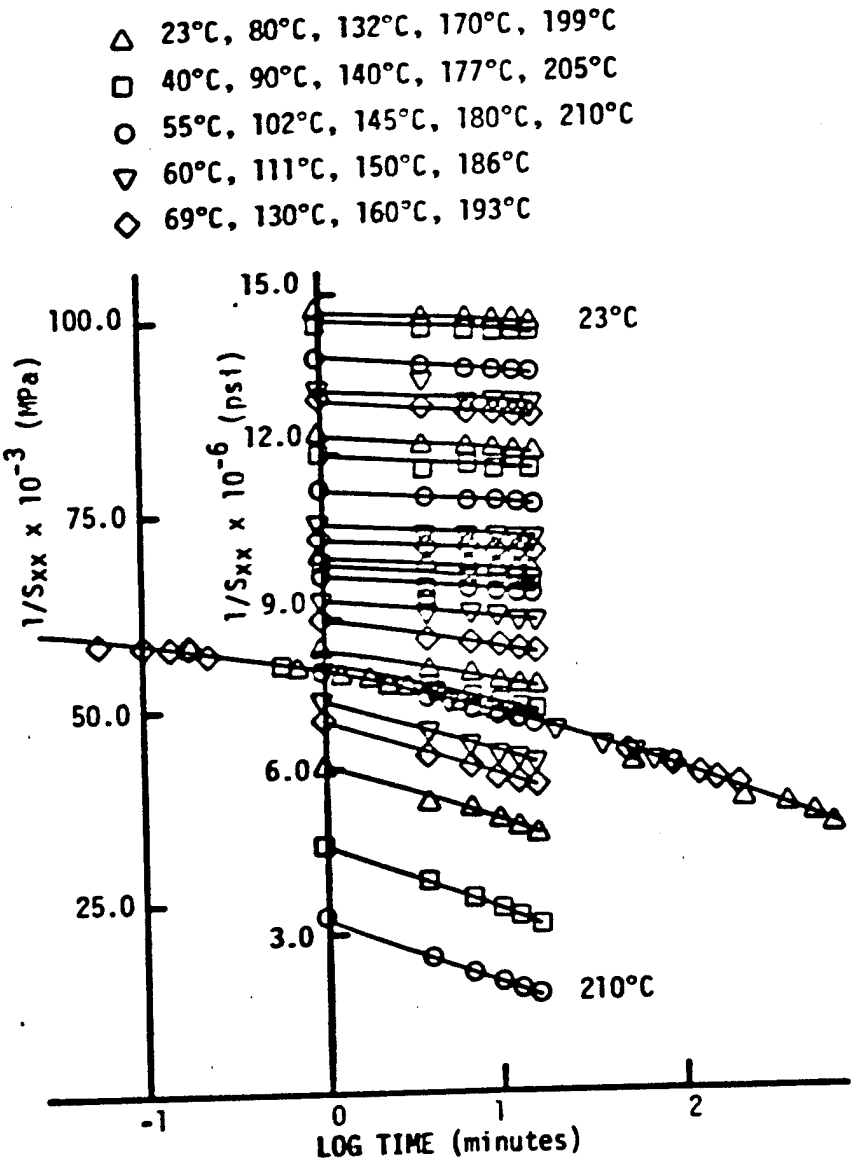

Figure 6. Reduced Reciprocal of Compliance, $1/S_{xx}$, and Portion of 180°C Master Curve for $[15°]_{8s}$ T300/934 Graphite/Epoxy Laminate.

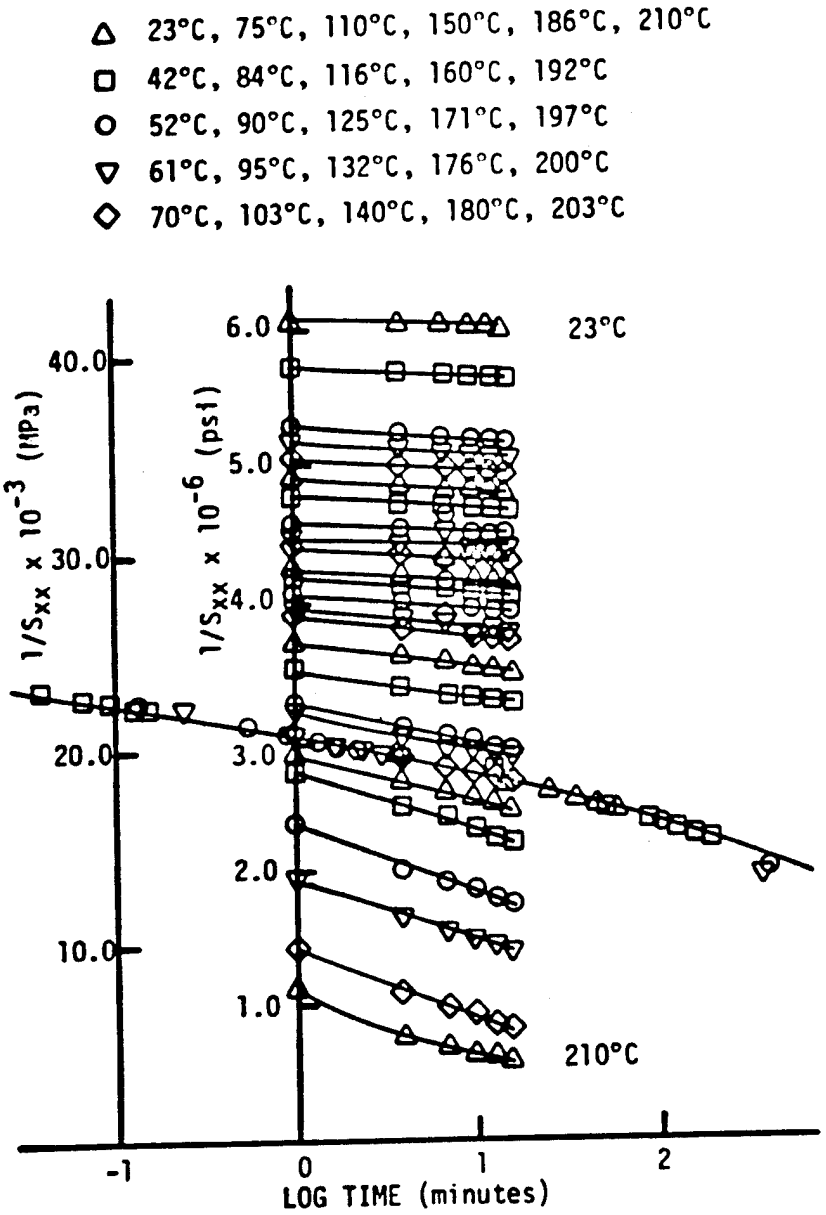

Figure 7. Reduced Reciprocal of Compliance, $1/S_{xx}$, and Portion of 180°C Master Curve for $[30°]_{8S}$ T300/934 Graphite/Epoxy Laminate.

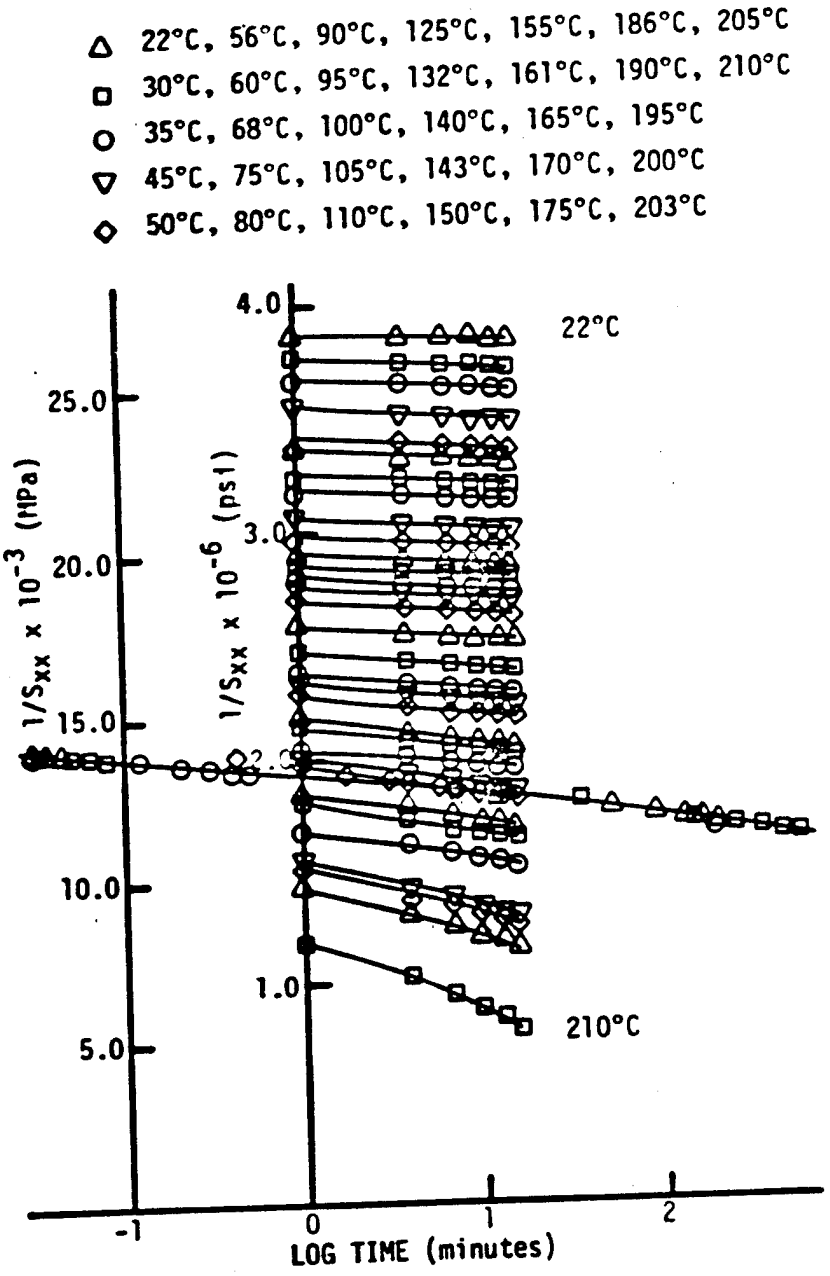

Figure 8. Reduced Reciprocal of Compliance, $1/S_{xx}$, and Portion of 180°C Master Curve for $[45°]_{8s}$ T300/934 Graphite/Epoxy Laminate.

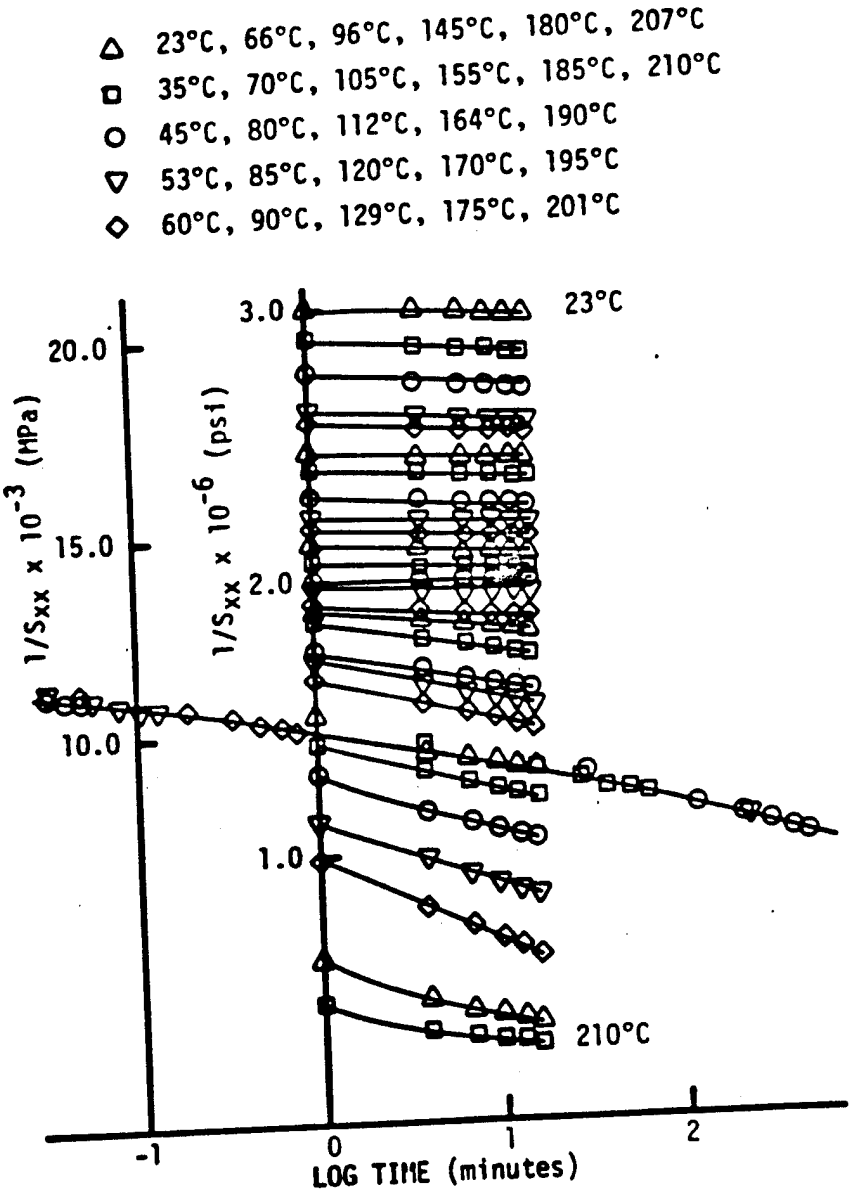

Figure 9. Reduced Reciprocal of Compliance, $1/S_{xx}$, and Portion of 180°C Master Curve for $[60°]_{8s}$ T300/934 Graphite/Epoxy Laminate.

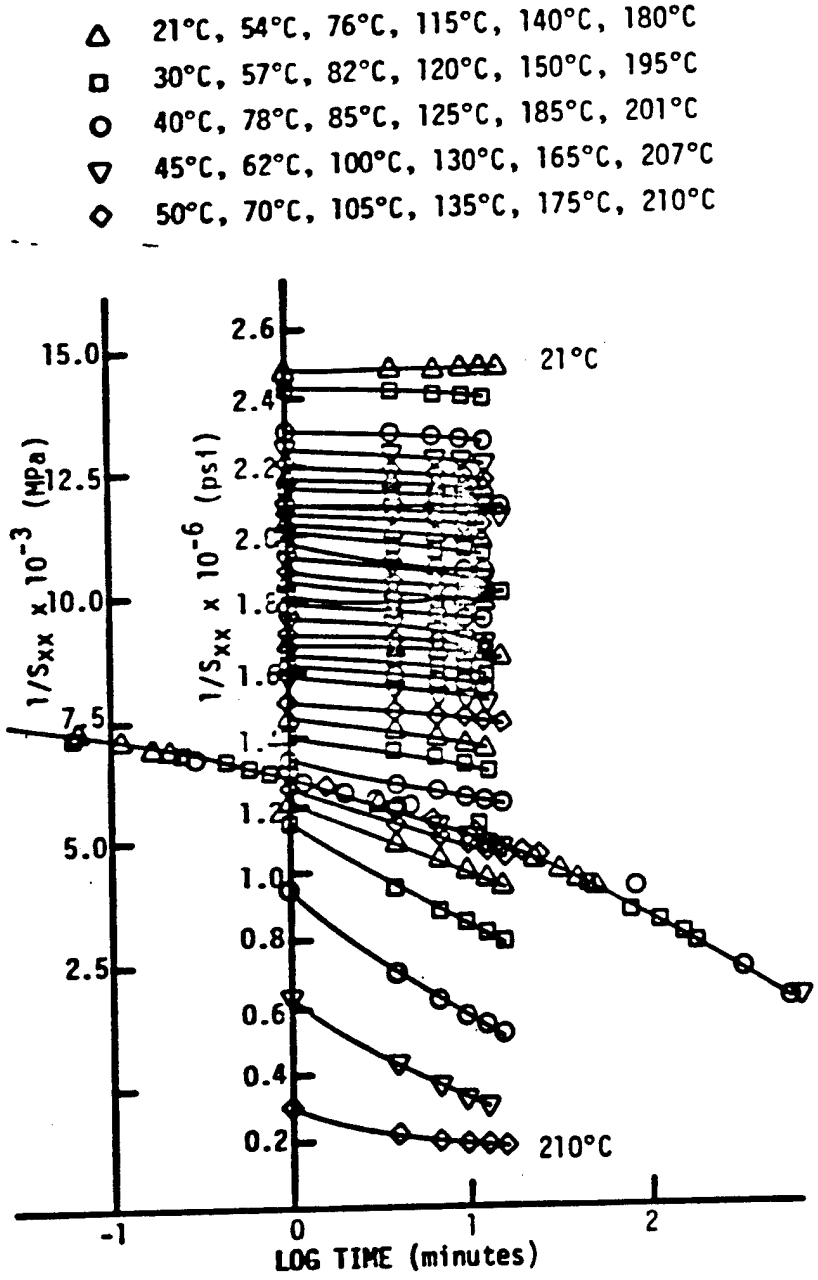

Figure 10. Reduced Reciprocal of Compliance, $1/S_{xx}$, and Portion of 180°C Master Curve for $[75°]_{8s}$ T300/934 Graphite/Epoxy Laminate.

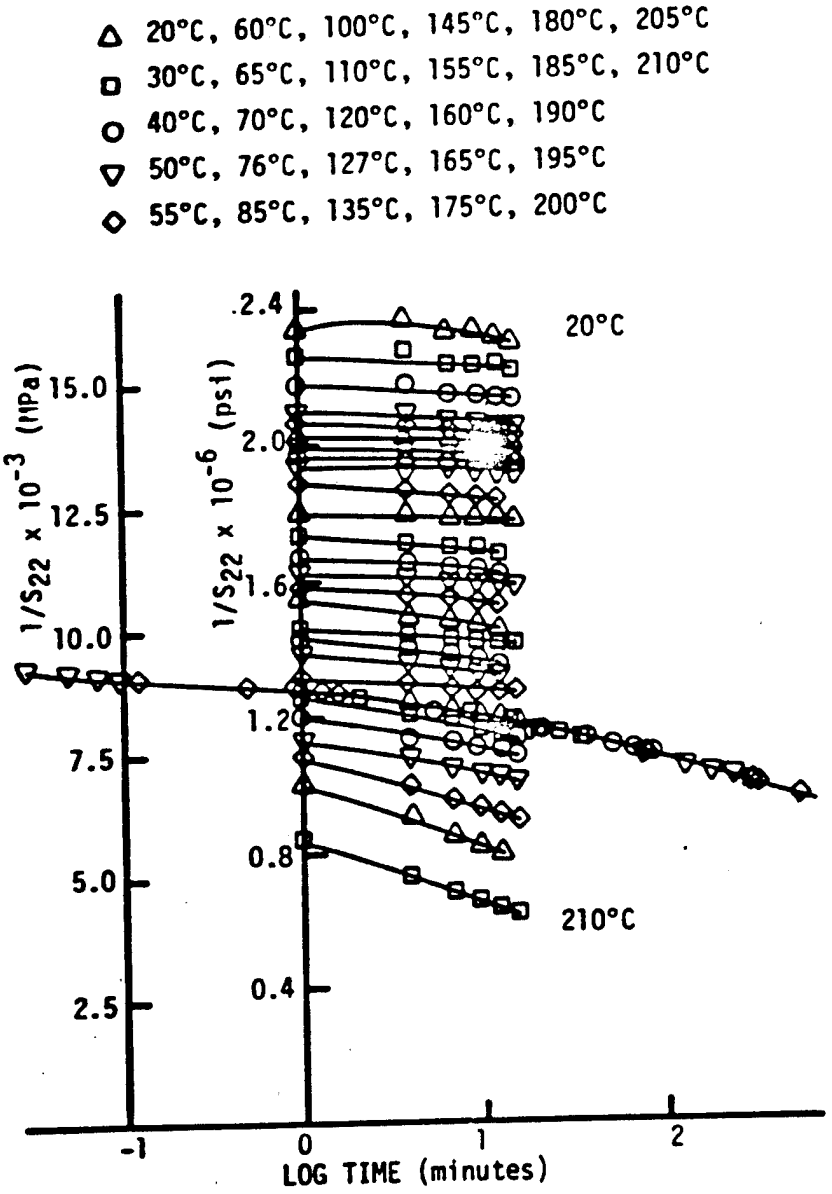

Figure 11. Reduced Reciprocal of Compliance, $1/S_{22}$, and Portion of 180°C Master Curve for $[90°]_{8S}$ T300/934 Graphite/Epoxy Laminate.

△ 23°C, 50°C, 78°C, 115°C, 160°C, 187°C
□ 30°C, 57°C, 84°C, 124°C, 165°C, 193°C
○ 35°C, 64°C, 89°C, 133°C, 170°C, 198°C
▽ 40°C, 60°C, 95°C, 140°C, 175°C, 204°C
◇ 45°C, 70°C, 101°C, 150°C, 180°C, 210°C

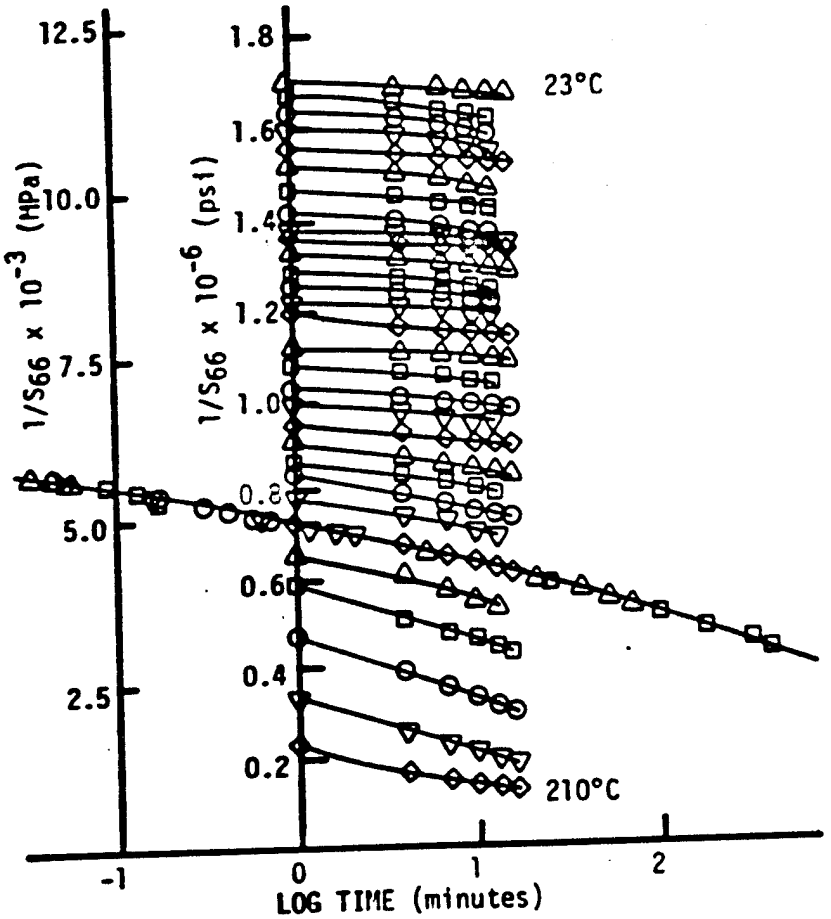

Figure 12. Reduced Reciprocal of Compliance, $1/S_{66}$, and Portion of 180°C Master Curve for T300/934 Graphite Epoxy.

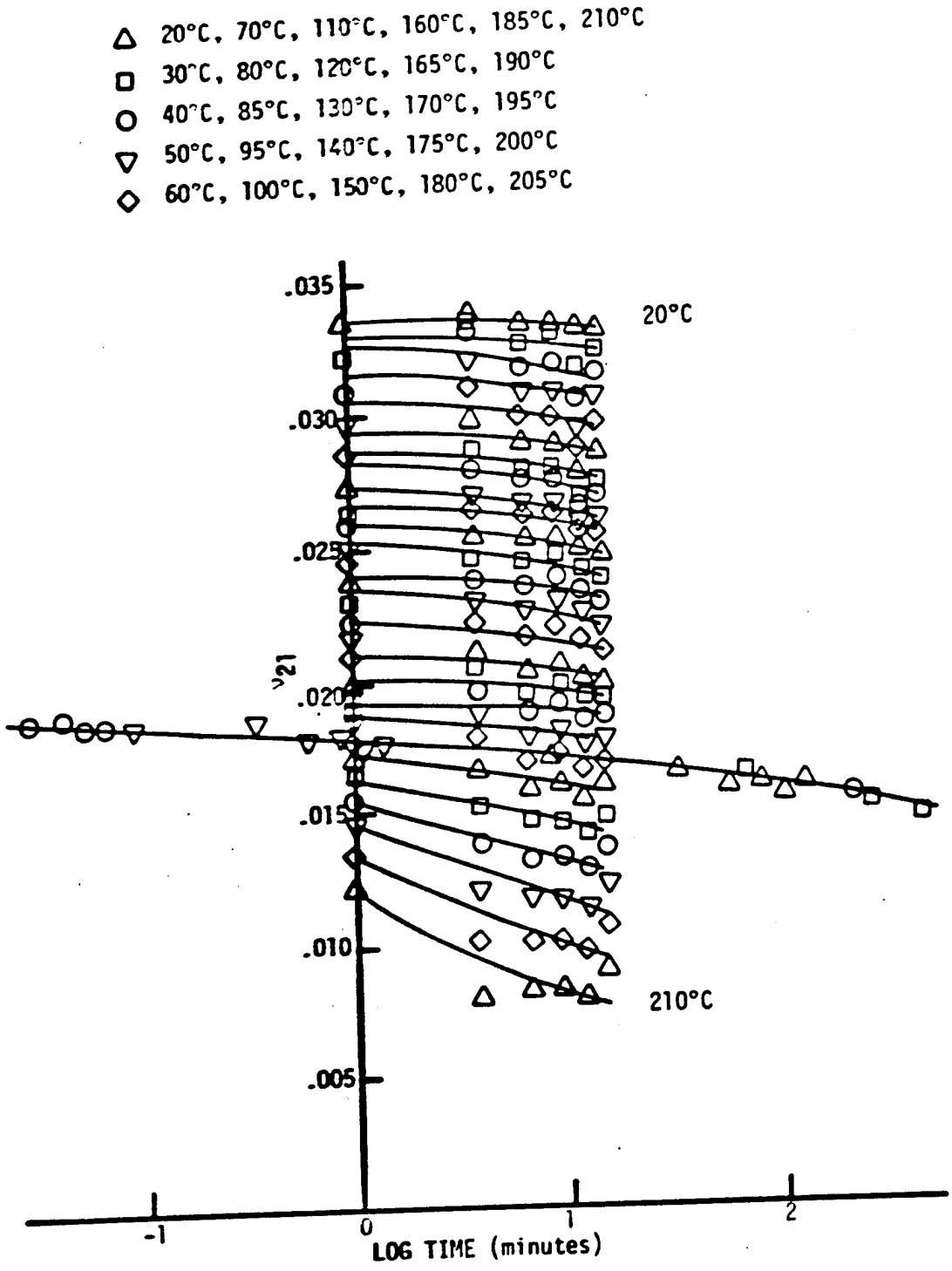

Figure 13. Reduced ν_{21} Data and Portion of 180°C Master Curve for T300/934 Graphite/Epoxy.

The shift factors ($a_T(T)$) are equivalent to the amount of horizontal shift of the respective isothermal reduced curves. Portions of the respective master curves are shown in Figures 5 to 13. It should be mentioned that this is a "trial and error" graphical smoothing procedure in which errors may arise. However, the principle yields important information over a broad time scale as indicated by the complete master curves of the three principal material properties shown in Figures 14 to 16. In these figures, the time scale of material response has been expanded to over twenty-six decades of time.

Master Curve Prediction

From an experimental and computational standpoint, the conventional procedure used in obtaining master curves is a very tedious and cumbersome one. This procedure, as it is, would have to be repeated for every arbitrarily oriented laminate. Obviously, from the designer's point of view and for economic reasons, this is a very serious drawback to the TTSP. Thus, a new technique, based on the principal material master curves, is proposed to overcome the disadvantages in the conventional master curve data reduction procedure and is discussed in detail subsequently.

Consider the orthotropic transformation equation (Chapter II) that is,

$$S_{xx}(t) = S_{11}(t)\,\mathrm{Cos}^4\theta + (S_{66}(t) + 2S_{12}(t))\,\mathrm{Cos}^2\theta\,\mathrm{Sin}^2\theta + S_{22}(t)\,\mathrm{Sin}^4\theta \qquad (17)$$

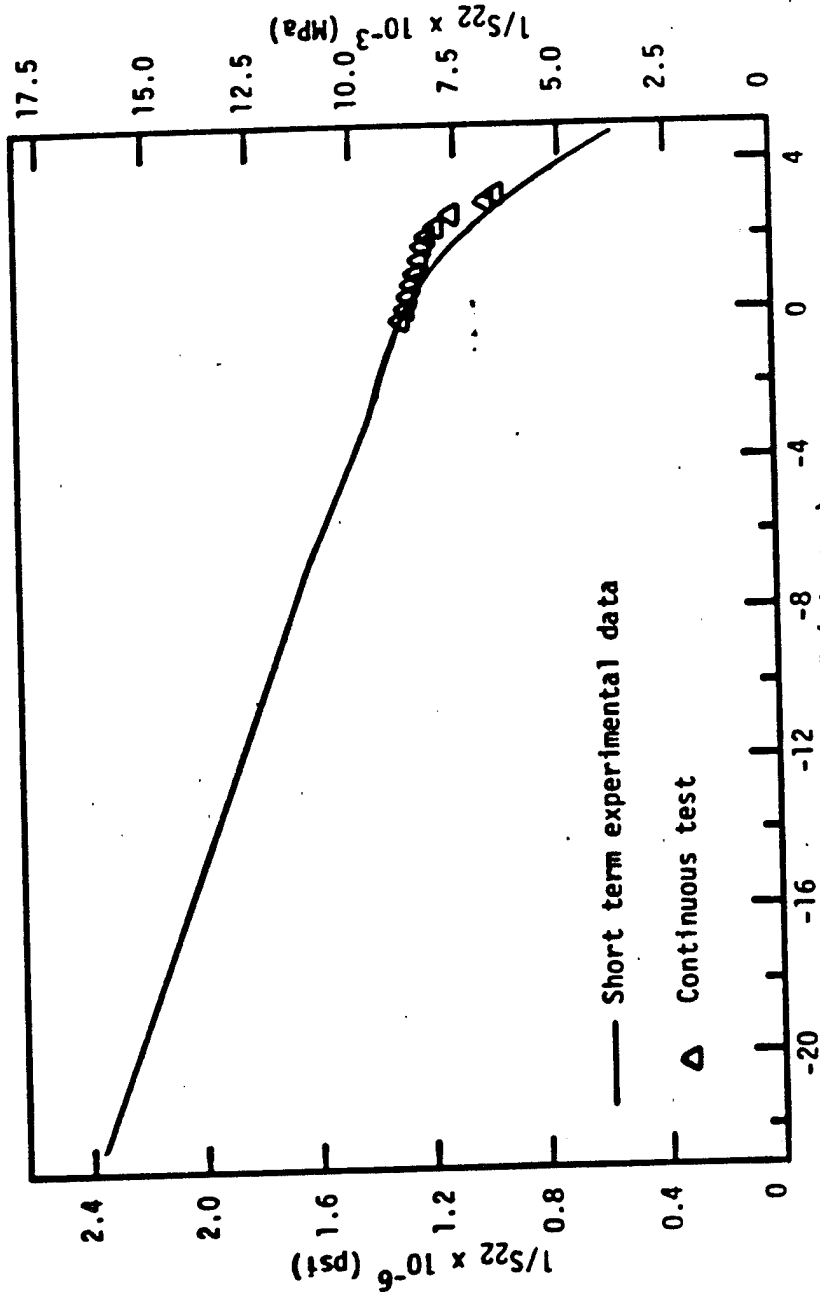

Figure 14. Master Curve of the Reciprocal of Reduced Compliance, $1/S_{22}$, for $[90°]_{8s}$ Laminate at 180°C.

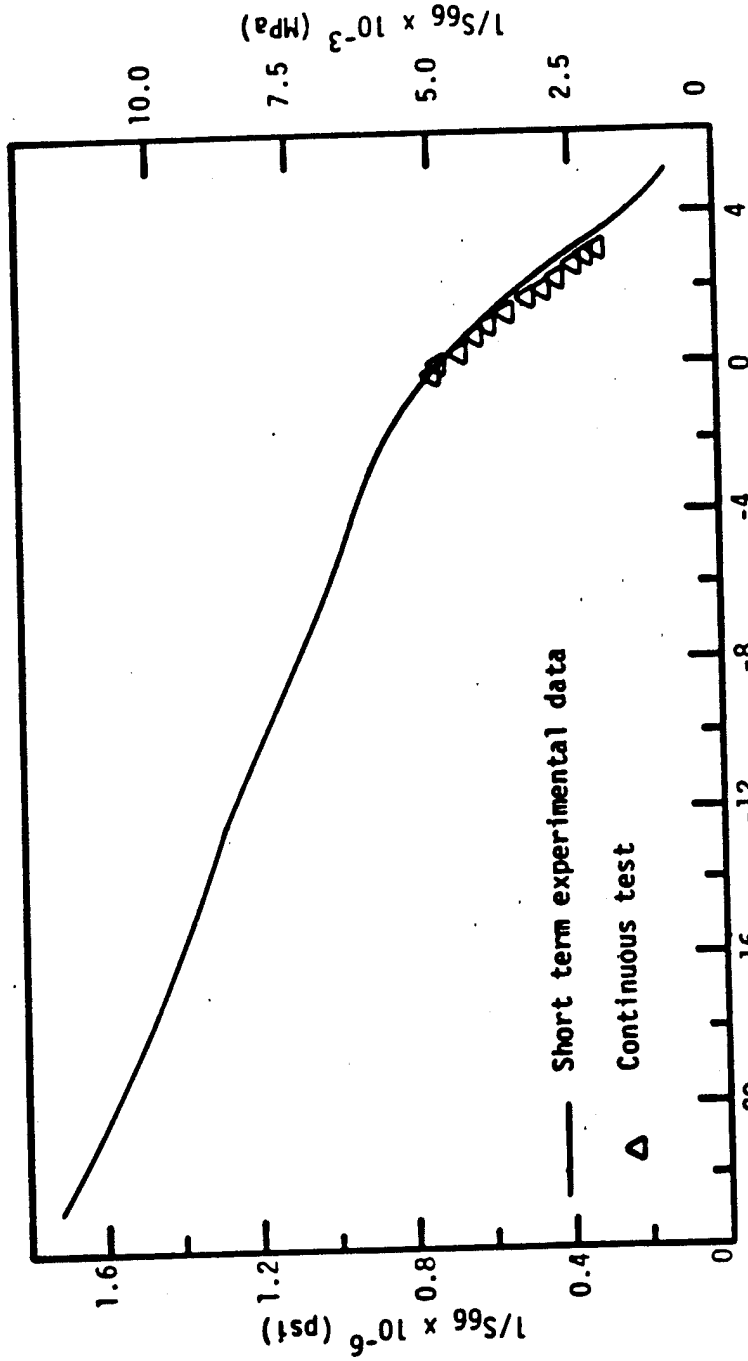

Figure 15. Master Curve of the Reciprocal of Reduced Shear Compliance, $1/S_{66}$, at 180°C.

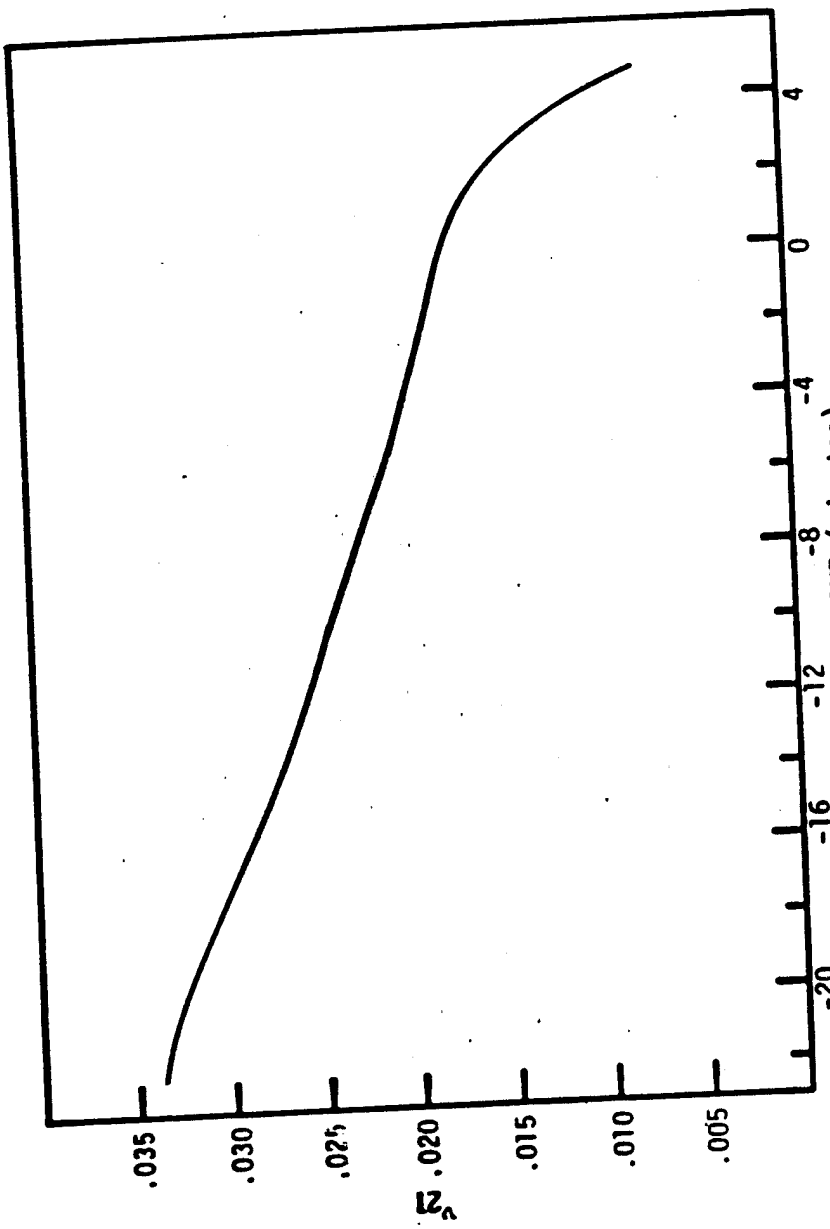

Figure 16. Master Curve of the Reduced Minor Poisson's Ratio, ν_{21}, at 180°C

For the type of two-phase materials considered herein and from our experimental observation on these materials as well as those of others [37,39], the $S_{11}(t)$ and $S_{12}(t)$ terms of equation (17) are found to be time-independent. The isochronal values of these two terms, tabulated in Table 1, do indicate time and temperature independence, at least within the temperature range considered. Thus, equation (17) can be further simplified as

$$S_{xx}(t) = S_{11}\text{Cos}^4\theta + (S_{66}(t) + 2S_{12})\text{Sin}^2\theta\ \text{Cos}^2\theta + S_{22}(t)\text{Sin}^4\theta \quad (28)$$

where time dependent terms are indicated by (t) and time independent terms are not so indicated. The difficulty in using equation (28) in conjunction with the four master curves is that reduced master curves of the S_{11} and ν_{12} for a particular temperature would have no meaning. Thus, the actual constant values of each have to be used. On the other hand, the $S_{66}(t)$ and $S_{22}(t)$ terms are reduced values. In short, equation (28) will not be composed of terms obtained by consistent procedures if the actual values of S_{11} and S_{12} and the reduced values of $S_{22}(t)$ and $S_{66}(t)$ are substituted directly therein. Any computational process performed using equation (28) would have to include a procedure to make all the terms consistent with each other. The procedure adopted was to use the actual values of all the terms in equation (28) as will be described subsequently.

Before proceeding into the computational procedure, it would be appropriate to discuss a few relevant and essential topics on the time-temperature behavior of two-phase materials in general. Consider equation (22), that is,

TABLE 1. VALUES OF THE RESPECTIVE 1-MINUTE COMPLIANCES.

Temperature °C	S_{11} x 10^6 psi^{-1} (x 10^4 MPa^{-1})	S_{12} x 10^6 psi^{-1} (x 10^4 MPa^{-1})	S_{21} x 10^6 psi (x 10^4 MPa^{-1})
22	0.0468 (0.0679)	-0.0149 (-0.0216)	-0.0143 (-0.0207)
100	0.0411 (0.0596)	-0.0124 (-0.0180)	-0.0148 (-0.0215)
180	0.0404 (0.0586)	-0.0132 (-0.0191)	-0.0144 (-0.0209)
200	0.0402 (0.0583)	-0.0140 (-0.0203)	-0.0147 (-0.0213)
210	0.0400 (0.0580)	-0.0136 (-0.0197)	-0.0157 (-0.0228)

$$\frac{1}{S_{xx}(t',T_o)} = \frac{T_o}{T\, S_{xx}(t,T)} \tag{22}$$

The physical interpretation of this relationship is that the time, t, required to reach a particular response (reciprocal of compliance in this case) at temperature, T, is equivalent to the time, t', required to reach the same response at temperature, T_o. By integrating equation (20), these two time parameters can be related by the shift factor as

$$t = a_T t'$$

or

$$\text{Log}_{10} t = \text{Log}_{10} a_T + \text{Log}_{10} t' \tag{29}$$

The main difficulty in applying equation (17) or (28) in conjunction with the TTSP to two-phase composite systems with time-dependent reinforcements is in the utilization of the shift factors. That is, the matrix and the fibers may possess different shift factors. The representation and/or interaction of the individual shift factor of these components would require further experimental and analytical study. However, in two-phase systems containing elastic reinforcement, Moehlenpah et al. showed that the shift factors are independent of the fiber orientation. Our present study has verified that observation. The subsequent computational procedure is based on this observation and the equivalent response relation of equation (22).

Consider the case where a $[\theta°]_s$ laminate master curve reduced at T_o'°C is required. Since the temperature dependence is represented by the variation of the shift factor with temperature and the time

dependence is represented by the master curves reduced at a particular temperature, T_o, the physical values of the two time-dependent terms ($S_{22}(t)$ and $S_{66}(t)$ of equation (28)) are obtained from the respective curves and the required master curves produced in the following manner:

1. For the particular isothermal ambient temperature, $T_o'°C$, a generic point on the $1/S_{22}(t)$ and $1/S_{66}(t)$ master curves (reduced at $T_o°C$) must be established first. This is accomplished by determining the shift factor, say t, for $T_o'°C$ on the $\log_{10}a_T$ versus temperature, as indicated in Figure 17a. Using this shift factor, the generic point, P, on the $1/S_{22}(t)$ and $1/S_{66}(t)$ master curves are located, as indicated in Figures 17b and 17c, respectively.
2. The two reduced time-dependent properties are obtained by measuring the ordinates of the point P on the respective curves.
3. Obtain the physical values of $1/S_{22}(t)$ and $1/S_{66}(t)$ by using

$$\frac{1}{S_{kk}(t,T)} = \frac{T}{T_o\, S_{kk}(t',T_o)}$$

where k = 2,6 (summation is not implied). It should be mentioned that $T = T_o'$ for the generic point and is equal to T' for all subsequent time increments, as indicated in step 8.

4. Substitute the values in step 3 and the other terms of the orthotropic transformation equation into equation (28) and compute the value of $S_{xx}(t)$.

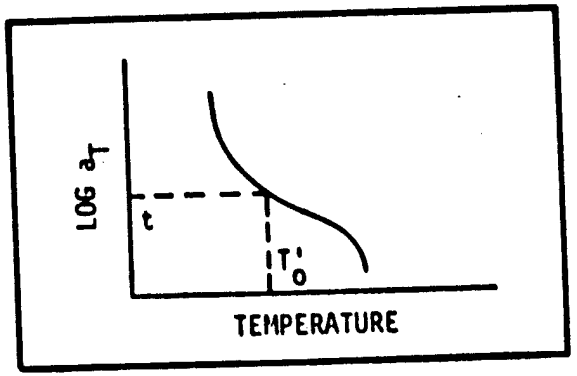

17a. $Log_{10}\ a_T$ Versus Temperature.

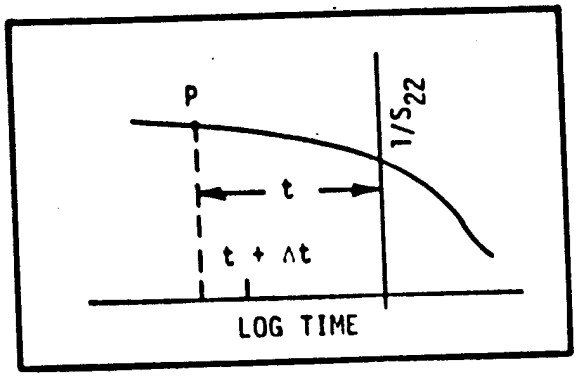

17b. $1/S_{22}$ Master Curve at T_o°C.

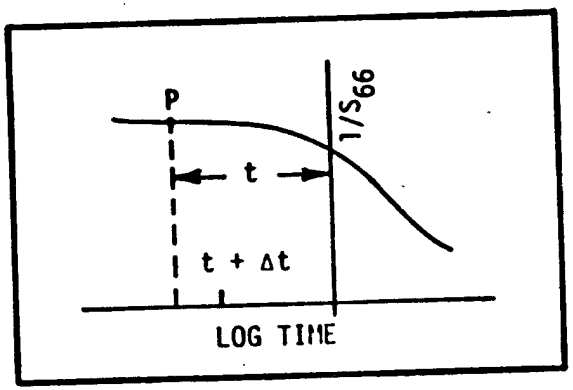

17c. $1/S_{66}$ Master Curve at T_o°C.

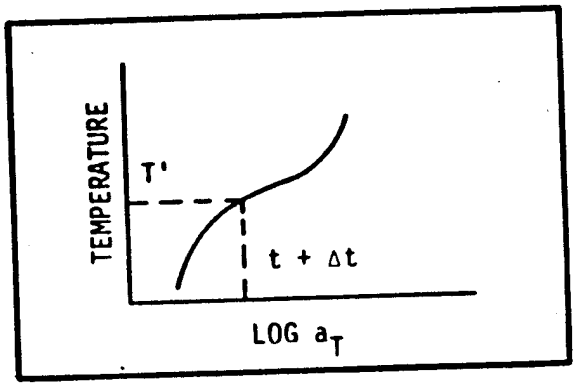

17d. Temperature Versus $Log_{10}\ a_T$.

Figure 17. Schematic for Master Curve Prediction Procedure.

5. Reduce the value of $S_{xx}(t)$, obtained in step 4, that is,

$$\frac{1}{S_{xx}(t,T_o')} = \frac{T_o'}{T\, S_{xx}(t',T)}$$

6. The next value at $t + \Delta t$, say, of the time-dependent properties are obtained by using $t + \Delta t$ to locate the $1/S_{22}(t + \Delta t)$ and $1/S_{66}(t + \Delta t)$ ordinates in Figures 17b and 17c, respectively.

7. Use the $t + \Delta t$ value to obtain the equivalent test temperature, T', from the temperature versus $\log_{10} a_T$ plot in Figure 17d.

8. Repeat steps 3 to 5 except use $T = T'$ (in steps 3 and 5) and $t = t + \Delta t$.

9. Repeat steps 6 to 8 for every additional time increment.

By plotting the reduced $1/S_{xx}(t)$ values obtained in the above manner versus $\log_{10}(\text{time})$, a curve representing the master curve of the $[\theta°]_s$ reduced at T_o' is obtained. This procedure can be used to generate any arbitrarily oriented unidirectional laminate reduced master curve for any length of time within the time scale of the input data, as well as any arbitrary ambient temperatures within the experimental range of the principal property master curves. The whole procedure can be further simplified by fitting all the curves in Figure 17 with a polynomial (known as POLYREG in the SSP library of the IBM 370/158 computer system) and used as input data for the computer program written to perform the computations described.

Strength Predictions

When predicting the delayed failure of a structure subjected to (say) creep loading, there are essentially two interrelated ways that one can pose the problem. One way is to determine the time required for the structure to fail when it is subjected to a known stress-level. An alternative is to determine the stress-level required to fail the structure at a given time. Although the objectives of both well posed problems are similar, the computational procedures are quite different. Thus, depending on one's preference, the choice is solely determined by the investigator. Both computational procedures and an alternative procedure are discussed in the subsequent paragraphs.

Consider the case of determining the stress-level required to fail a specimen at a particular ambient temperature, T, and a given length of time, t. Sequentially, using the analysis described in Chapter II, the computations are performed as follows:

1. Using the known principal strength of the respective laminates (obtained from tests performed at T'), calculate the respective isochronal strengths expressed in equation (26).
2. Substitute these calculated isochronal strengths at T, into equations (27a) and (27b). By expressing the prescribed state of creep stress in terms of the local coordinates and increasing the applied stress incrementally, the failure stress-level is determined when the sum of the terms on the left hand side of equations (27a) and (27b) equals to unity.

One may have to perform some iterations (in terms of the applied stresses) in step 2, in order to achieve unity. For uniaxially applied stress, σ_x, the incremental procedure of step 2 can be avoided and σ_x can be calculated directly as follows: Transform σ_x to the local coordinates,

$$\left.\begin{aligned} \sigma_{11} &= \sigma_x \cos^2\theta \\ \sigma_{22} &= \sigma_x \sin^2\theta \\ \tau_{12} &= \sigma_x \cos\theta \sin\theta \end{aligned}\right\} \qquad (30)$$

Now substitute equations (30) into equations (27a) and (27b) to obtain the following equations,

$$\frac{1}{\sigma_x^2} = \left[\frac{\cos^2\theta}{X_{11}}\right]^2 - \gamma\left[\frac{X_{11}}{X_{22}}\right]\left[\frac{\cos^2\theta}{X_{11}}\right]\left[\frac{\sin^2\theta}{X_{22}}\right] + \gamma\left[\frac{\sin^2\theta}{X_{22}}\right]^2 + \left[\frac{\cos\theta\ \sin\theta}{X_{66}}\right]^2 \qquad (31a)$$

$$\frac{1}{\sigma_x^2} = \gamma\left[\frac{\cos^2\theta}{X_{11}}\right]^2 - \gamma\left[\frac{X_{22}}{X_{11}}\right]\left[\frac{\cos^2\theta}{X_{11}}\right]\left[\frac{\sin^2\theta}{X_{22}}\right] + \left[\frac{\sin^2\theta}{X_{22}}\right]^2 + \left[\frac{\cos\theta\ \sin\theta}{X_{66}}\right]^2 \qquad (31b)$$

in which the terms are as previously defined. Thus, using these latter equations one can determine directly the required uniaxial stress-level.

In the case when the stresses are known and the time-frame is required, increments of time would have to be used regardless of the types of in-plane applied stresses. Except for some modifications, essentially the same procedure described in the previous paragraph can be used for this prediction. That is, the isochronal strengths of step 1 is required. The main difference is in step 2 where the applied stresses are constant. By taking time increments and substituting the time-dependent strengths into equations (27a) and (27b), the required

time frame is obtained when the sum of the terms on the left hand side of the failure criterion equals to unity. Again, some iterations may be required in the computations.

The third procedure for determining either the time-frame or stress-level is to compute creep strength master curves for the given states of stress at a reference temperature using the procedure described for the first case. The required quantity is obtained from the time-dependent failure surface directly by measuring it from the plot of the failure surface. The main disadvantage in the simultaneous acquisition of both quantities is that different surfaces would be required for different ambient temperatures. However, this procedure is very convenient when a number of predictions at a particular ambient temperature are required.

V. RESULTS AND DISCUSSION

The master curves of all the laminates (except the $[0°]_{8s}$ laminate) obtained from the short-term (16-minute) tests, are shown in Figures 14 to 16 and Figures 18 to 23. The results in these figures represent the measured master curves obtained from short-term, 16-minute tests, the predicted master curves obtained using the computational procedure described in the previous section and the results of our 25-hour creep tests for each orientation indicated. In all these figures, except Figure 16, a linear scale was used to represent the magnitude of the reciprocal of axial compliance instead of the logarithmic scale normally used in the master curves of single-phase polymeric materials. This is primarily due to the small volume fraction of the epoxy in the laminates which resulted in the relatively small variations in creep compliances. A reason for using the reciprocal of the reduced compliance in these figures rather than simply the reduced compliance is essentially for future investigative purposes. That is, a number of authors [1,37,39] had conjectured that for temperatures below the T_g, one can assume the behavior of the material to be quasi-elastic, that is

$$E_{ij}(t) = \frac{1}{S_{ij}(t)}$$

Normally, in single-phase polymeric materials such an assumption is invalid [41]. The only means of validating the quasi-elastic assumption is to perform relaxation tests on the same material and compare

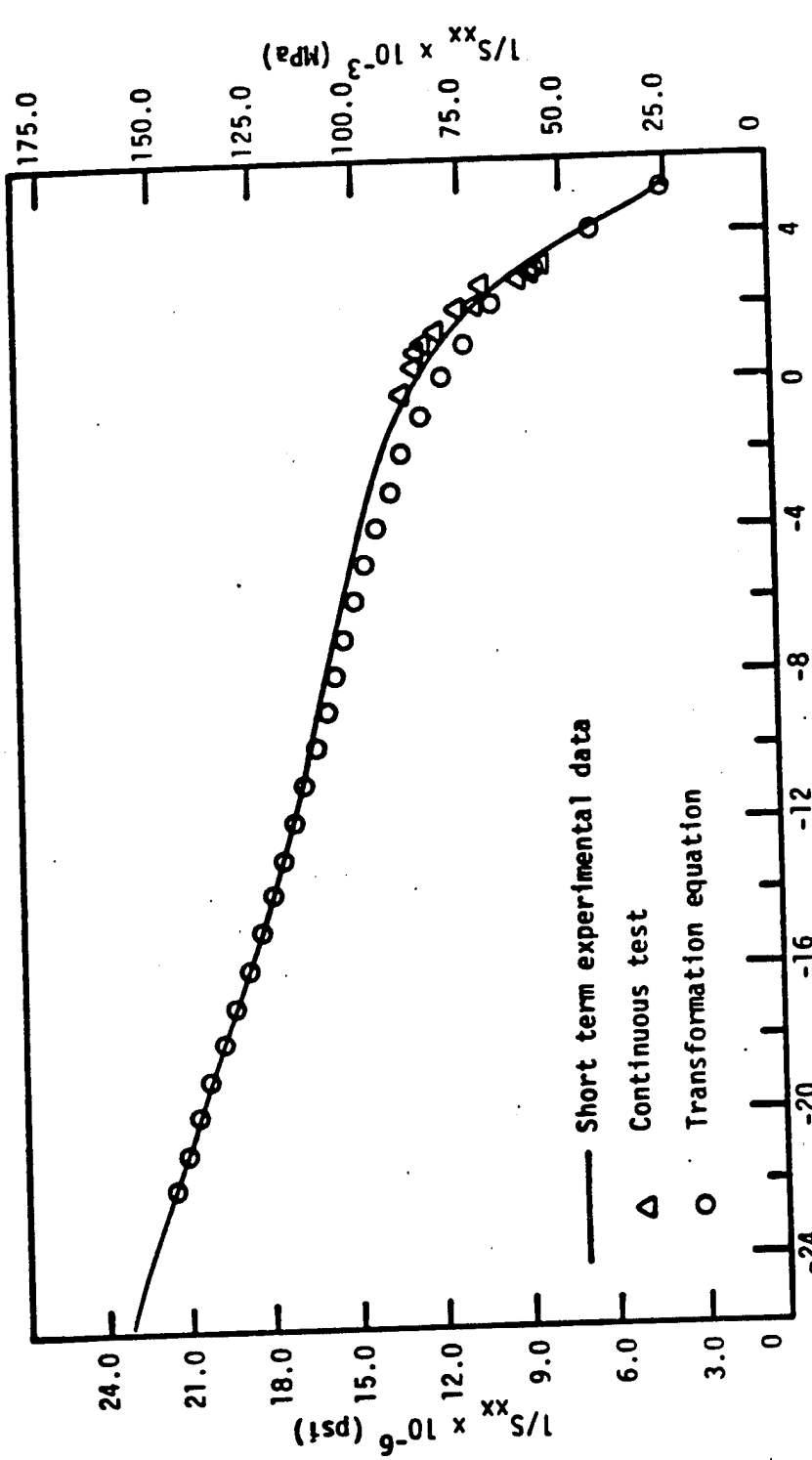

Figure 18. Master Curve of the Reciprocal of Reduced Compliance, $1/S_{xx}$, of $[10°]_{8s}$ Laminate at 180°C.

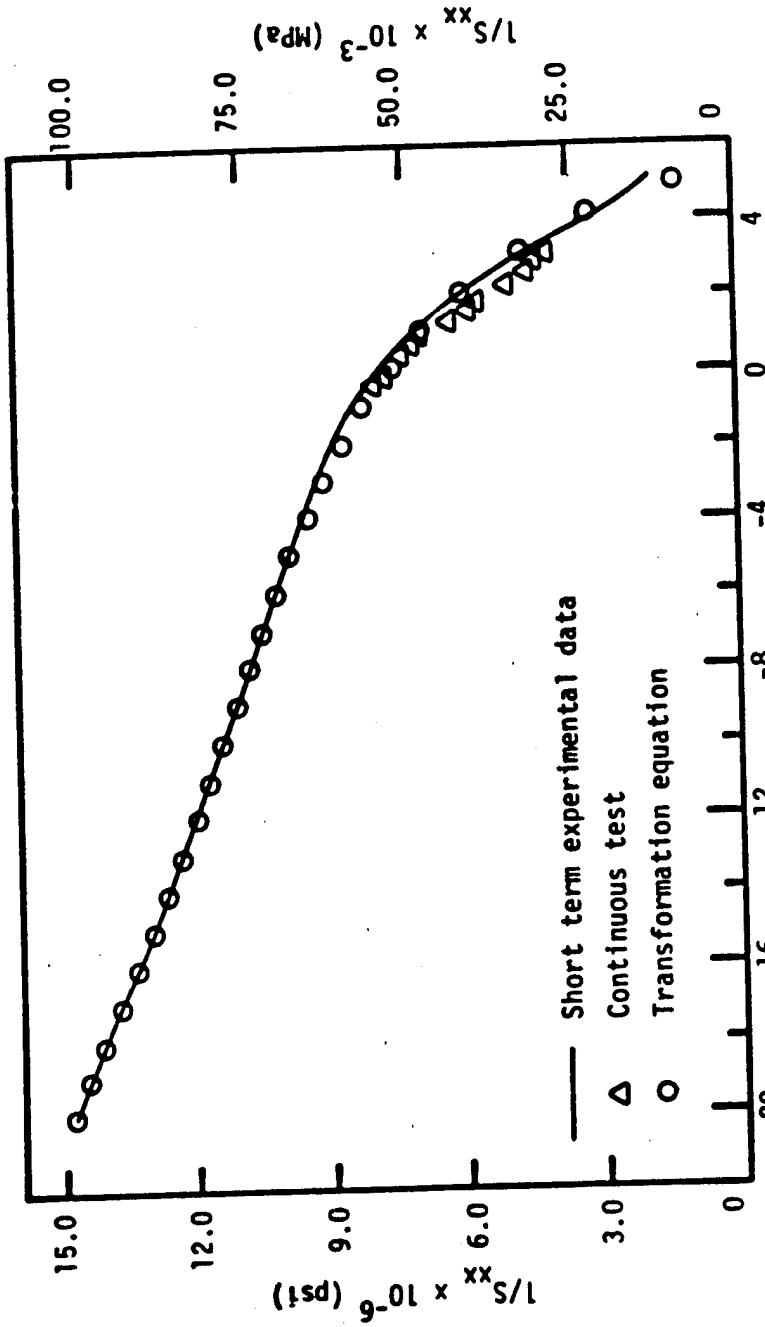

Figure 19. Master Curve of the Reciprocal of Reduced Compliance, $1/S_{xx}$, of $[15°]_{8s}$ Laminate at 180°C.

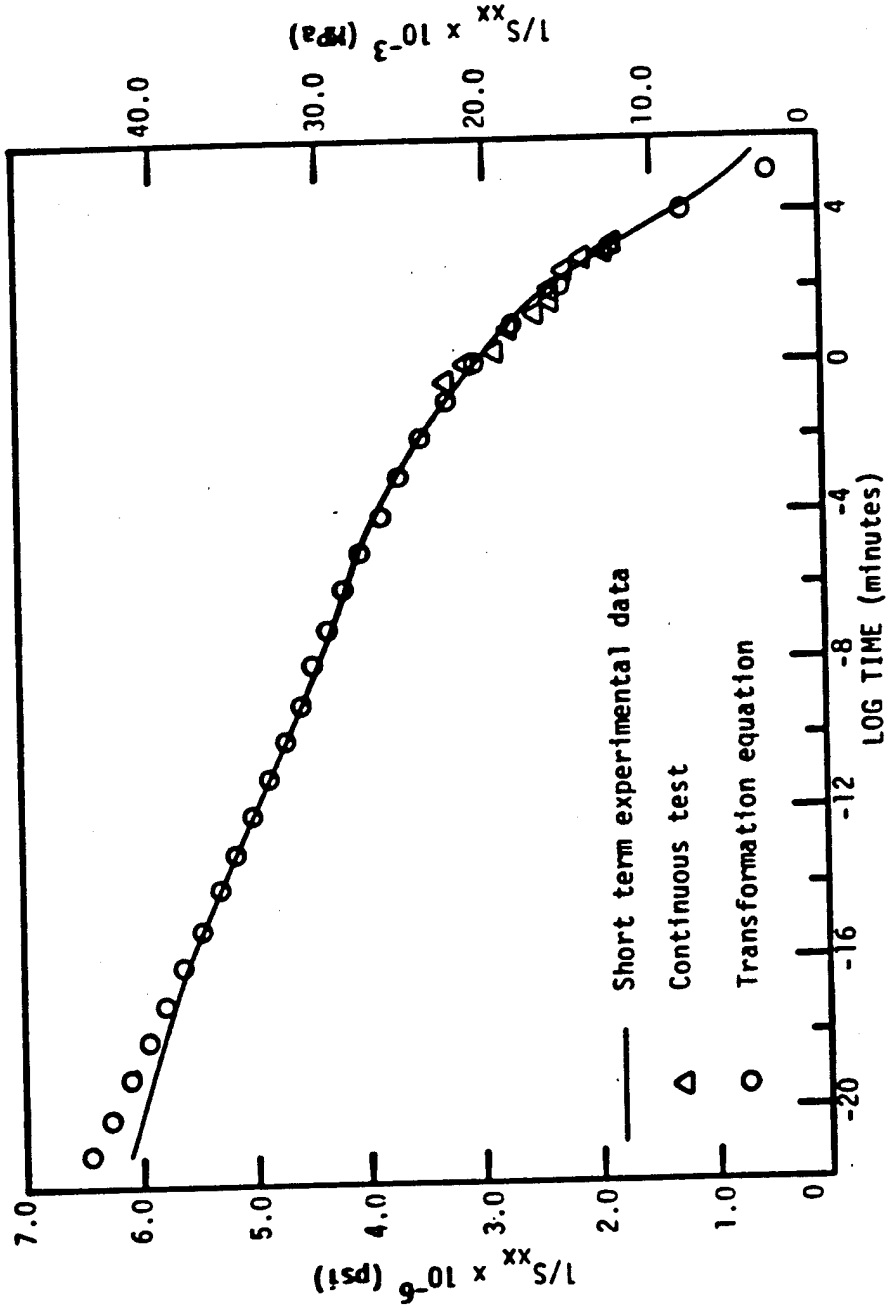

Figure 20. Master Curve of the Reciprocal of Reduced Compliance, $1/S_{xx}$, of $[30°]_{8s}$ Laminate at 180°C.

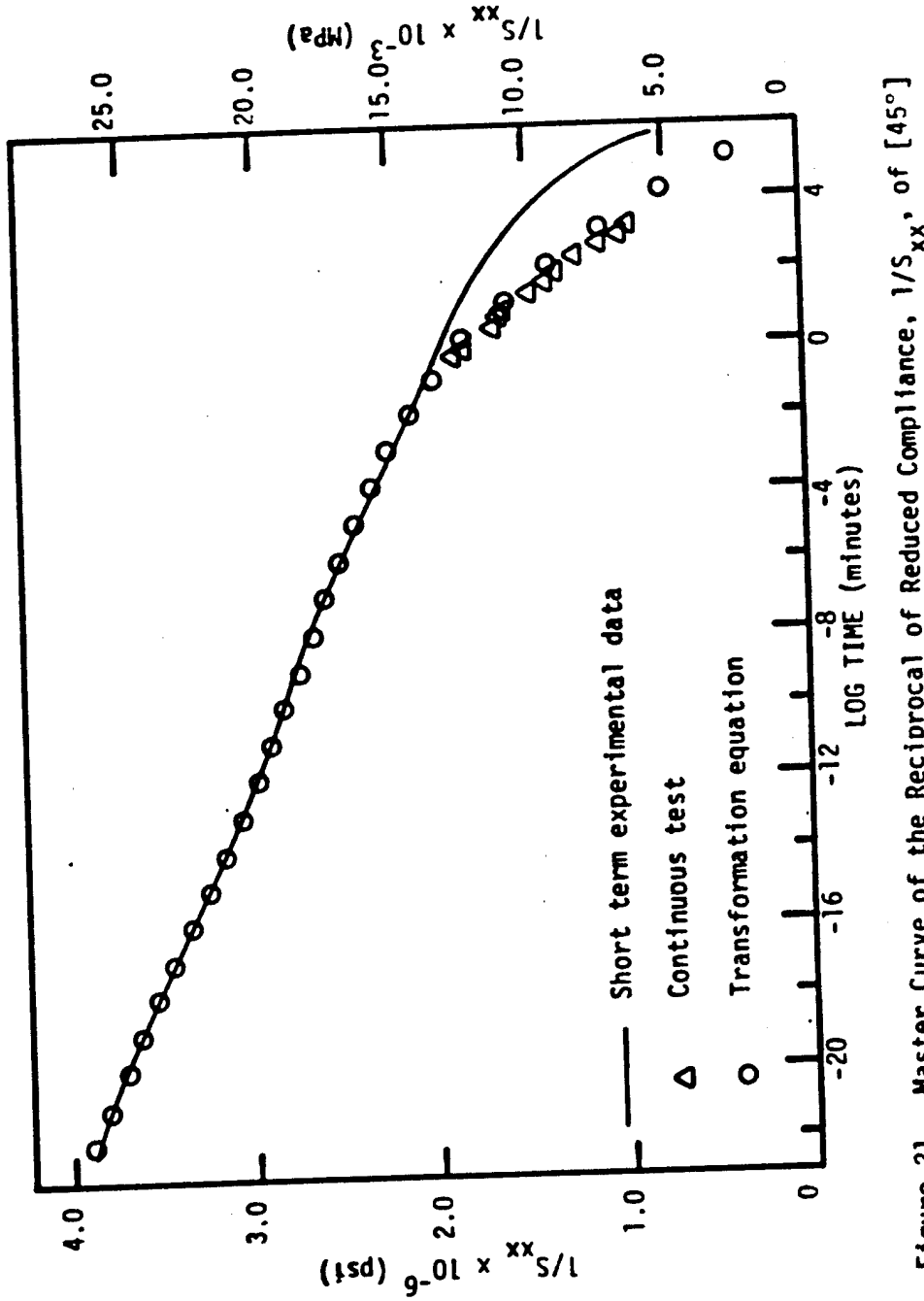

Figure 21. Master Curve of the Reciprocal of Reduced Compliance, $1/S_{xx}$, of [45°] Laminate at 180°C.

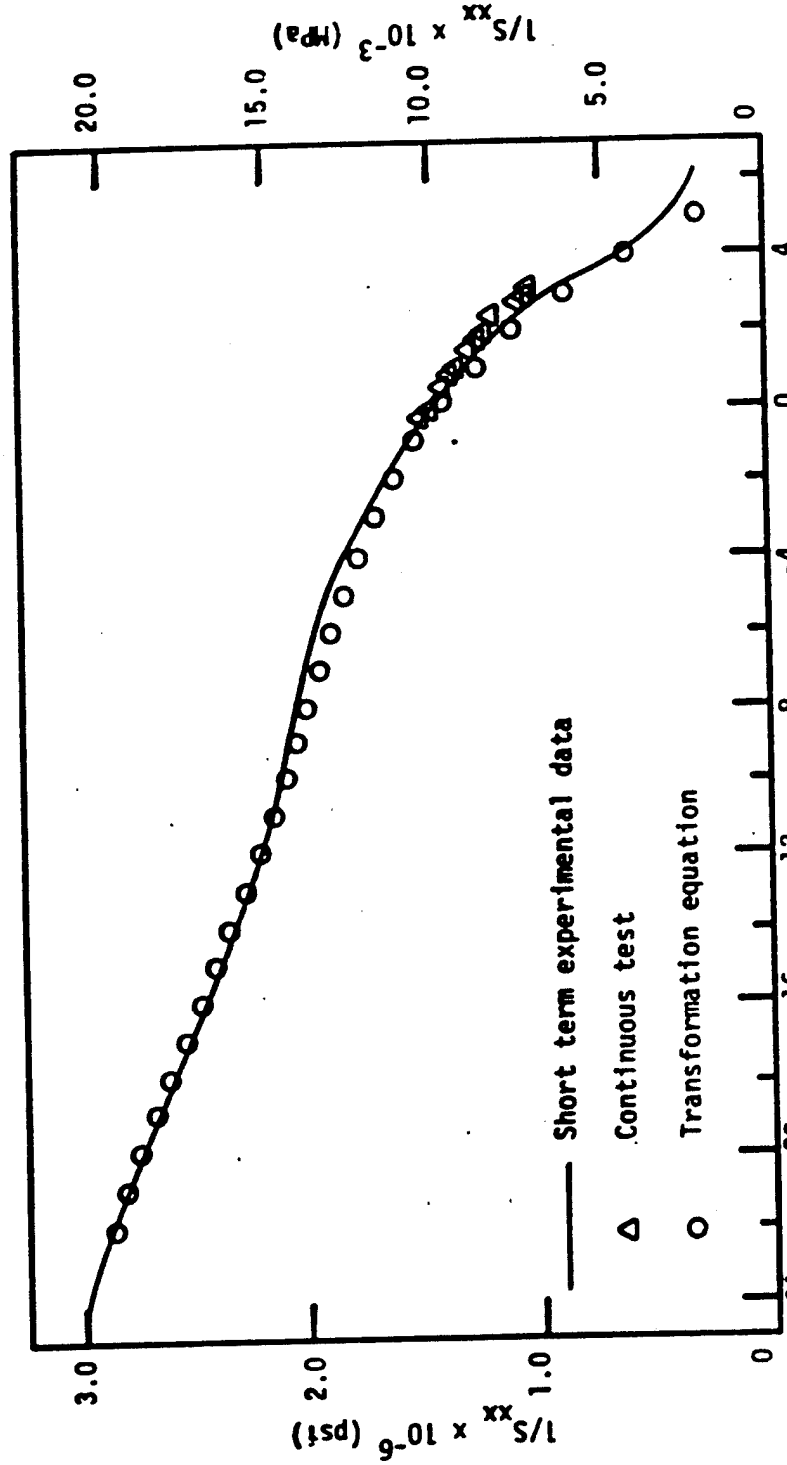

Figure 22. Master Curve of the Reciprocal of Reduced Compliance, $1/S_{xx}$, of $[60°]_{8s}$ Laminate at 180°C.

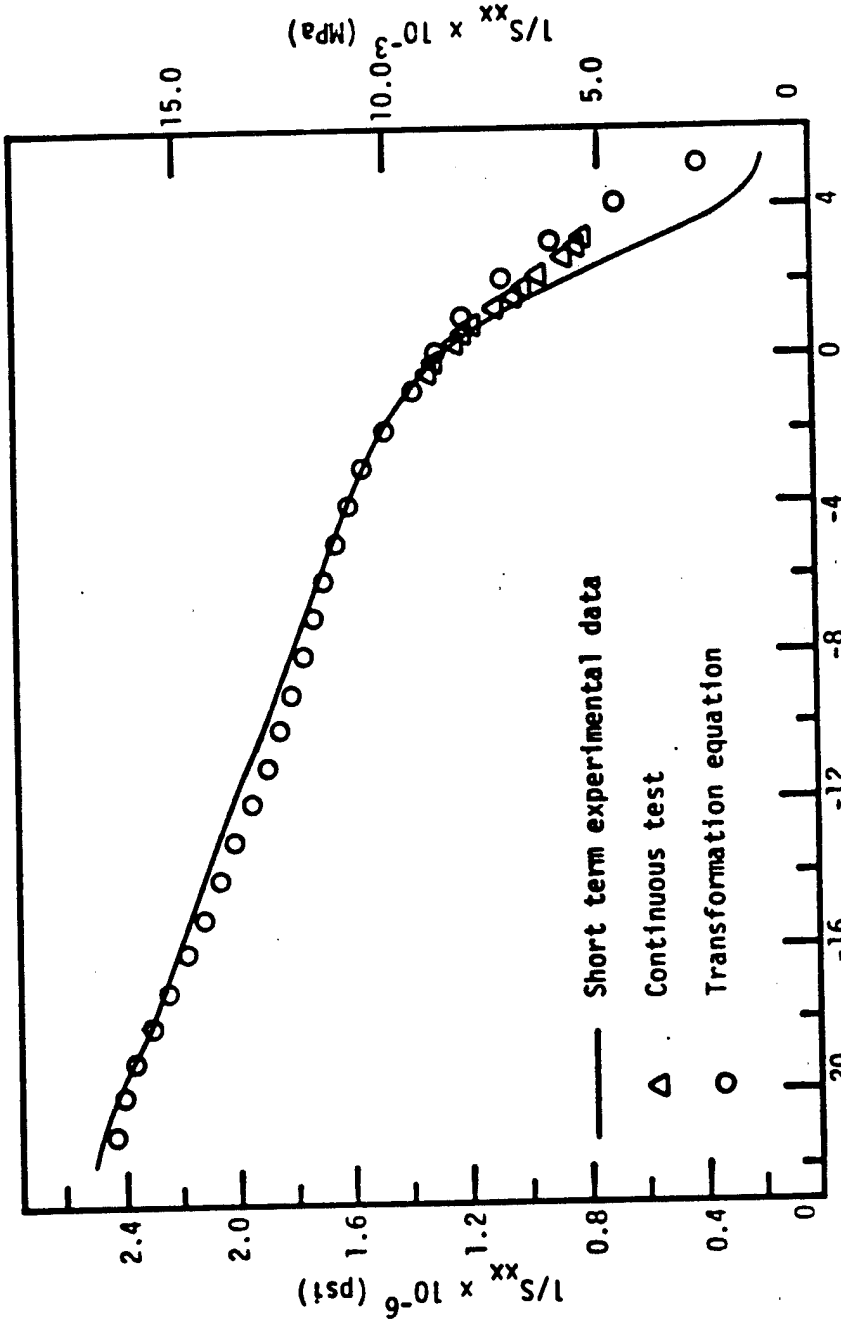

Figure 23. Master Curve of the Reciprocal of Reduced Compliance, $1/S_{xx}$, of $[75°]_{8s}$ Laminate at 180°C.

the relaxation results with the reciprocal of reduced compliance results presented here. On the other hand, if this quasi-elastic assumption is valid then its use would simplify the computation of the responses of general laminates considerably. Primarily, however, we preferred to have the vertical scale be comparable to moduli rather than compliance simply as a convenience for ourselves and for others.

As indicated earlier, the major Poisson's ratio (ν_{12}) was found to be time-independent. However, the minor Poisson's ratio (ν_{21}, obtained from the $[90°]_{8s}$ uniaxial test) was time-dependent. This difference in behavior is due to the definition of Poisson's ratio. That is, in the latter case it is defined as

$$\nu_{21} = \frac{\varepsilon_{yy}(t)}{\varepsilon_{xx}(t)}$$

The experimental results of the $[90°]_{8s}$ laminate indicated that the transverse strain, $\varepsilon_{yy}(t)$, was time-independent and the axial strain, $\varepsilon_{xx}(t)$, was time-dependent. Thus, ν_{21} was found to be a time-dependent quantity. Its master curve is shown in Figure 16. Similar results for ν_{21} of glass/epoxy laminate were reported by Beckwith [39]. However, he attributed such a result to experimental scatter. Based on the above explanation and the results here, perhaps Beckwith's conclusion was incorrect.

Except for Figure 16, the continuous 25-hour tests correlated well with the predicted master curves as shown in Figures 18 to 23. Generally, reasonable agreement was obtained for all the three results as indicated in Figures 14 to 23. The large deviations in the

short-term $[45°]_{8s}$ and $[75°]_{8s}$ results (Figures 21 and 23, respectively) may have been due to experimental and/or the graphical procedure used to construct the master curve from the short-term results. A comparison of the $1/S_{xx}$(1-minute) results obtained from the transformation equation and experiment, Figure 24, indicates that for these two particular laminates deviations occur at elevated temperatures of about 180°C and above. The large deviations of the $[45°]_{8s}$ and $[75°]_{8s}$ master curves tends to substantiate the earlier comment on the conventional procedure used in constructing master curves from short-term tests, that is, the graphical smoothing procedure may create errors. These deviations also imply that the master curve prediction computational procedure proposed here is not only less error prone but is a very cost-effective technique for the accelerated characterization of composite materials.

Another advantage of the master curve prediction procedure is that master curves of off-axis specimens reduced at any arbitrary reference temperature can be produced at a relatively small cost of less than a minute of computer time. For example, consider the master curves generated for the $[30°]_{8s}$ laminate shown in Figure 25. These master curves were generated for the three reference temperatures of 150°C, 180°C and 200°C with the aid of the shift factor versus temperature plot.

The temperature dependence of the material studied here is shown by the $Log_{10}a_T$ versus temperature plot of Figure 26. The deviations of the $\nu_{21}(t)$ results, at temperature-levels less than the T_g, from the other two principal properties results is primarily due to the

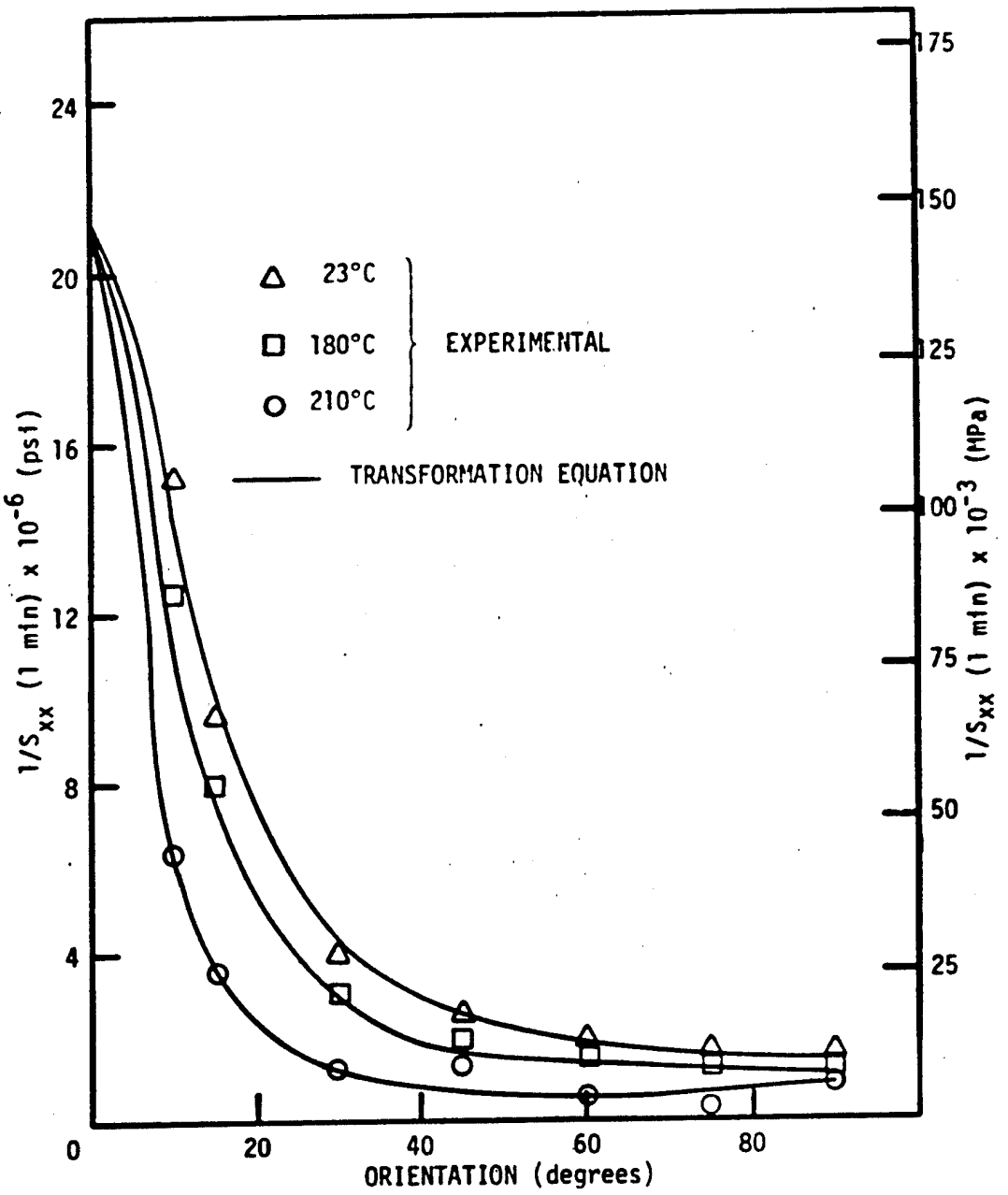

Figure 24. Comparison of Reciprocal of Compliance with Respect to Orientation and Temperature.

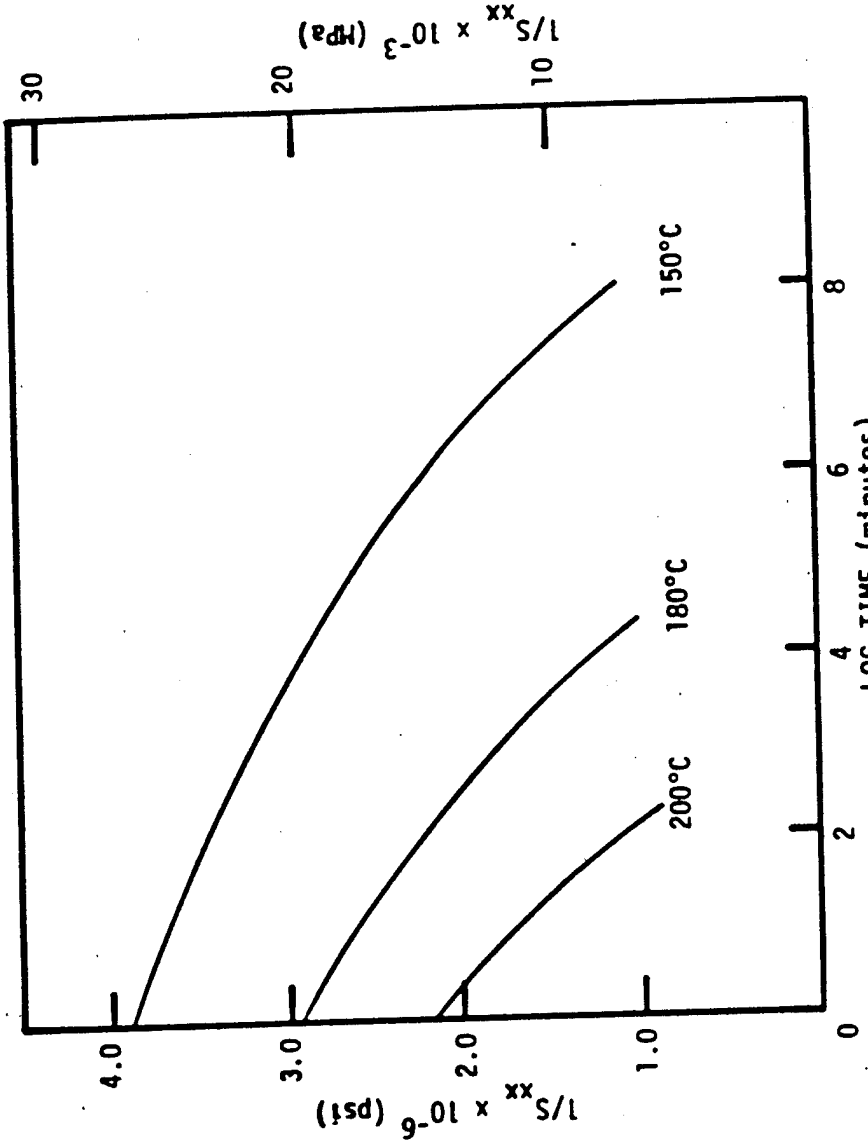

Figure 25. Predicted Master Curves of the Reciprocal of Reduced Compliance, $1/S_{xx}$, of $[30°]_{8s}$ Laminate at Different Temperatures.

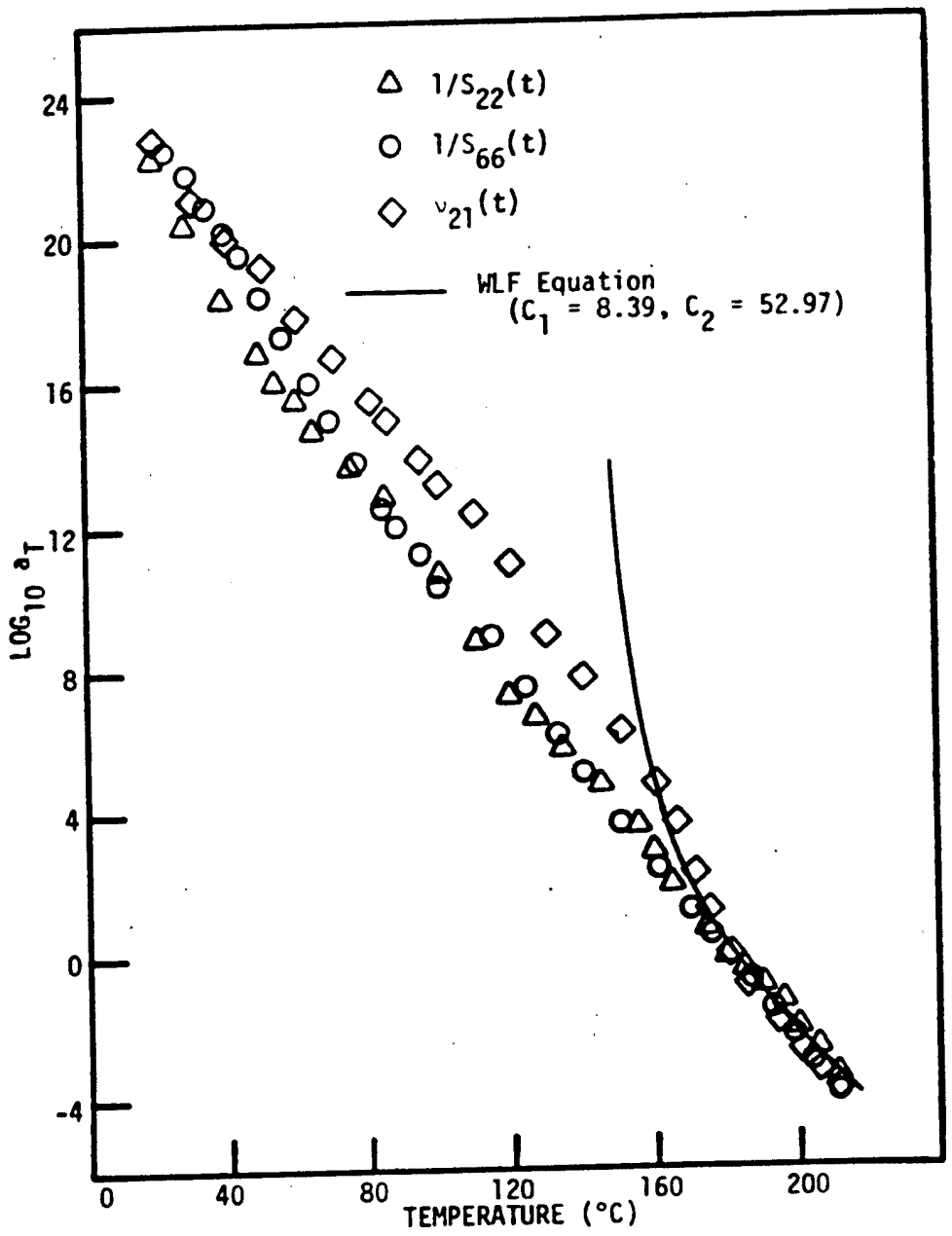

Figure 26. $Log_{10}\ a_T$ Versus Temperature.

relatively small transverse strains produced by the uniaxially stressed $[90°]_{8s}$ specimen. This behavior is always observed in these types of two-phase materials. It should be mentioned that the $\nu_{21}(t)$ results are not used in any of the predictions. The reasons for presenting results for $\nu_{21}(t)$ are mainly to validate the elastic symmetry of the material (Table 1, where $S_{12}(1 \text{ minute}) = S_{21}(1 \text{ minute})$) and for completeness sake.

Also shown in Figure 26 is the correlation between the WLF equation and the experimental results. Good correlations were obtained for temperatures ranging from slightly below the T_g to 210°C. The values of the material constants used to obtain this correlation were $C_1 = 8.39$ and $C_2 = 52.97$, as expressed in equation (25). Figure 27 indicates that $\log_{10} a_T$ as a function of 1/T is non-linear for temperatures below the T_g. This tends to invalidate equation (24) which assumes a linear function and, for this reason, equation (23) would have to be used to determine apparent activation energies.

The effect of temperature on the strength of the material investigated here is shown in Figure 28. The experimental strengths of the respective laminates were obtained by ramp loading the specimens to failure at 0.050 inch/minute (0.127 cm/minute) head-rate and at the two isothermal ambient temperatures indicated in the figure. This test is sometimes assumed to be a very short-term creep to rupture test [32]. The predictions were made using the failure theory of Puppo-Evensen which was discussed earlier. Reasonable correlations were obtained between experiments and predictions as shown. It should be

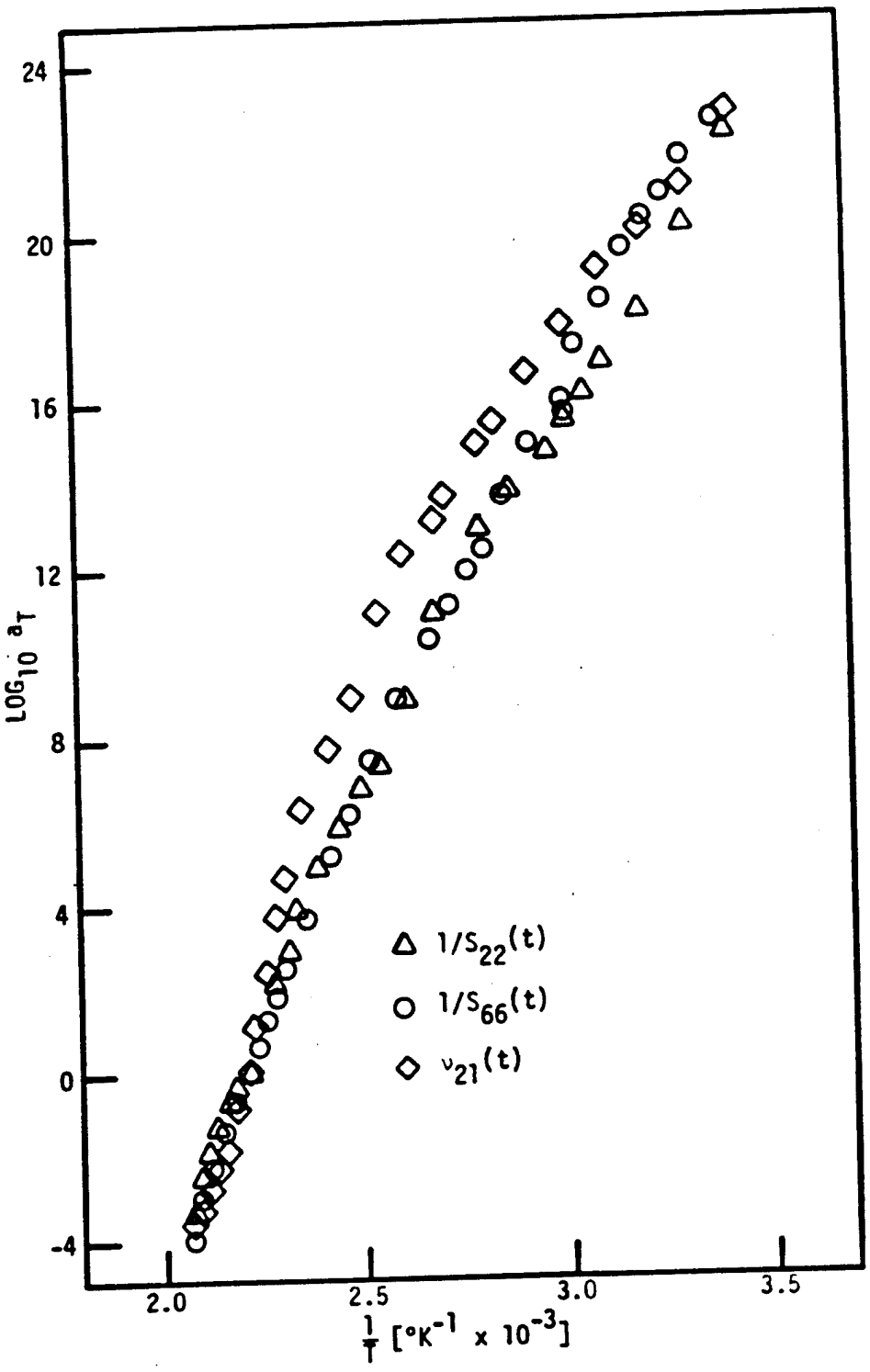

Figure 27. $Log_{10}\ a_T$ Versus Reciprocal of Absolute Temperature.

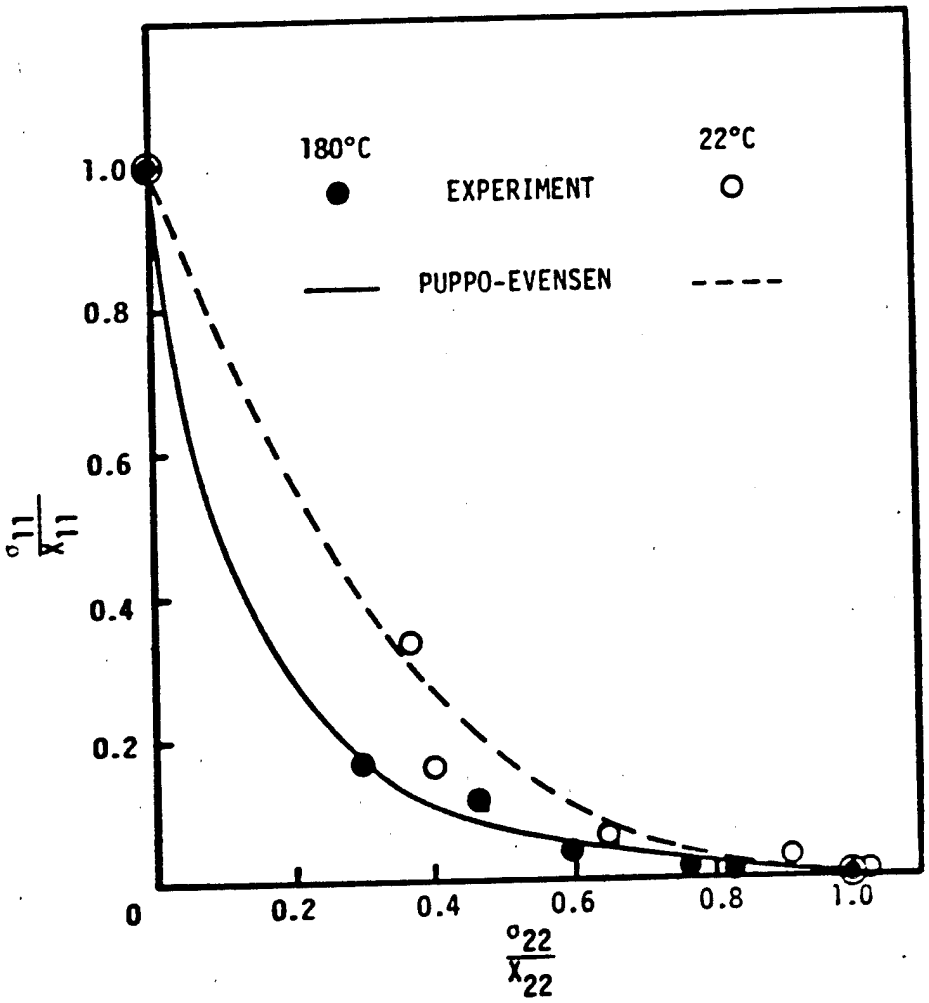

Figure 28. Comparison of Normalized Experimental and Predicted Off-Axis Strengths (Ramp Loaded Uniaxially to Failure) at Room Temperature (22°C) and Glass-Transition Temperature (180°C).

mentioned that by using the value of 0.1 for the exponent of the interaction factor of equations (27a) and (27b) in the 180°C tests, a slightly better correlation was obtained as opposed to using the value of unity. However, the value of 0.1, for the exponent of the interaction factor, gave a much better correlation with the delayed failure test results.

The third data reduction procedure for predicting delayed failures and a value of 0.1 for the exponent of the interaction factor of equation (31) were used to produce the analytical results of the respective laminates shown in Figure 29, together with experimental results. The open symbols represent the tests where delayed failures were observed and the solid symbols represent tests where the specimens did not fail. The solid lines represent the analytical results. All the specimens were subjected to uniaxial tensile load. The three orthogonal axes represent σ_{11}, σ_{22}, and time, respectively. The ramp-loaded to failure results at 180°C are represented by the σ_{11}-σ_{22} plane at 10^0 minute and are assumed to be the very short-term creep to rupture tests. All the open symbols either coincide with their respective strength master curves or are in the vicinity of it. The solid symbols are always below their respective strength master curves. In addition, the variations of the failure surface with time are compared in this figure. That is, the failure surface appears to "shrink" as the duration of the tests increases.

A better representation of the experimental and predicted delayed failure results are tabulated in Table 2. In this table, for laminate orientations equal to and less than 45°, reasonable correlations were

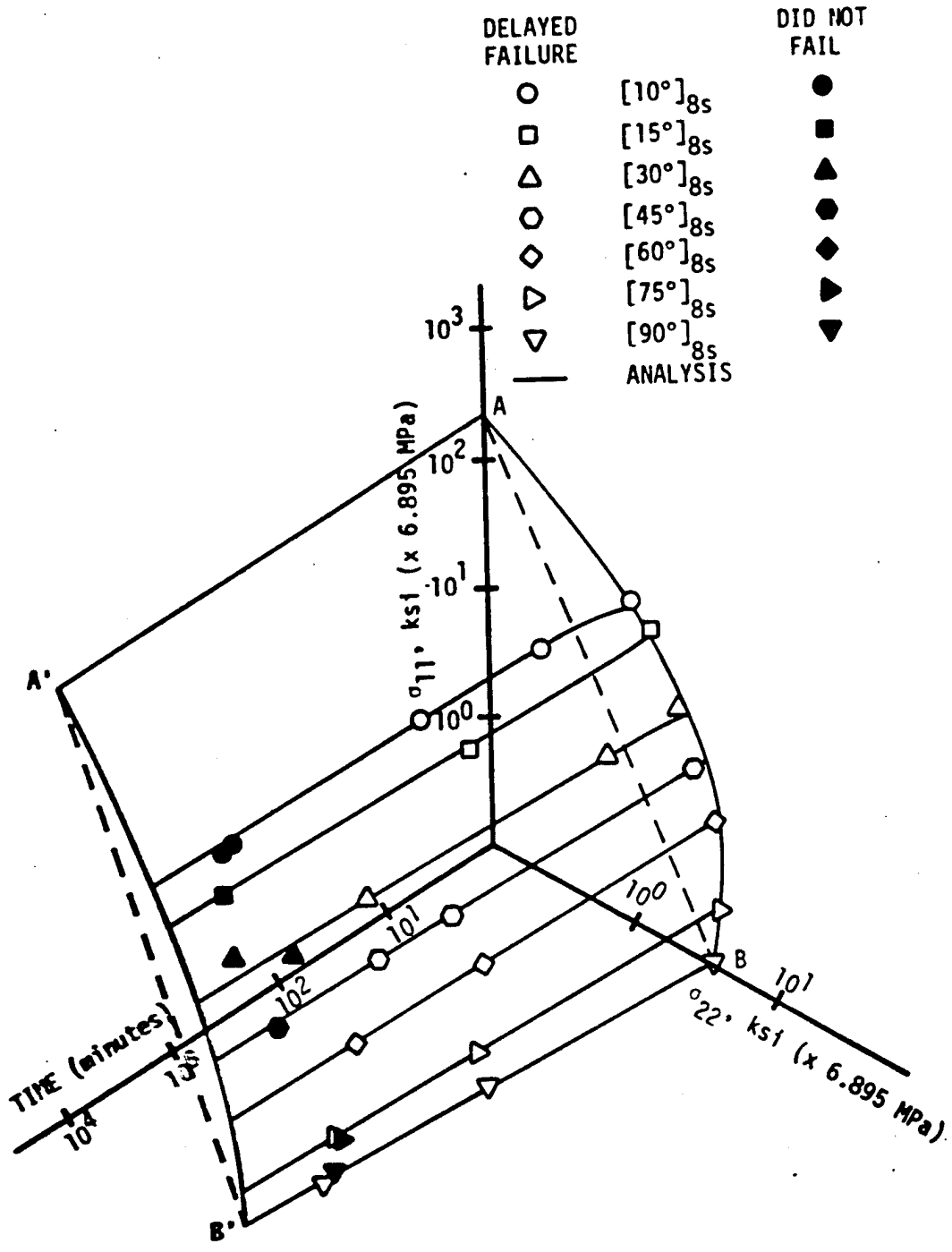

Figure 29. Time-Dependent Failure Surface of Unidirectional Graphite/Epoxy Laminates at 180°C.

TABLE 2. COMPARISON OF EXPERIMENTAL AND PREDICTED AXIAL CREEP STRENGTH AT 180°C.

Laminate Orientation	Duration of Test (minutes)	Experimental x ksi (MPa)	Predictions	
			Equation (31a) x ksi (MPa)	Equation (31b) x ksi (MPa)
$[15°]_{8s}$	29.5	14.286 (98.502)	20.072 (138.396)	14.971 (103.225)
$[30°]_{8s}$	4.8	9.146 (63.062)	18.648 (128.578)	7.811 (53.857)
$[30°]_{8s}$	586.0	7.317 (50.451)	22.664 (156.268)	5.513 (38.012)
$[45°]_{8s}$	136.0	4.699 (32.400)	7.088 (48.872)	4.058 (27.980)
$[45°]_{8s}$	613.0	4.293 (29.600)	6.000 (41.370)	3.623 (24.981)
$[60°]_{8s}$	104.0	3.976 (27.415)	4.081 (28.139)	3.114 (21.471)
$[60°]_{8s}$	1230.0	3.171 (21.864)	3.400 (23.443)	2.589 (17.851)
$[75°]_{8s}$	115.0	3.090 (21.306)	3.088 (21.292)	2.632 (18.148)
$[75°]_{8s}$	2304.0	2.584 (17.817)	2.530 (17.444)	2.108 (14.535)

obtained when the second failure criterion, equation (31b), was used. The first criterion, equation (31a), gave excellent correlations for laminate orientations greater than 45°. This would imply that for the material used here, the first criterion would be appropriate for $\theta > 45°$ and the second criterion is suitable for $45° \geq \theta \geq 0°$.

Besides the good overall correlations between the predictions and experiments on the delayed failures, Figure 29 clearly illustrates the dependence of the creep strength master curves on the state of stress. That is, for orientations between 0° and 90°, the location of the creep strength master curve on the envelope is determined by the principal stresses (the stresses along the local coordinates). These principal stresses are dependent on the laminate orientations. Consequently, one would have to produce creep strength master curves for all the required orientations either from experiments or other means. From the designer's point of view, a rational and convenient methodology should be available to predict delayed failures. Based on the results here, it is felt that the methodology proposed can be used confidently and easily to generate either creep strength master curves of any arbitrary unidirectional laminate or time-dependent failure envelopes at the required ambient temperature.

Finally, the embrittlement of the material due to the duration of the test is also clearly illustrated in Figure 29. Consider the straight dashed lines connecting points A, B and A', B' as indicated in Figure 29. For very short-term creep to rupture tests (1 minute), the material failed in a ductile manner as indicated by the degree of curvature of the surface with respect to line AB. Over a long term

(10^4 minutes), the degree of curvature of the surface with respect to line A'B' decreases. This would imply a more brittle failure at 10^4 minutes than 10^0 minute. This type behavior is similar to the ones observed for single phase material subjected to different biaxial states of stress [32]. The implication is that methodologies currently being used for unfilled polymeric materials can be extended to epoxy based composite materials.

VI. CONCLUSIONS AND FUTURE CONSIDERATIONS

The present investigation has been concerned with the time-temperature behavior of unidirectional graphite/epoxy laminates at room and elevated temperatures while general laminates have been only concerned with room temperature behavior. For elevated temperatures, the investigation can be summarized as follows:

- The expansional behavior of the material, at temperatures ranging from 22°C to 210°C, is tri-linear. Consequently, two "knees" are observed to occur at 60°C and 180°C. The first "knee" (at 60°C) is assumed to be the secondary T_g and the other "knee" (at 180°C) is assumed to be the primary T_g.
- The viscoelastic linearity check indicated the material behavior to be linear at low stress levels and non-linear at higher stress-levels. Our material was, therefore, thermo-rheologically complex but a thermorheologically simple behavior was assumed due to the low stress-levels applied.
- Thermal and mechanical conditioning of the material used here was found to be unnecessary.
- Among the four principal material properties, two (S_{11} and ν_{12}) were found to be time-independent and the others ($S_{22}(t)$ and $S_{66}(t)$) were found to be time-dependent.
- Master curves of the off-axis specimens were obtained by using the TTSP.

- Using the four principal material properties and TTSP, master curves of off-axis specimens were produced from the computational scheme proposed herein.
- The predicted master curves generally agreed better with the 25-hour continuous test than the ones obtained from the short-term tests.
- Delayed failures were observed for all the off-axis specimens.
- A computational scheme for producing master creep strength curves of any arbitrarily orientated unidirectional laminates at any reference temperature was proposed.
- Reasonable to good correlations were obtained from the experimental and predicted creep to rupture results.
- The master creep strength curves were dependent on the state of stress.
- Depending on the duration of the creep to rupture tests, the material failure mode varied from ductile (1 minute) to quasi-brittle (10^4 minutes). Both experimental and analytical results substantiated the embrittlement behavior.

Unnotched and notched quasi-elastic investigations had been reported and presented in the appendices including a summary and conclusion and will not be repeated here.

On the whole, the agreement between analyses and experiments were satisfactory. The methodology outlined here was essentially intended to be used for the accelerated characterization of epoxy based continuous and elastic fiber reinforced composite materials. This new methodology is only the preliminary portion of an investigation of a

major effort undertaken for the purpose of evaluating the possibility of forecasting the effects of the four accelerators (vibration, stress, moisture and temperature) on the time-dependent behavior of epoxy based composite materials. However, before the larger issue can be addressed, additional verifications and/or modifications on the present time-temperature methodology are required. Namely,

1) The master curves presented herein were all reduced at 180°C. Longer term continuous testing at 180°C and a few other lower isothermal ambient temperatures should be performed. The results of these additional tests will not only validate the predictions of the proposed master curve computational procedure but also the applicability of TTSP.

2) More delayed failure tests should be performed at lower ambient temperatures and for longer time periods. The results of such tests would be useful to further validate the delayed failure prediction methodology.

3) Relaxation tests should be done, in order to determine whether the quasi-elastic assumption

$$\frac{1}{E_{ij}(t)} = S_{ij}(t)$$

is valid at temperatures below the T_g. In addition, these tests can be used to determine the interrelationship between the creep compliance and relaxation moduli [42] if different than given in the above equation. Such a relationship would in turn be needed to determine the creep-relaxation behavior of cured general laminates.

4) Develop an incremental time-temperature computational method (similar to the one in Appendix A) to determine the behavior of general laminates. The methodology developed should consider creep and relaxation responses and should be verified experimentally along the lines of the first two recommendations.

5) Explore the possibilities of a more effective time-temperature failure criterion.

The above items, when completed, would subsequently lead to a stress-dependent TTSP. Before attempting to use such a joint methodology (referred to as the time-stress-temperature superposition (TSTS) [11]), the time-stress superposition principle (TSSP) should be verified. At present there are at least two approaches [8,26] on the TSSP. These approaches should be reviewed and experimentally verified to determine their feasibility. The methodology developed from this study should be incorporated into the TTSP and the resulting methodology, TSTS, should be verified experimentally using the rationale and procedure described in the manuscript. Subsequently, the constitutive equations used in the TSTS methodology can be used in the analysis of the notched behavior of composites subjected to different stress and/or temperature levels.

Finally, the confidence and experience gained from the TSTS methodology would enable one to incorporate the other two time analogies (time-vibration and time-moisture) into the multi-parametric predictions. Again, a symbiosis between analysis and experiment must exist if the resulting methodology is to be meaningful.

VII. BIBLIOGRAPHY

1. Halpin, J. C., "Introduction to Viscoelasticity", Composite Materials Workshop, Progress in Materials Science Series, Vol. 1, 1968.

2. Kovriga, V. V.; Osipova, E. S.; Faberova, I. I.; and Artanova, K. Ya., "Time-Temperature Superposition Applied to the Relaxation Properties of a Glass-Reinforced Plastic and Its Matrix", Polymer Mechanics, March-April, 1972.

3. Roy, A., and Murthy, P. N., "Viscoelastic Analysis of the Residual Stress in Glass Fiber-Reinforced Plastics", Fibre Science and Technology, Vol. 9, 1976.

4. Urzhumtsev, Yu. S., "Prediction of the Deformation and Fracture of Polymeric Materials", Polymer Mechanics, May-June, 1972.

5. Halpin, J. C., and Pagano, N. J., "Observations on Linear Anisotropic Viscoelasticity", J. of Composite Materials, Vol. 2, 1968.

6. Urzhumtsev, Yu. S., and Maksimov, R. D., "Multi-parametric Prediction of the Creep of Polymer Materials", Polymer Mechanics, May-June, 1970.

7. Turtsin'sh, R. P., Urzhumtsev, Yu. S., and Maksimov, R. D., "Static and Vibrational Creep of a Fabric-Reinforced Plastic in Shear in the Plane of Reinforcement", Polymer Mechanics, July-August, 1971.

8. Urzhumtsev, Yu. S., "Time-Temperature Superposition for Thermorheologically Complex Materials", Polymer Mechanics, March-April, 1974.

9. Sims, D. F., and Halpin, J. C., "Methods for Determining the Elastic and Viscoelastic Response of Composite Materials", Composite Materials: Testing and Design (Third Conference), ASTM STP 546, 1974.

10. Maksimov, R. D., Mochalov, V. P., and Urzhumtsev, Yu. S., "Time-Moisture Superposition", Polymer Mechanics, September-October, 1972.

11. Sandhu, R. S., "Nonlinear Behavior of Unidirectional and Angle-Ply Laminates", Journal of Aircraft, February, 1976.

12. Sendeckyj, G. P., Richardson, G. P., and Pappas, J. E., "Fracture Behavior of Thornel 300/5208 Graphite/Epoxy Laminates--Part 1: Unnotched Laminates", Composite Reliability, ASTM STP 580, 1975.

13. Petit, P. H., and Waddoups, E. M., "A Method of Predicting Non-linear Behavior of Laminated Composites", J. of Composite Materials, January, 1969.

14. Daniel, I. M., and Liber, T., "Strain Rate Effects on Mechanical Properties of Fiber Composites", IIT Research Institute, Report No. IITRI D6073-IV, June, 1976.

15. Urzhumtsev, Yu. S., and Maksimov, R. D., "Graphoanalytical Determination of Rheological Coefficients", Polymer Mechanics, July-August, 1968.

16. Morland, L. W., and Lee, E. H., "Stress Analysis for Linear Viscoelastic Materials with Temperature Variation", Trans. of Society of Rheology, 1960.

17. Schapery, R. A., "Application of Thermodynamics to Thermomechanical, Fracture and Birefringent Phenomena in Viscoelastic Media", J. Applied Physics, Vol. 35, 1964.

18. Ferry, J. D., "Viscoelastic Properties of Polymers", John Wiley & Sons, Second Edition, New York, 1970.

19. Urzhumtsev, Yu. S., "Time-Temperature Superposition Review", Polymer Mechanics, January-February, 1975.

20. Tobolsky, A. V., "Properties and Structures of Polymers", John Wiley & Sons, Inc., New York, 1960.

21. Bartenev, G. M., and Zelenev, Yu. V., Polymer Mechanics, No. 2, 1971.

22. Molotkov, A. P., Zelenev, Yu. V., and Bartenev, G. M., Polymer Mechanics, No. 6, 1971.

23. Bahadur, S., and Ludema, K. C., "Time-Temperature Superposition of Large-Strain Shear Properties of the Ethylene-Propylene Copolymer System", J. of Applied Polymer Science, Vol. 16, 1972.

24. Urzhumtsev, Yu. S., "Time-Temperature Superposition for Thermorheologically Complex Materials", Polymer Mechanics, March-June, 1974.

25. Daugste, Ch. L., "Joint Application of Time-Temperature and Time-Stress Analogies to Constructing Unified Curves", Polymer Mechanics, May-June, 1974.

26. Schapery, R. A., "On the Characterization of Nonlinear Viscoelastic Materials", Polymer Engineering and Science, July, 1969.

27. Sandhu, R. S., "A Survey of Failure Theories of Isotropic and Anisotropic Materials", Tech. Rep. AFFDL-TR-72-71, Air Force Flight Dynamics Lab., Wright-Patterson Air Force Base, Ohio.

28. Flugge, W., "Viscoelasticity", Springer-Verlag, New York, 1975.

29. Schapery, R. A., "Approximate Methods for Transform Inversion for Viscoelastic Stress Analysis", Proceedings of U.S. Congress for Applied Mechanics, ASME, 1962.

30. Williams, M. L., and Arenz, R. J., "The Engineering Analysis of Linear Photoviscoelastic Materials", Experimental Mechanics, September, 1964.

31. Wang, A. S. D., Drexel University, [Private Communication].

32. Grinman, A. M., and Gol'dman, A. Ya., "Long-Time Strength of Polyethylene in Biaxial Tension", Polymer Mechanics, May-June, 1976.

33. Landel, R. F., and Fedors, R. F., "Rupture of Unfilled Amorphous Polymers", Fracture Processes in Polymeric Solids: Phenomena and Theory, Interscience Publishers, John Wiley & Sons, Inc., 1964.

34. Puppo, A. H., and Evensen, H. A., "Strength of Anisotropic Materials under Combined Stresses", AIAA Journal, April, 1972.

35. Chamis, C. C., and Sinclair, J. H., "10-deg Off-Axis Test for Shear Properties of Fiber Composites", S.E.S.A. Spring Meeting, Dallas, Texas, May 1977.

36. Pagano, N. J., and Halpin, J. C., "Influence of End Constraints in the Testing of Anisotropic Bodies", J. of Composite Materials, January 1968.

37. Lou, Y. C., and Schapery, R. A., "Viscoelastic Characterization of a Nonlinear Fiber-Reinforced Plastic", J. of Composite Materials, April 1971.

38. Schapery, R. A., "Survey on Time-Dependent and Fracture Behavior", Composite Materials: Testing and Design, 5th Conference, New Orleans, La., March 20-22, 1978.

39. Beckwith, S. W., "Viscoelastic Characterization of a Nonlinear Glass/Epoxy Composite Using Micromechanics Theory", Annual Meeting of JANNAF, San Francisco, February 26, 1976.

40. Moehlenpah, A. E., Ishai, O., and Di Benedetto, A. T., "The Effect of Temperature on the Mechanical Behavior of Epoxy Composites", Polymer Science and Engineering, March, 1971.

41. Theocaris, P. S., "Creep and Relaxation Contraction Ratio of Linear Viscoelastic Materials", J. of Mech. Phys. Solids, Vol. 12, 1964.

42. De Runtz, J. A., Jr., and Crossman, F. W., "Time and Temperature Effects in Laminated Composites", Proceedings of Computer Simulation of Materials Application, Nuclear Materials, Vol. 20, 1976.

43. Ashton, J. E., and Whitney, J. M., "Theory of Laminated Plates", Progress Mat. Sc. Series, IV, Technomic Pub. Co., 1970.

44. Jones, R. M., "Mechanics of Composite Materials", McGraw-Hill Book Company.

45. Yeow, Y. T., and Brinson, H. F., "Stress-Strain and Failure Properties of Graphite/Epoxy Laminates", VPI-E-76-21, V.P.I. & S.U., Sept., 1976.

46. Yeow, Y. T., and Brinson, H. F., "An Investigation on the Tensile Moduli and Strengths of Graphite/Epoxy Laminates", Experimental Mechanics, Nov. 1977.

47. Yeow, Y. T., and Brinson, H. F., "A Comparison of Simple Shear Characterization Methods for Composite Laminates", Composite, Jan. 1978.

48. Rowlands, R. E., "Flow and Failure of Biaxially Loaded Composites", Inelastic Behavior of Composites, A.S.M.E., AMD-Vol 13, 1975.

49. a. Ashkenazi, E. K., "Anisotropy in the Strength Construction Material", C. M. Kirov Wood Tech. Academy, Leningrad, May 1961.

    b. Ashkenazi, E. K., "The Construction of Limiting Surfaces for Biaxial Stressed Condition of Anisotropic Materials", Zavodskaya Laboratoriyz, Leningrad Forestry Academy, Feb. 1964.

    c. Ashkenazi, E. K., "Problems of the Anistropy Strength", Polymer Mechanics, 1965.

50. Hill, R., "A Theory of the Yielding and Plastic Flow of Anisotropic Metals", Proc. Royal Society, Series A, 1948.

51. Cole, B. W., and Pipes, R. B., "Filamentary Composite Laminates Subjected to Biaxial Stress Fields", Tech. Rep., AFFDL-TR-73-115, Air Force Flight Dynamics Lab., Wright-Patterson Air Force Base, Ohio.

52. Bert, C. W., "Static Testing Techniques for Filament-Wound Composite Materials", Composites, January, 1974.

53. Daniel, I. M., and Liber, T., "Lamination Residual Stresses in Hybrid Composites", Part 1-4, NASA CR-135085, June 1976.

54. Petit, P. H., "A Simplified Method for Determining the In-plane Shear Stress-Strain Response of Unidirectional Composites", A.S.T.M. STP 460, 1969.

55. Rosen, B. W., "A Simple Procedure for Experimental Determination of the Longitudinal Shear Modulus of Unidirectional Composites", J. Composite Materials, Oct. 1972.

56. Sims, D. F., "In-plane Shear Stress-Strain Response of Unidirectional Composite Materials", J. Composite Materials, Jan. 1973.

57. Brinson, H. F., and Yeow, Y. T., "An Investigation of the Failure and Fracture Behavior of Graphite/Epoxy Laminates", V.P.I.& S.U., Report, VPI-E-75-23, September, 1975.

58. Brinson, H. F., and Yeow, Y. T., "An Experimental Study of the Fracture Behavior of Laminated Graphite/Epoxy Composites", Composite Materials: Testing and Design, ASTM STP 617, 1977.

59. Yeow, Y. T., and Brinson, H. F., "The Fracture Behavior of Graphite/Epoxy Laminates", SESA Spring Meeting, Dallas, Texas, May 15-20, 1977.

60. Yeow, Y. T., and Brinson, H. F., "A Correlative Study Between Analysis and Experiment on the Fracture Behavior of Graphite/Epoxy Laminates", V.P.I.& S.U. Report, VPI-E-77-20, August, 1977.

61. Cooper, G. A., and Kelly, A., "Tensile Properties of Fiber-Reinforced Materials: Fracture Mechanics", J. Mech. Phys. Solids, Vol. 15, 1967, pp. 279-297.

62. Kelly, A., "Interface Effects and the Work of Fracture of a Fibrous Composite", Proc. Roy. Soc., A 319, 1970, pp. 95-116.

63. Piggott, M. R., "Theoretical Estimation of Fracture Toughness of Fibrous Composites", J. Mat. Sci., Vol. 5, 1970, pp. 669-675.

64. Harrison, N. L., "The Toughness of a Glass Fibre/Epoxy Resin Composite", Fibre Sci. and Tech., Vol. 4, 1971, pp. 101-114.

65. Waddoups, M. E., Eisenmann, J. R., and Kaminski, B. E., "Macroscopic Fracture Mechanics of Advanced Composite Materials", J. Comp. Mat., Vol. 5, 1971, pp. 446-454.

66. Sih, G. C., and Liebowitz, H., "Mathematical Theories of Brittle Fracture", Fracture, Vol. II, Academic Press, New York, 1968, p. 67.

67. Sih, G. C., and Chen, E. P., "Fracture Analysis of Unidirectional Composites", J. Comp. Mat., Vol. 7, 1973, pp. 230-244.

68. Sih, G. C., Chen, E. P., and Huang, S. L., "Fracture Mechanics of Plastic-Fiber Composites", Eng. Fracture Mech., Vol. 6, 1974, pp. 343-359.

69. Sih, G. C.; Chen, E. P.; Huang, S. L.; and McQuillen, E. N., "Material Chracterization on the Fracture of Filament-Reinforced Composites", J. Comp. Mat., Vol. 9, 1973, pp. 167-186.

70. Whitney, J. M., and Nuismer, R. J., "Stress Fracture Criteria for Laminated Composites Containing Stress Concentrations", J. Comp. Mat., Vol. 8, 1974, pp. 253-265.

71. Nuismer, R. J., and Whitney, J. M., "Uniaxial Failure of Composite Laminates Containing Stress Concentrations", ASTM-STP 593, American Society for Testing and Materials, 1975, pp. 117-142.

72. Cruse, T. A., "Tensile Strength of Notched Composites", J. Comp. Mat., Vol. 7, 1973, pp. 218-229.

73. Konish, H. J., Jr., and Cruse, T. A., "Determination of Fracture Strength in Orthotropic Graphite-Epoxy Laminates", ASTM-STP 580, American Society for Testing and Materials, 1975, pp. 490-503.

74. Snyder, M. D., and Cruse, T. A., "Boundary-Integral Equation Analysis of Cracked Anisotropic Plates", Int. J. Fracture, Vol. 11, 1975, pp. 315-328.

75. Zweben, C., "Fracture Mechanics and Composite Materials: A Critical Analysis", ASTM-STP 521, American Society for Testing and Materials, 1973, pp. 65-97.

76. Rosen, B. W., Kulkarni, S. V., and McLaughlin, P. V., Jr., "Failure and Fatigue Mechanisms in Composite Materials", in Inelastic Behavior of Composite Materials, AMD - Vol. 13, ASME, 1975.

77. Kanninen, M. F., Rybicki, and Griffith, W. I., "Preliminary Development of a Fundamental Analysis Model for Crack Growth in a Fiber Reinforced Composite Material", ASTM-STP 617, American Society for Testing and Materials, 1977, pp. 53-69.

78. Lekhnitskii, S. G., Anisotropic Plates, Translated from the Second Russian Edition by S. W. Tsai and T. Cheron, Gordon and Breach, Science Publishers, Inc., New York, 1968, p. 157.

79. Tsai, S. W., and Hahn, H. T., "Failure Analysis of Composite Materials", in Inelastic Behavior of Composite Materials, AMD - Vol. 13, ASME, 1975, pp. 73-96.

80. Brown, W. F., and Srawley, J. E., Plane Strain Crack Toughness Testing of High Strength Metallic Materials, ASTM-STP 410, American Society for Testing and Materials, 1966.

81. Cruse, T. A., and Osias, J. R., "Exploratory Development on Fracture Mechanics of Composite Materials", AFML-TR-74-111, Air Force Materials Laboratory, 1974.

82. Konish, H. J., Jr., "Mode I Stress Intensity Factors for Symmetrically-Cracked Orthotropic Strips", ASTM-STP 593, American Society for Testing and Materials, 1974, pp. 99-116.

83. Snyder, M. A., and Cruse, T. A., "Crack Tip Stress Intensity Factors in Finite Anisotropic Plates", AFML-TR-73-209, Air Force Materials Laboratory, 1973.

84. Cruse, T. A., "User's Manual for T4O4CRX: A 2-D Fracture Mechanics Deck", Pratt and Whitney Aircraft, 1975.

85. Gaggar, S., and Broutman, L. J., "Crack Growth Resistance of Random Fiber Composites", Journal of Composites, Vol. 9, July 1975.

86. Dally, J. W., and Alfirevich, I., "Application of Birefringent Coatings to Glass-Fiber Reinforced Plastics", Experimental Mechanics, March 1969.

APPENDIX A

STRESS-STRAIN BEHAVIOR AT ROOM TEMPERATURE

The purpose of this section is to present an analytical technique for determining the non-linear stress-strain response to failure of symmetric general laminates subjected to in-plane loads using the lamina non-linear stress-strain response to failure properties. In this technique, the constitutive relations and concepts of laminated plate theory [43,44] are employed in an incremental manner to predict the behavior of general laminates under monotonic loading. As such, lamina-wise stress calculations can be performed and sub-critical failures can be predicted. For the sake of brevity, only pertinent discussion and results will be presented here as more extensive documentation can be obtained in references 45 to 47. In addition, an excellent survey and discussion on the types of analytical techniques proposed to date has been given by Rowlands [48].

Method of Analysis

A non-linear stress-strain curve can be approximated quite well by a series of linear increments provided that sufficiently small increments are taken. Assuming that an increment of stress is proportional to an increment of strain, the constitutive relations for a lamina under generalized plane stress for a given increment can be expressed as,

$$d\sigma_i = C_{ij}(\sigma_i)\, d\epsilon_j \qquad (i,j = 1,2,6)$$

that is,

$$\begin{Bmatrix} d\sigma_1 \\ d\sigma_2 \\ d\sigma_6 \end{Bmatrix} = \begin{bmatrix} C_{11} & C_{12} & C_{16} \\ C_{21} & C_{22} & C_{26} \\ C_{61} & C_{62} & C_{66} \end{bmatrix} \begin{Bmatrix} d\varepsilon_1 \\ d\varepsilon_2 \\ d\sigma_6 \end{Bmatrix}$$

or simply,

$$\{d\sigma\} = [C]\ \{d\varepsilon\} \qquad \text{(A-1)}$$

where $d\sigma_i$, $d\varepsilon_j$ are the stress and strain increments respectively, and the stiffness, C_{ij}, is a function of σ_i. In the case of a general laminate, the incremental constitutive relations for the k^{th} lamina are written as

$$\{d\sigma^k\} = [C^k]\ \{d\varepsilon^k\} \qquad \text{(A-2)}$$

The implication of equation (A-2) is that the applied stress and material axes coincide. Generally, this is not the case. However, the two coordinate systems can be related by a transformation matrix [1,2], $[T^k]$, that is,

$$\{d\sigma^k\} = [T^k]\ \{d\bar{\sigma}^k\} \qquad \text{(A-3)}$$

and,

$$\{d\varepsilon^k\} = [T^k]\ \{d\bar{\varepsilon}^k\} \qquad \text{(A-4)}$$

where $d\bar{\sigma}^k$ and $d\bar{\varepsilon}^k$ are the stress and strain increments in the k^{th} lamina with respect to the load or global axes. Substituting equations (A-3) and (A-4) into (A-2) yields,

$$\{d\bar{\sigma}^k\} = [\bar{C}^k]\ \{d\bar{\varepsilon}^k\} \qquad \text{(A-5)}$$

where,

$$[\bar{C}^k] = [T^k]^{-1} [C^k] [T^k]$$

Assuming that the stresses are uniform through the thickness of the lamina, the resultant force increment, {dN}, with respect to the global coordinates is given by,

$$\{dN\} = \sum_{k=1}^{k=L} t_k \{d\bar{\sigma}^k\} \qquad \text{(A-6)}$$

where t_k is the thickness of the k^{th} lamina and L is the total number of laminae in the laminate. Combining equations (A-5) and (A-6), the resultant force increment becomes

$$\{dN\} = \sum_{k=1}^{k=L} t_k [\bar{C}^k] \{d\bar{\varepsilon}^k\} \qquad \text{(A-7)}$$

By further assuming that the incremental strains are the same in all laminae, that is,

$$\{d\bar{\varepsilon}^k\} = \{d\varepsilon^\circ\} \qquad \text{(A-8)}$$

and equation (A-7) reduces to,

$$\{dN\} = [A]\{d\varepsilon^\circ\} \qquad \text{(A-9)}$$

where

$$[A] = \sum_{k=1}^{k=L} t_k [\bar{C}^k]$$

Equation (A-9) can also be expressed as,

$$\{d\varepsilon^\circ\} = [A]^{-1}\{dN\} \qquad \text{(A-10)}$$

In equation (A-10), $[A]^{-1}$ represents the average laminate compliance during the $(n+1)^{th}$ load increment. However, these properties are not

known when the $(n+1)^{th}$ load increment is applied. Consequently, the principal elastic properties at the end of the n^{th} load increment are used to compute the laminate compliance for the $(n+1)^{th}$ load increment. Sequentially, knowing the $(n+1)^{th}$ load increment and the laminate compliance at the end of the n^{th} load increment, the laminate strain increment $\{d\varepsilon^{\circ}\}$ and each lamina strain increment $\{d\varepsilon^{k}\}$ and stress increment $\{d\bar{\sigma}^{k}\}$ can be calculated by using equations (A-10), (A-4) and (A-2), respectively. These laminae stress and strain increments are added to the stresses and strains at the end of the n^{th} load increment to obtain the current stresses and strains in each of the laminae.

The incremental loading procedure described above is continued until a lamina reaches a state of stress when it can no longer sustain additional load. Analytically, this state of stress is determined by a failure criterion. Numerous failure criterion are available [27] for predicting the strength of composite materials and these criteria can be classified as either having independent or dependent failure modes. The maximum stress or strain criteria are the ones with independent failure modes. The criteria proposed by Ashkenazi [49], Hill [50] and Puppo and Evensen [34] are examples of failure criteria with dependent failure modes. Between the two classes, experimental results [51] tend to confirm that the criteria with dependent failure modes are more appropriate for composite materials.

The assumptions made in Ashkenazi's criterion are that the material is a macroscopic continuum, the strength properties are fourth order tensors and environmental effects are neglected. His

criterion for a plane orthotropic material under uniaxial load is,

$$\frac{1}{\sigma_x} = \frac{\cos^4\theta}{X} + \left(\frac{4}{X_{45}} - \frac{1}{X} - \frac{1}{Y}\right)\cos^2\theta \sin^2\theta + \frac{\sin^4\theta}{Y} \qquad \text{(A-11)}$$

where σ_x is the applied axial stress, θ is the angle between σ_x and the direction of the applied load and X, Y and X_{45} are the tensile strengths along, transverse and at 45° to the fibers, respectively. While equation (A-11) is written for uniaxial loading only, other states or stress were considered by Ashkenazi.

Using assumptions similar to Ashkenazi, Hill developed an anisotropic yield criterion which can be modified into a failure criterion for an orthotropic material under a generalized state of plane stress. It can be expressed as,

$$\left(\frac{\sigma_1}{X}\right)^2 + \left(\frac{\sigma_2}{Y}\right)^2 - \frac{\sigma_1\sigma_2}{XY} + \left(\frac{\tau_{12}}{S}\right)^2 = 1 \qquad \text{(A-12)}$$

where the stresses σ_1, σ_2 and τ_{12} are along the material axes, S is the intralamina shear strength and X and Y are as defined for equation (A-11).

Finally, a more general failure criterion proposed by Puppo and Evensen can be expressed as

$$\left.\begin{aligned} \left(\frac{\sigma_1}{X}\right)^2 - \gamma\left(\frac{X}{Y}\right)\left(\frac{\sigma_1}{X}\right)\left(\frac{\sigma_2}{Y}\right) + \gamma\left(\frac{\sigma_2}{Y}\right)^2 + \left(\frac{\tau_{12}}{S}\right)^2 = 1 \\ \gamma\left(\frac{\sigma_1}{X}\right)^2 - \gamma\left(\frac{X}{Y}\right)\left(\frac{\sigma_1}{X}\right)\left(\frac{\sigma_2}{Y}\right) + \left(\frac{\sigma_2}{Y}\right)^2 + \left(\frac{\tau_{12}}{S}\right)^2 = 1 \end{aligned}\right\} \qquad \text{(A-13)}$$

where $\gamma = \frac{3S^2}{XY}$ is an interaction factor and the other quantities are as previously defined. Further, the authors indicated that their theory could be adapted to a wide range of materials by writing the interaction factor as $\gamma = \left(\frac{3S^2}{XY}\right)^n$ where the exponent, n, is a material parameter.

So far, the discussion has been related to the determination of the states of stress in a lamina and the subsequent failure resulting therefrom. The most difficult and fundamental question to answer in such investigations is how to represent failed laminae mathematically when some laminae in the laminate are still intact or have not reached their critical stress state. An easy analytical technique is to mathematically remove failed laminae from the laminate by zeroing the thicknesses and stiffnesses of the failed laminae. However, this procedure leads to conservative or ultra-conservative strength predictions depending on the laminate lay-up. An alternative is to uncouple the constitutive equation of the failed laminae from the laminate stiffness or compliance calculations. This can be done by assigning zero stiffnesses to the three off-diagonal terms of the $[\overline{C}^k]$ matrix in equation (A-5) and the appropriate diagonal term when its ultimate strain is reached or exceeded.

Results and Discussion

Using the incremental procedure previously explained, the total stress-strain response of general laminates subjected to uniaxial loading are generated. The results obtained are shown in Figures A-1 to A-3. Figure A-1 shows the analytical and experimental results for the

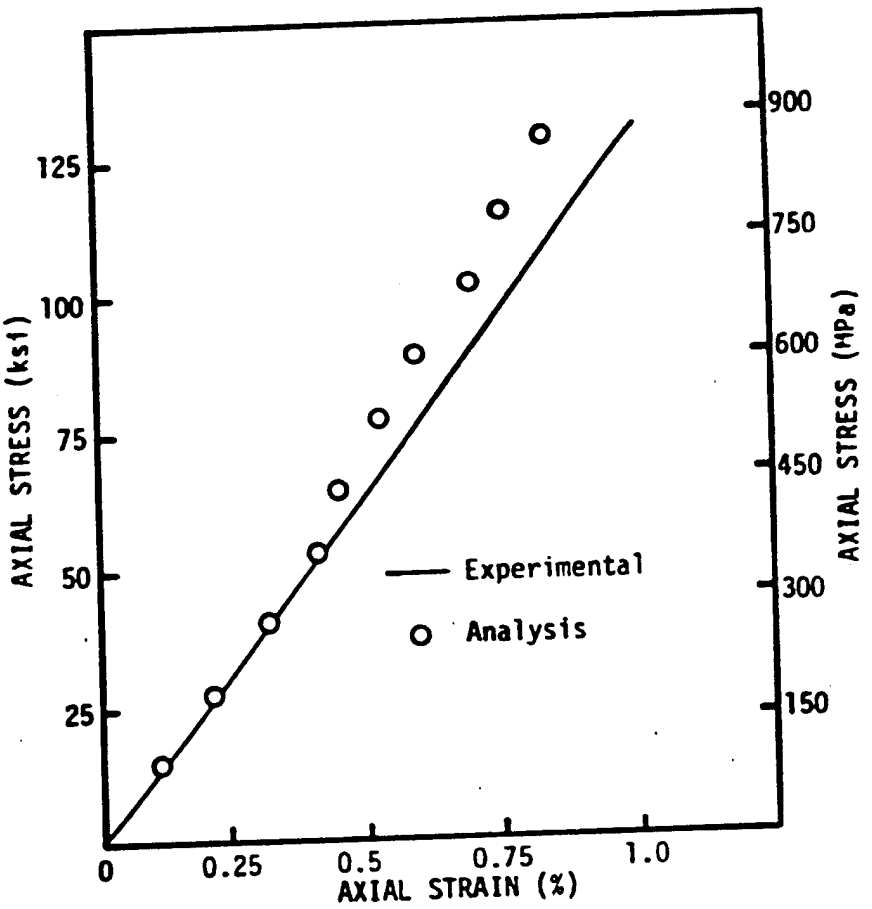

Figure A-1. Comparison of Experimental Results with Analytical Predictions of AS-3501 $[0°/\pm30°/0°]_{2s}$ Graphite/Epoxy Laminate.

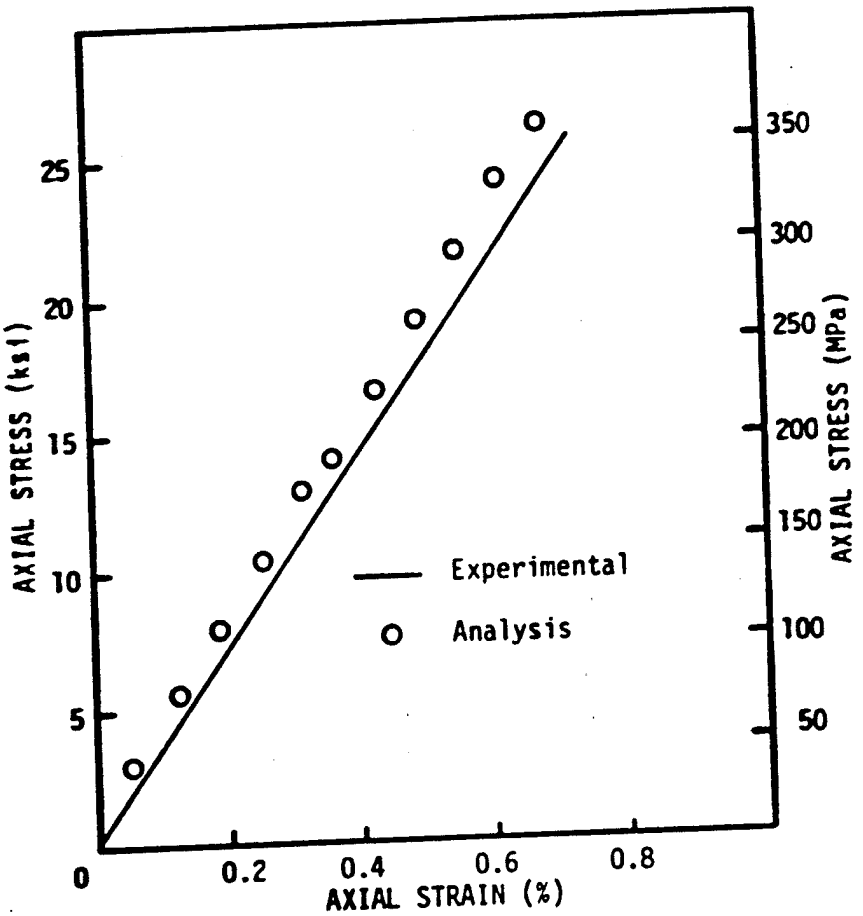

Figure A-2. Comparison of Experimental Results with Analytical Predictions of AS-3501 $[45°/15°/75°/45°]_{2s}$ Graphite/Epoxy Laminate.

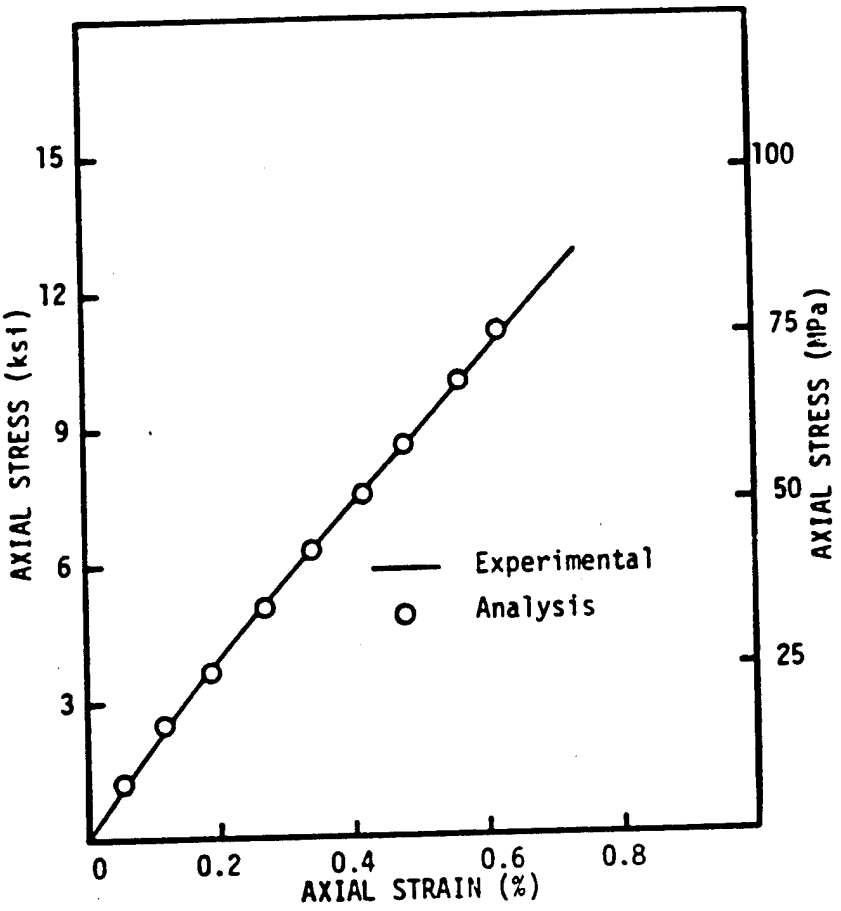

Figure A-3. Comparison of Experimental Results with Analytical Predictions of AS-3501 $[90°/\pm60°/90°]_{2s}$ Graphite/ Epoxy Laminate.

$[0°/\pm30°/0°]_{2s}$ laminate. Excellent correlation is seen up to about 50 ksi (344.8 MPa). At this stress level, failure of the ±30° laminae is predicted and is indicated by the steeper slope of the experimental stress-strain curve. After this sub-critical failure stress level, the analysis predicted higher stresses than experiment. This is probably due to the omission of interlamina stresses. Reasonable correlation between analysis and experiment is observed in the case of the $[45°/15°/75°/45°]_{2s}$ laminate, Figure A-2. Excellent correlation is seen in the case of the $[90°/\pm60°/90°]_{2s}$ laminate, Figure A-3.

A comparison of the normalized laminate failure strengths, as predicted by the three failure criteria used in the analysis, are as shown in Table A-1. Among the three failure criteria used, Ashkenazi's appears to be the best. It should be noted that the exponent of the

Table A-1. Predicted Failure Strength, Normalized with Respect to the Experimental Strength.

Laminate Orientation	Ashkenazi	Hill	Puppo-Evensen
$[0°/\pm30°/0°]_{2s}$	0.971	0.965	0.968
$[45°/15°/75°/45°]_{2s}$	1.002	1.168	1.054
$[90°/\pm60°/90°]_{2s}$	0.827	0.786	0.864

interaction factor in equation (A-13) was taken as unity. By adjusting this exponent, for the laminates investigated, identical analytical and experimental strengths can be obtained. Unfortunately, the exponent was not constant even though the specimens were obtained from a single

large panel. Nevertheless, the Puppo-Evensen criteria appear to be the most promising as it can be used for multi-axial loading, allows for material variations through the interaction factor and can be used without a lamina-wise analysis as shown here.

On the whole, good stress-strain response was obtained from the non-linear incremental analysis proposed here.

Application of Analysis

Besides the total stress-strain prediction capability, the incremental procedure described here can be used to validate test methods such as intralamina shear response determination. Presently, a variety of test methods has been proposed [52] to obtain this in-plane shear stress-strain response. Because among the four principal material properties required in the two-dimensional analysis, the most difficult experimental quantity to obtain is the intralamina shear stress-strain response. This difficulty is best clarified by Figure A-4, where variations in the response of five different test methods are observed. In this figure, the 10-deg off-axis test method of Daniel [53] and Chamis et al [35] and the calculated $[15]_{8s}$ results appear to correlate. In the case of the $[\pm 45°]_{4s}$ tensile test, the methods of Petit [54] and Rosen [55] tend to agree. The results obtained from the $[0°/90°]_{4s}$ symmetric rail-shear method of Sims [51] indicates the most ductility. Thus, depending on the test method used, the intralamina shear stress-strain response may vary from a brittle to ductile nature.

To validate the various test methods, an easy method is to compare the actual initial axial modulus of the off-axis tensile tests

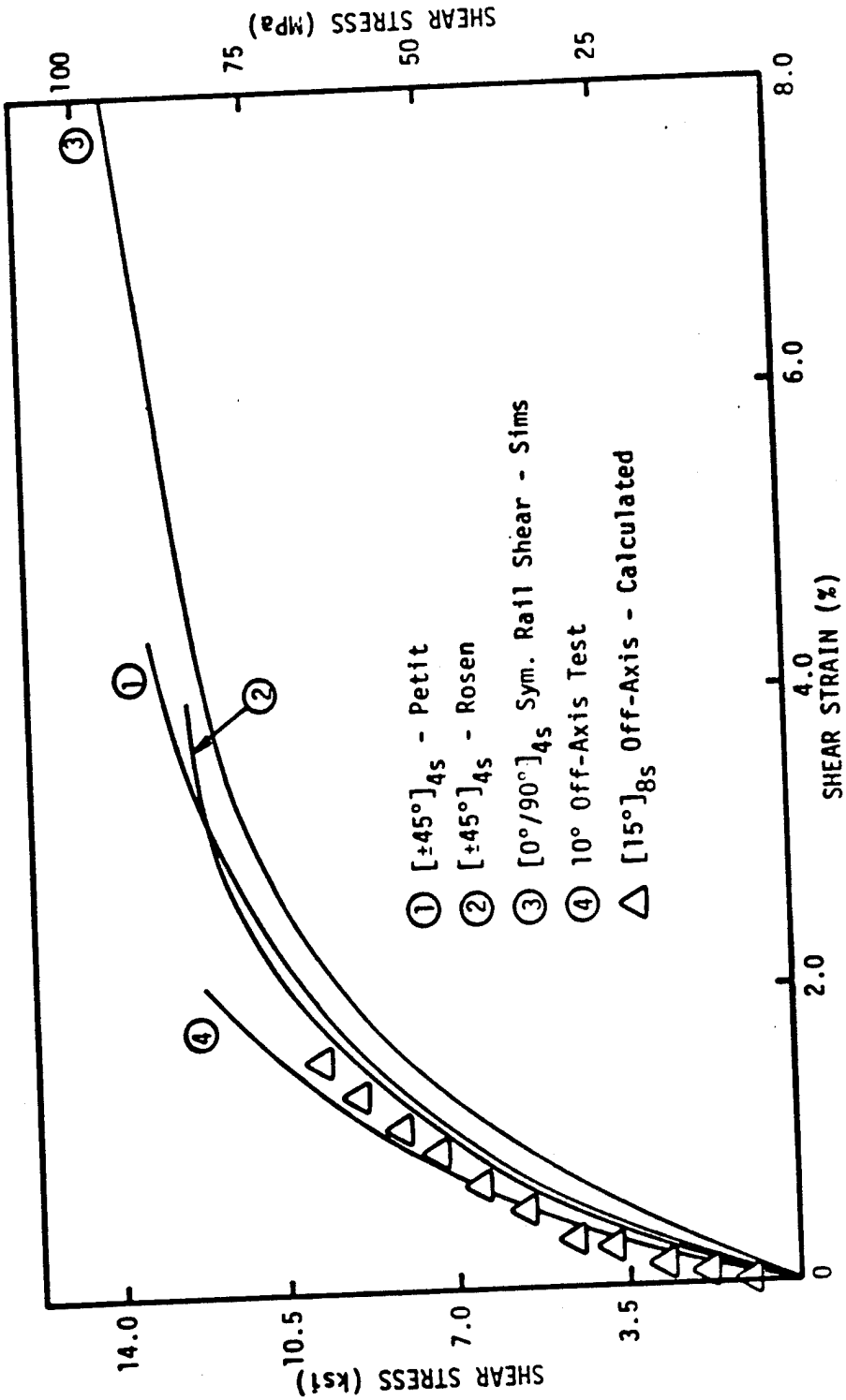

Figure A-4. Lamina Shear Stress-Strain Response of T300/934 Graphite/Epoxy Material as Determined by Different Methods.

with the orthotropic transformation equation which can be expressed as,

$$\frac{1}{E_x} = \frac{\cos^4\theta}{E_{11}} + \left(\frac{1}{G_{12}} - \frac{2\nu_{12}}{E_{11}}\right) \cos^2\theta \sin^2\theta + \frac{\sin^4\theta}{E_{22}} \qquad \text{(A-14)}$$

The quantities used in equation (A-14) are as previously defined. By substituting the initial G_{12} value from the $[15°]_{8s}$ off-axis calculated results and the initial G_{12} value by Rosen's $[\pm 45°]_s$ method into equation (A-14), an analytical and experimental comparison can be made as shown in Figure A-5. In this figure, excellent correlation is seen between experiment and analysis when the $[15°]_{8s}$ results are used. It must be noted that the reason for the choice of these two methods among the five methods is that the responses of the two chosen methods appear to be the average upper and lower bounds.

To further validate the effect of the two lamina shear responses on laminate behavior, the total response curves obtained from the two methods ($[15°]_{8s}$ calculated and Rosen's $[\pm 45°]_s$ method) are used in the incremental analysis, previously described, with the other three parameters (E_{11}, E_{22} and ν_{12}) kept constant to predict the tensile behavior of general laminates. The analytical results obtained from the two shear results are compared to the experimental tensile test results as shown in Figures A-6 to A-8. In the case of the $[0°/90°]_{4s}$, $[0°/\pm 45°/0°]_{2s}$, and $[90°/\pm 60°/90°]_{2s}$ laminates, Figures A-6 to A-7, little difference between the analytical results were observed. Apparently in these cases, intralaminar shear response does not play an important role as in the case of the $[45°/0°/90°/-45°]_{2s}$, $[30°]_{8s}$

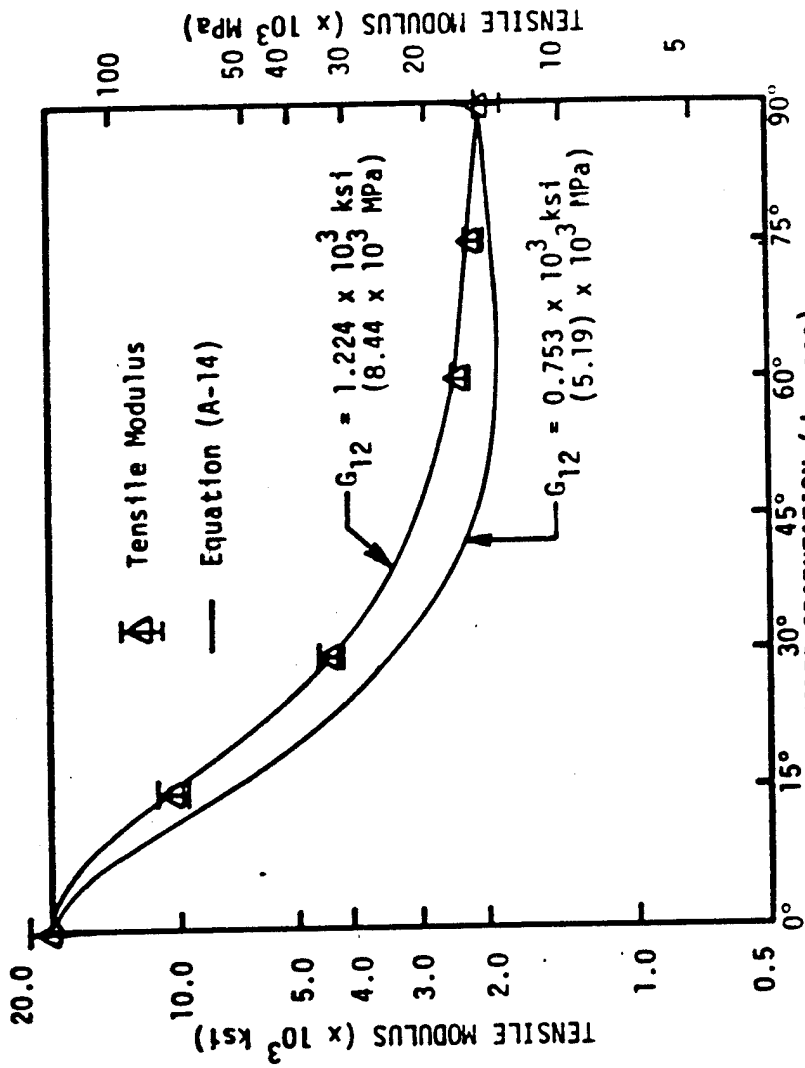

Figure A-5. Variation of the Tensile Moduli with Fiber Orientation for Unidirectional T300/934 Graphite/Epoxy Laminates.

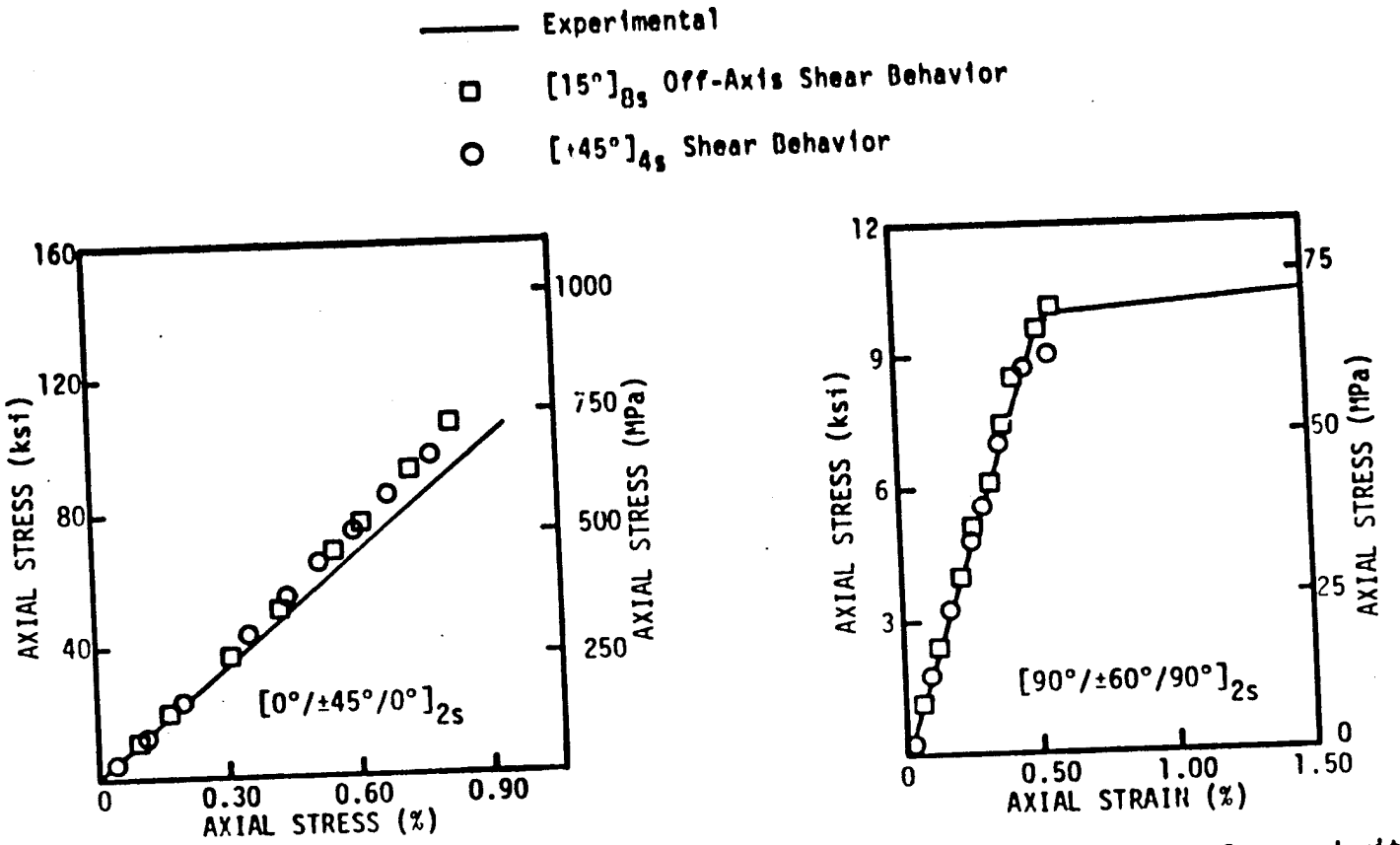

Figure A-6. Predicted Laminate Tensile Response Using Indicated Shear Behavior Compared with Experimental Results.

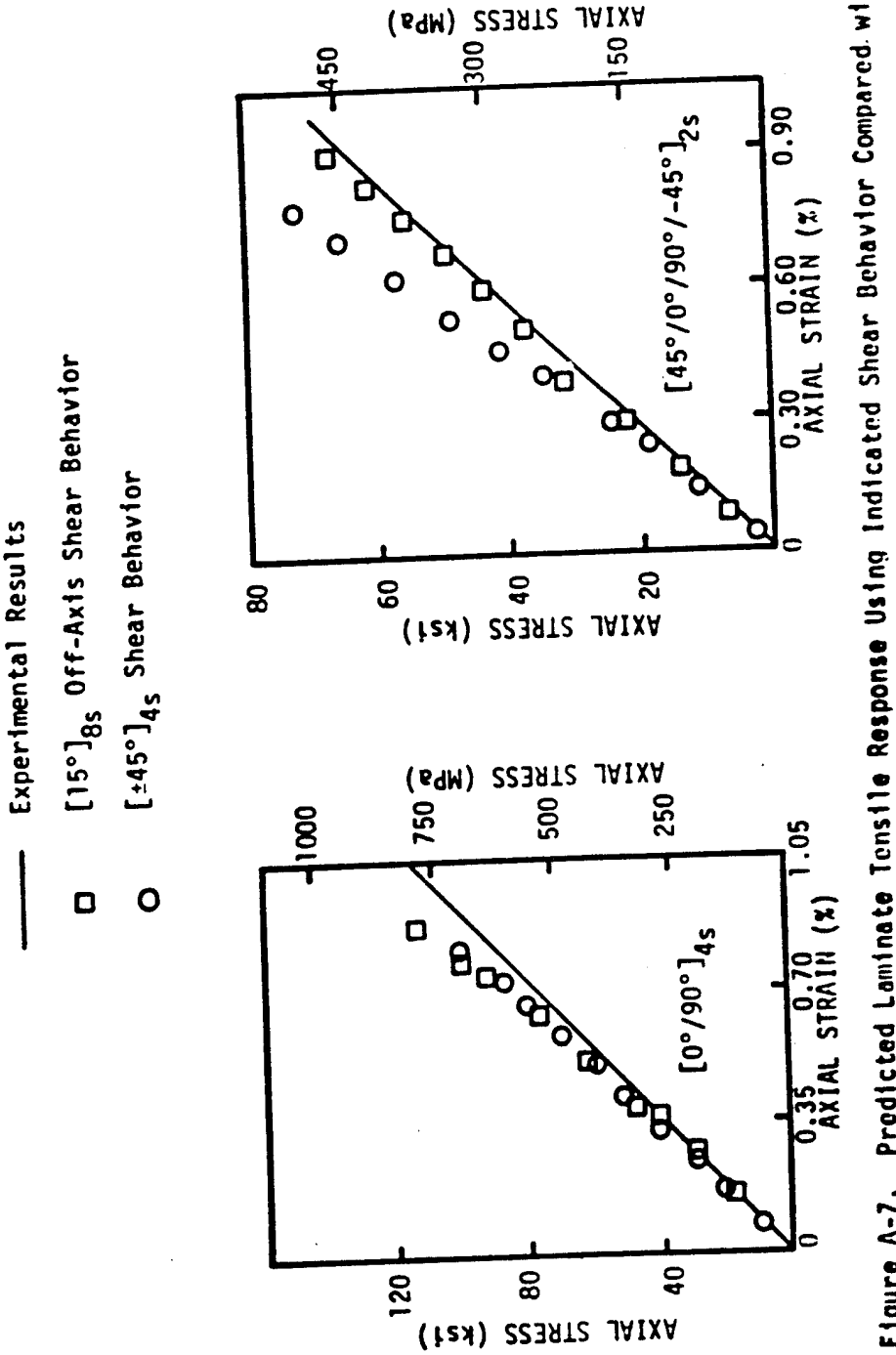

Figure A-7. Predicted Laminate Tensile Response Using Indicated Shear Behavior Compared with Experimental Results.

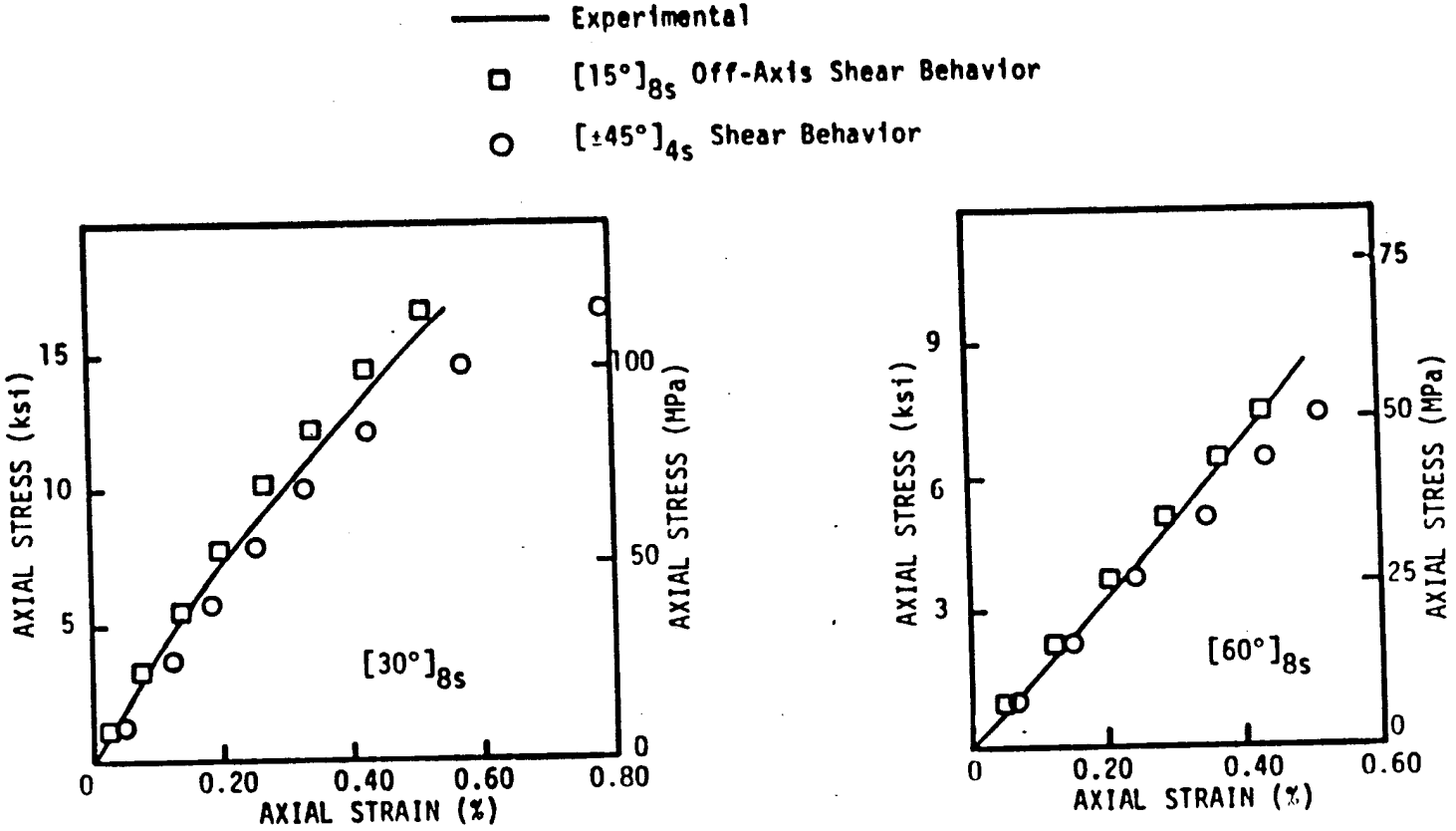

Figure A-8. Predicted Laminate Tensile Response Using Indicated Shear Behavior Compared with Experimental Results.

and $[60°]_{8s}$ laminates shown in Figures A-7 to A-8, where good correlations are obtained from the $[15°]_{8s}$ calculated results.

The main conclusion drawn from these results is that the off-axis test is the better method for the determination of the shear response of unidirectional laminates. On the other hand, the $[\pm 45°]_s$ tensile and $[0°/90°]_s$ rail shear methods seem to include interlamina effects. Thus, it appears that the appropriate test method would depend primarily upon what is sought. For example, if the effect of a variable, say environment (temperature and humidity), on the shear properties within a lamina are to be determined, the off-axis test would be appropriate. If, on the other hand, the effect of the same variables on laminate shear response, including intralamina and interlamina effects, the $[\pm 45°]_s$ tension or the $[0°/90°]_s$ rail shear test would be the appropriate test.

APPENDIX B

A SYNOPSIS OF FRACTURE BEHAVIOR OF NOTCHED COMPOSITES AT ROOM TEMPERATURE

In this appendix, a brief perspective of some of the proposed analytical models for the fracture behavior of notched composites is presented. This is followed by the analytical methodology used for the macroscopic fracture behavior of composites, experimental considerations, and an evaluation of the available fracture models with available experimental data. The application of these concepts are used to discuss possible future time-temperature investigations on notched composites. Only pertinent discussion and results are presented here as more extensive documentation can be obtained in references 57 to 60.

Fracture Models

The fracture behavior of composite materials has been studied using mainly three aspects: Linear elastic fracture mechanics (LEFM) on a microscopic scale with the material being heterogeneous and anisotropic; LEFM on a macroscopic scale with the material being homogeneous and anisotropic; and the material modelling approach using approximate models to represent the major effects of heterogeneity and anisotropy.

Chronologically, the fracture behavior of notched composites was analyzed from the micromechanical viewpoint [61-64] first and later was examined from the macromechanical viewpoint [65-74]. The primary limitations of the micro and macro approaches are: The former, due to

its simplicity, is not feasible when multi-axial loading is considered and in the latter, the non-self-similar crack propagation (which exists for certain laminate lay-ups) is not considered. Since the mathematical theory of LEFM assumes self-similar crack propagation, the latter approach will not be applicable when this assumption is violated. To overcome these limitations, the "Materials Science" model [75,76] and the "Local Heterogeneous Region" (LHR) model [77] were proposed. The advantages gained in these material modelling methods are that the structural response and various failure modes and mechanisms can be incorporated and predicted regardless of the boundary loadings. Consequently, the number of parameters required by the models increases as its analytical capabilities increase.

Analytical Methodology

The mode I critical stress intensity factor, K_{IC}, for an infinite isotropic plate containing a crack is expressed as

$$K_{IC} = \sigma_c\sqrt{\pi a} \tag{B-1}$$

and the modified K_{IC} using an Irwin type plasticity correction factor is expressed as

$$K_{IC} = \sigma_c\sqrt{\pi(a + a_o)} \tag{B-2}$$

where σ_c is the critical remote stress normal to the crack, 2a (Figure B-1) is the total crack length, and a_o is the characteristic length or inherent flaw length as denoted by Waddoups et al. [65]. These authors assumed that an unnotched laminate is equivalent to a notched laminate with a notch length of $2a_o$. That is, for the unnotched laminate

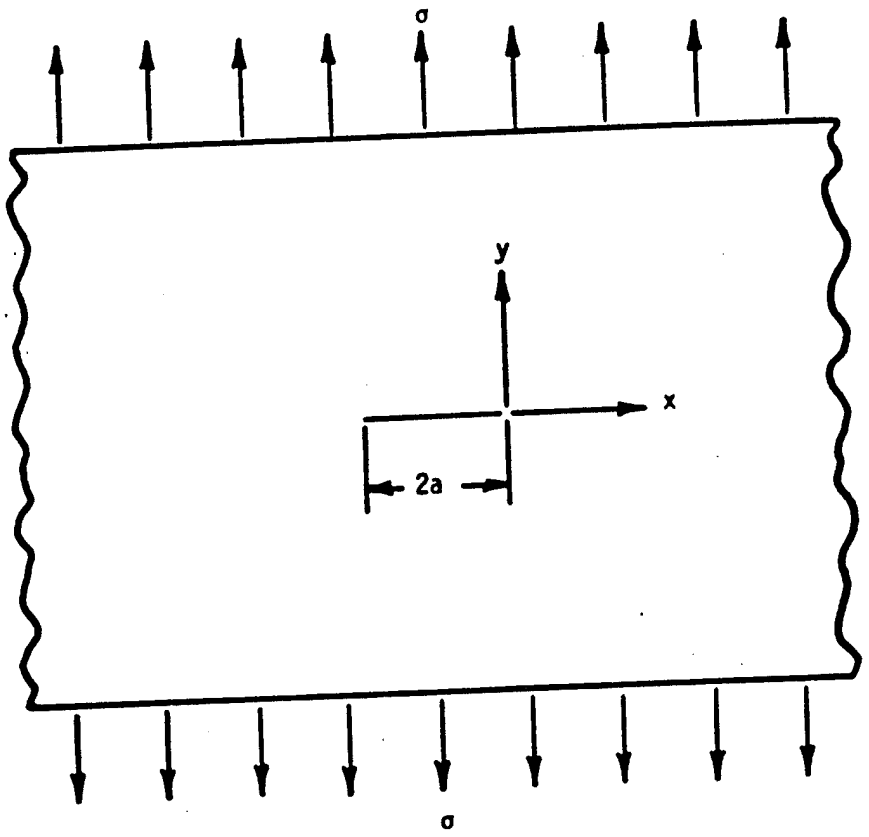

Figure B-1. Mode I Loading of a Center Cracked Infinite Plate.

$$K_{IC} = \sigma_o\sqrt{\pi a_o} \tag{B-3}$$

where σ_o is the ultimate strength of the unnotched laminate. By performing two tests, one on an unnotched laminate and the other on a notched laminate, the two parameters a_o and σ_o are determined. Using equations (B-2) and (B-3), the critical remote stress, σ_c, for the same laminate containing another flaw size, 2b, is related to σ_o and a_o as [65]

$$\frac{\sigma_o}{\sigma_c} = \sqrt{\frac{b + a_o}{a_o}} \tag{B-4}$$

Using a similar procedure as Waddoups et al. but with a different rationale, Whitney and Nuismer [70,71] use the exact anisotropic center cracked solution of Lekhnitskii [78] to derive two failure criteria for center notched specimens. The normal stress distribution for an infinite plate, Figure B-1, containing a crack and subjected to uniaxial tension σ is

$$\sigma_y(x,o) = \frac{\sigma_x}{\sqrt{x^2 - a^2}} = \frac{K_I x}{\sqrt{\pi a(x^2 - a^2)}} \tag{B-5}$$

where K_I from LEFM is expressed as $K_I = \sigma\sqrt{\pi a}$. The first failure criterion of Whitney and Nuismer, known as the point stress criterion, states that failure of a notched laminate will occur when the local stress $\sigma_y(a_1,o)$ at a certain distance, a_1, from the implanted notch tip reaches the strength of the unnotched laminate, σ_o. Using equation (B-5) and the definition of the point stress criterion, results in

$$\frac{\sigma_c}{\sigma_o} = \sqrt{1 - \xi^2} \tag{B-6}$$

where

$$\xi = \frac{a}{a + a_1}$$

The second failure criterion, known as the average stress criterion, stated that failure will occur when the average stress $\sigma_y(d_o,o)$, over a distance d_o from the notch tip reaches the strength of the unnotched laminate, σ_o. Substituting equation (B-5) into the definition of the average stress criterion gives

$$\frac{\sigma_c}{\sigma_o} = \sqrt{\frac{1 - \xi_1}{1 + \xi_1}} \tag{B-7}$$

where

$$\xi_1 = \frac{a}{a + d_o}$$

The parameters σ_o, a_1, and d_o are found experimentally using the same two required tests as in the Waddoups et al.'s method. As discussed by Tsai and Hahn [79], the characteristic lengths d_o and a_o are related by a factor of two, that is, $d_o = 2a_o$.

As shown in reference [70], the fracture toughness according to the point stress criterion is given by

$$K_Q = \sigma_o\sqrt{\pi a(1 - \xi^2)} \tag{B-8}$$

whereas for the average stress criterion the fracture toughness is

$$K_Q = \sigma_o\sqrt{\pi a(1 - \xi_1)/(1 + \xi_1)} \tag{B-9}$$

The analysis discussed so far is for an infinite plate while for economic reasons and experimental convenience finite width plates are used. In order to correlate the two types of results, the experimental data is corrected to the analytical results by applying appropriate finite width correction factors. The usual procedure is to determine the infinite plate notched strength from the equation

$$\sigma_c = F(a/W)\sigma_c^f \qquad \text{(B-10)}$$

where σ_c is the infinite plate notched strength, σ_c^f is the notched strength of a finite width specimen, and F(a/W) is the finite width correction factor. The value of F(a/W) is determined from the equation for isotropic materials [80].

$$F(a/W) = \sqrt{(W/\pi a)\tan(\pi a/W)} \qquad \text{(B-11)}$$

where W is the width of the finite plate.

The analytical methodology mentioned to this point depends very strongly on the isotropic treatment of the analysis as seen in the correlation of the finite width experimental data with the infinite plate analytical solution, or vice versa. However, the difference between the correction factor for isotropic and anisotropic materials is of the order of 10%, as shown by Cruse and Osias [81] and Konish [82]. Thus, as a matter of convenience, the isotropic correction factor is used.

To avoid the assumption of an isotropic factor, Snyder and Cruse [74,83] developed a boundary-integral equation (BIE) method to calculate finite width effects and stress intensity factors for modes I and II, for various geometries and in-plane loadings. In this approach the

material is modelled as a homogeneous, linearly elastic, anisotropic continuum using the assumptions of lamination theory. The BIE method is based upon an appropriate fundamental solution to the field equations of elasticity. The fundamental solution is used to derive a set of integral equations relating boundary values of displacement and traction corresponding to a well-posed boundary value problem. The boundary integral equations are solved using approximate techniques, e.g., modeling the boundary by constant-displacement, constant-traction segments.

The boundary integral equations relate boundary values of traction and displacement on that portion of the boundary excluding the crack boundary, thus avoiding the problem of modeling the crack boundary. An additional advantage of the method is that it provides a direct means for obtaining both of the stress intensity factors K_I and K_{II}, i.e., equations are derived for obtaining K_I and K_{II} directly from the boundary solution. Thus, the boundary solution may be computed using other numerical methods, such as the finite element method.

As developed by Snyder and Cruse, the basic equation of the BIE method may be written as

$$u_j(P)/2 + \int_S u_i(Q)\, T_{ji}(P,Q)ds(Q) = \int_S t_i(Q)\, U_{ji}(P,Q)ds(Q) \qquad \text{(B-12)}$$

In equation (B-12), $u_i(Q)$ and $t_i(Q)$ refer to, respectively, displacements and tractions at boundary points Q, not including the crack boundary. The BIE method uses special kernels, $T^*_{ji}(P,Q)$ and $U^*_{ji}(P,Q)$, for $T_{ji}(P,Q)$ and $U_{ji}(P,Q)$ in equation (B-12) to mathematically model a traction-free straight crack of length 2a. Since T^*_{ji} and t_i are

identically zero on the crack surface, the crack need not be modelled.

The expression for determining mode I and mode II stress intensity factors is an integral of boundary displacements and boundary tractions on an arbitrary path in the body, and is given by

$$K_{I,II} = \int_S R_i^{I,II}(Q)u_i(Q)ds(Q) + \int_S L_i^{I,II}(Q)t_i(Q)ds(Q) \qquad \text{(B-13)}$$

The kernels R_i and L_i are complex variable functions which include crack size and location, as well as material properties. As discussed in reference [84], while the derivation of equation (B-12) leads to the definition of equation (B-13), equation (B-13) may use boundary data taken from any numerical model of the cracked geometry. The only input information needed in the technique is geometry, material properties, and grid sizes and spacings.

Experimental Considerations

In order to determine the versatility of the three two-parameter models and the one one-parameter model described in the previous section, a series of center notched specimens containing narrow slits with variations in aspect ratio (2a/w, where w is the total width of the specimen) and/or anisotropy were tested. In the second series of tests, the aspect ratio variations were the same as the first, but the flaw geometry was changed to that of a hole or square slot rather than a slit. The objective of the second series was to ascertain the types of fracture, if more than one existed and the fracture strength variation when the height of the slit was increased. In these series of tests, experimental methodologies such as crack opening displacement (COD)

gages, two types of photoelastic coatings and photographic recording of crack propagation were employed. In addition, in-situ and post microscopic observation of the crack growth and similar observations of the free surfaces of the specimens were made.

In the third series of tests, the implanted flaw geometries and/or location, material anisotropy and aspect ratios were again varied. The notch geometries and/or locations chosen were the single-edged notch (SEN), double-edged notch (DEN) and centrally located circular holes. The reasons for this series of tests were to compare the fracture toughnesses of the SEN and DEN specimens using the BIE method and the experimental fracture strengths of the specimens containing holes with the predictions of the three two-parameter models.

Results and Discussion

COD Measurements

Typical load-COD traces for all the laminates in the first series of tests are as shown in Figure B-2. The measurements were taken from the relative motion of the center of the opposite faces of the notch in the direction of the remote tensile load. Similar traces were also obtained from the second series of tests (slots). Generally, as indicated in Figure B-2, the $[0°/\pm45°/0°]_{2s}$ laminates exhibited nearly linear response while the $[0°]_{8s}$ and $[\pm45°]_{4s}$ laminates were highly non-linear. In most cases, the displacements of the two latter laminates exceeded the range of the COD gage.

Gaggar and Broutman [86] attributed such non-linear behavior and discontinuities in load-COD measurements to deformations and

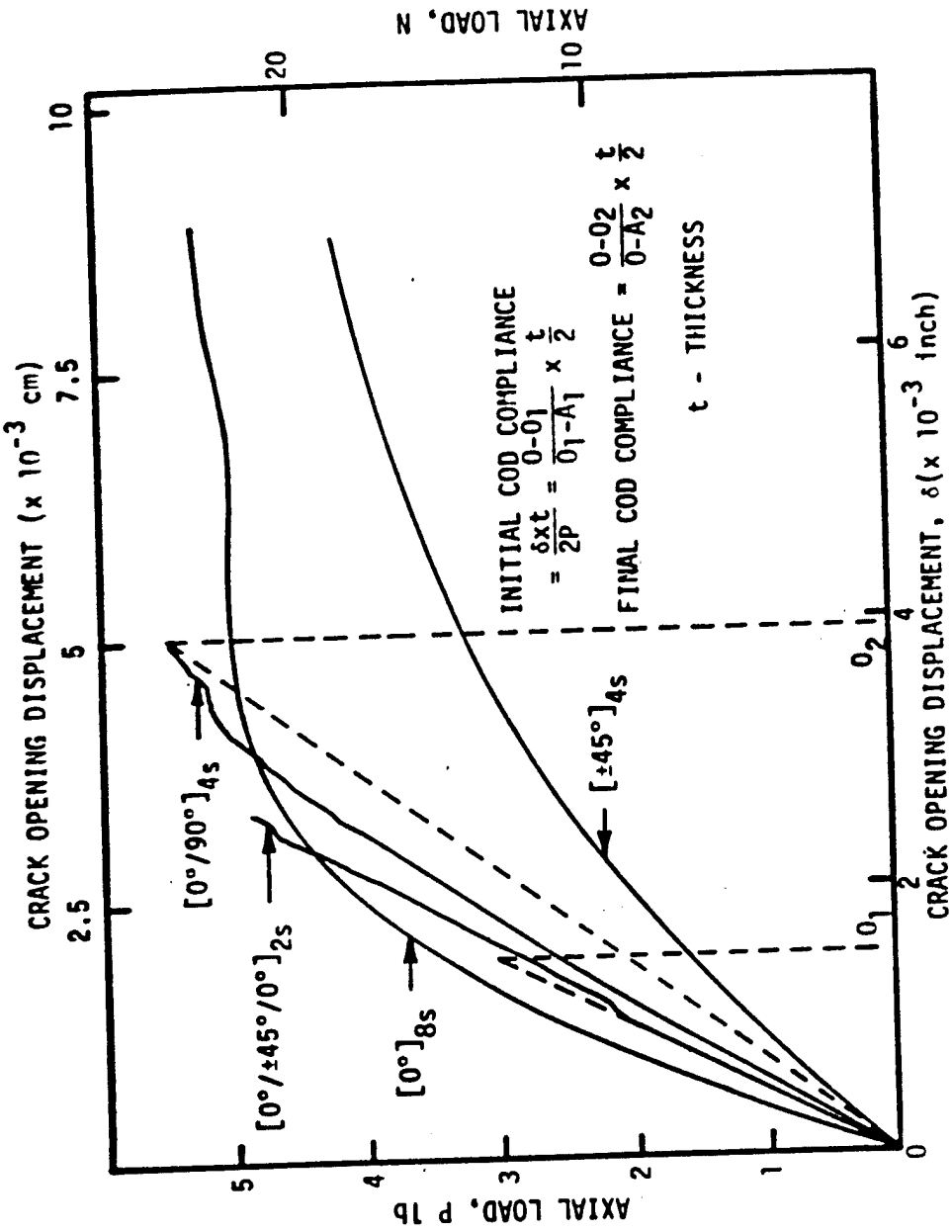

Figure B-2. Load-displacement curves for slits, 2a/w = 0.25

extensions of the notch tips. Assuming self-similar crack propagation, those authors suggested a compliance matching procedure, which is illustrated in Figure B-2, to quantify the amount of actual or apparent crack extension at any arbitrary load level. Using this procedure, the compliances of the slots were always higher than their slit counterparts. The more flexible nature of the slots was expected as there was less constraint than in the case of the slits.

Fracture Strengths

The variation of the average value of the critical gross stresses with aspect ratios for the first and second series of tests (i.e., slits and slots) are as shown in Figure B-3. Although the trends of the critical gross stresses were similar, the slots always fractured at a higher stress level than the slits irrespective of the aspect ratio or laminate orientation. This was probably due to the more flexible nature of the slots as determined by the COD measurements.

In the case of the $[\pm 45°]_{4s}$ laminate, the specimens containing circular holes fractured at about the same or slightly lower stress levels than the ones containing narrow slits for all aspect ratios as shown in Figure B-3. Examination of the photoelastic fringes of Figures B-4a and B-4c tended to indicate that the size of the region of the intense stress gradient was larger for the hole than for the slit at about the same remote stress level. This would imply that the holes were more critical than the slits for the $[\pm 45°]_{4s}$ laminate.

It should be noted that the trends of the variation of the critical remote stresses with aspect ratio were the same for all

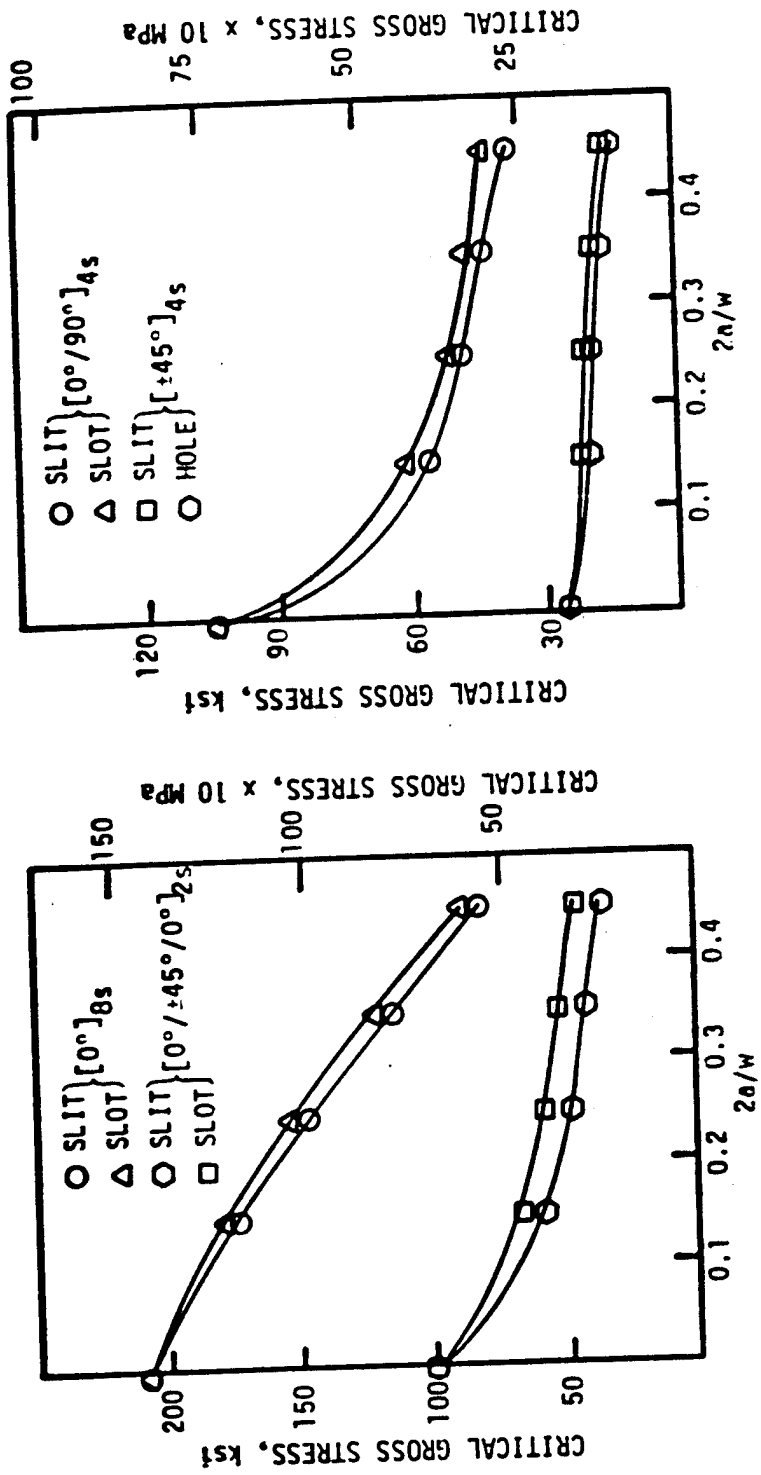

Figure B-3. Remote Failures Stresses of T300/934 Graphite/Epoxy Laminates.

a) 13.10 ksi
(90.29 MPa)

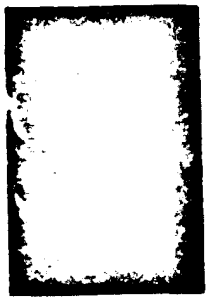

b) Fracture

c) 13.22 ksi
(91.16 MPa)

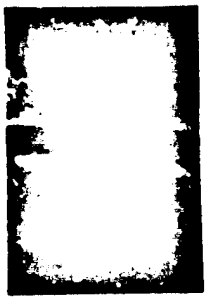

d) Fracture

e) 16.39 ksi
(113.00 MPa)

f) Fracture

Figure B-4. Isochromatics of $[\pm 45°]_{4s}$ Laminate with Perforated (a-d) and Continuous (e,f) Coatings ($2r/w = 0.45$).

cutouts as shown in Figure B-3. This observation tends to substantiate the "Materials Science" model for fracture which assumes that flaw geometry does not have a major influence on the laminate fracture strength and the strength is more closely related to the size and shape of the damage zone surrounding the flaw tip.

Finally, the critical remote stresses of the specimens containing SEN, DEN and holes with aspect ratio are shown in Figures B-5, B-6 and B-7, respectively. Except for the $[0°]_{8s}$ laminate, the trends of the variation of the fracture strengths with aspect ratios in every case were similar to the ones observed for isotropic materials. The deviations of the $[0°]_{8s}$ laminate from these trends were likely due to the axial crack propagation which propagated into the gripped sections of the specimen prior to transverse failure.

Birefringent Coatings

Typical results obtained for each laminate orientation using both continuous and perforated coatings are shown in Figures B-4c and B-4e. That is, the fringe density was less in the case of the continuous coatings but the shapes of the patterns were similar.

Figure B-8 shows the types of stress fields and fracture planes obtained for specimens containing center slits. In the case of the $[0°]_{8s}$ and $[0°/90°]_{4s}$ specimens, although both laminates could be considered to be orthotropic and the intense shear stress regions were in the axial direction (see Figure B-8a and B-8b), the final fracture planes were different. Non-self-similar crack propagation was observed for the $[0°]_{8s}$ laminates and self-similar crack propagation

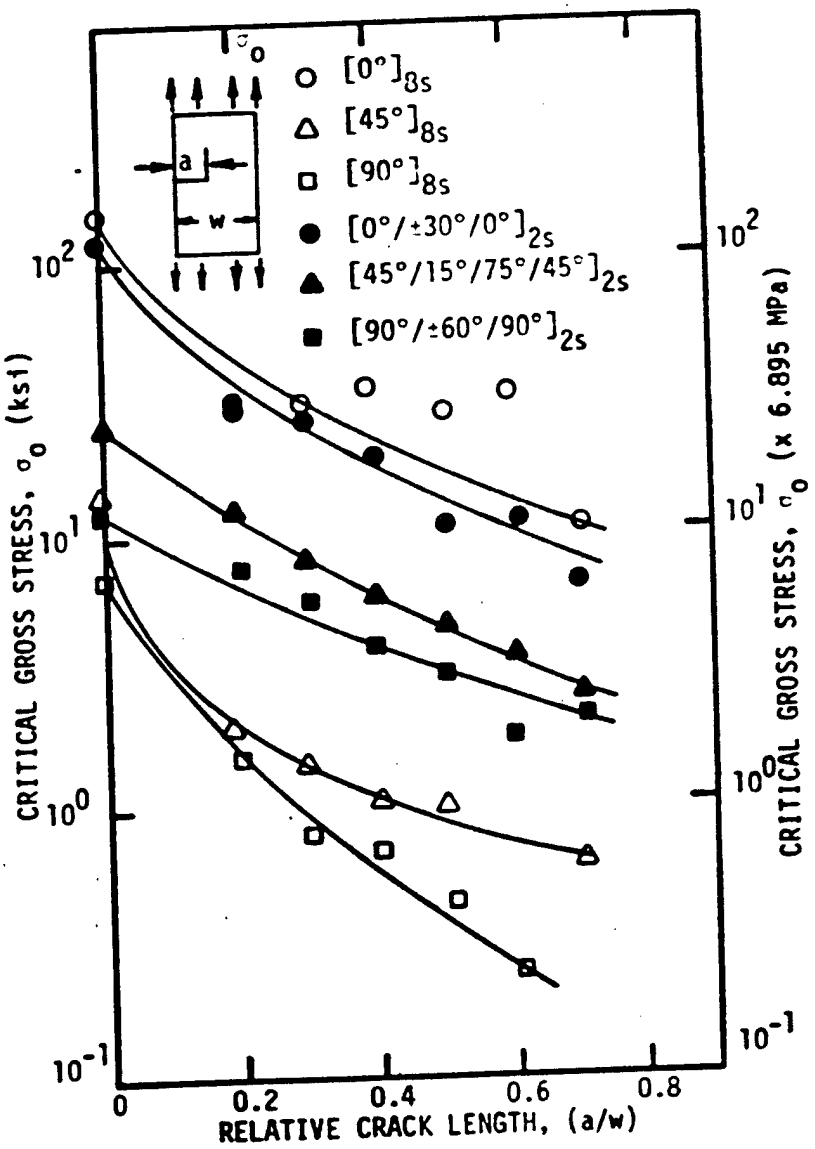

Figure B-5. Single Edge Notch (SEN) Gross Fracture Stresses for AS-3501 Graphite/Epoxy Laminates.

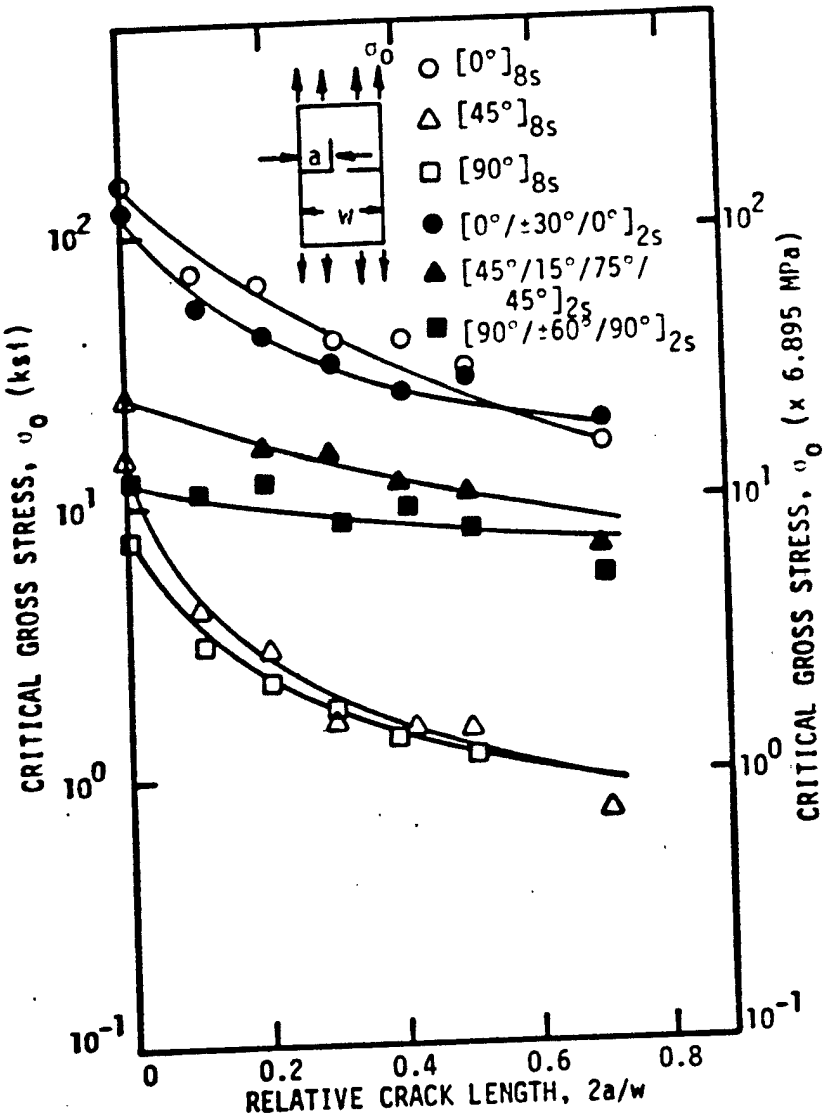

Figure B-6. Double Edge Notch Gross Fracture Stresses for AS-3501 Graphite/Epoxy Laminates.

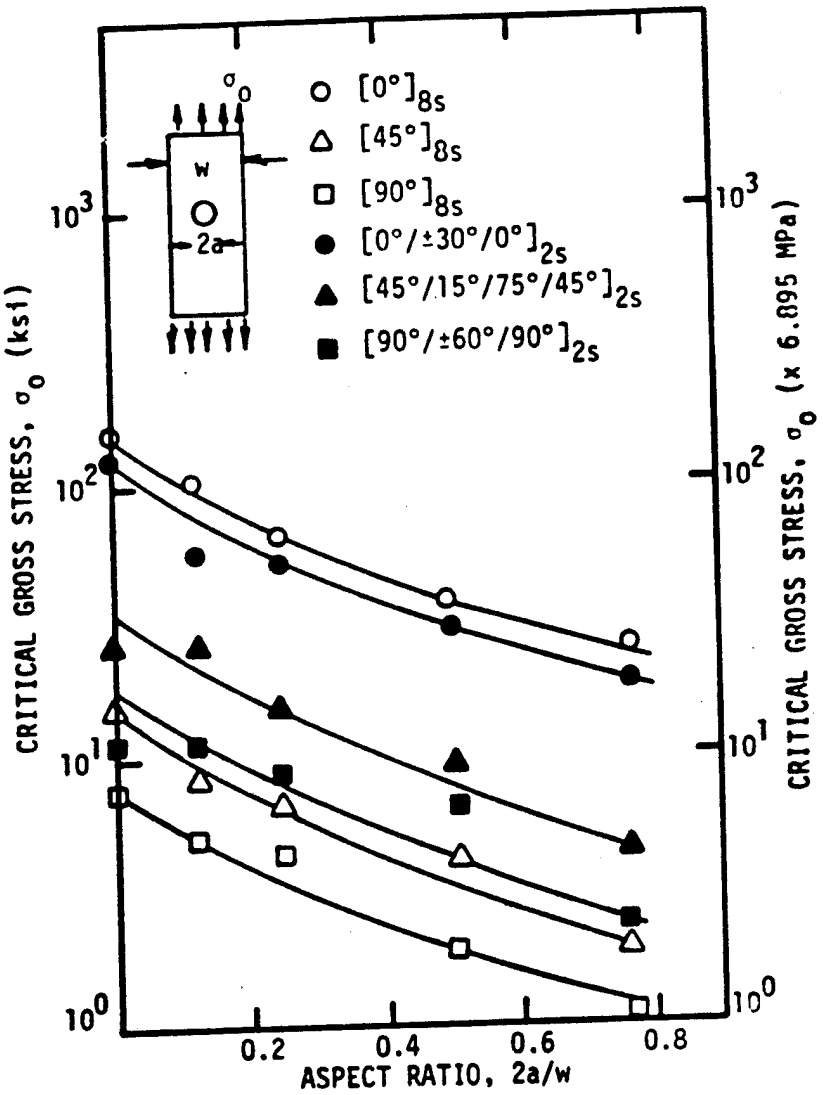

Figure B-7. Circular Hole Gross Fracture Stresses for AS-3501 Graphite/Epoxy Laminates.

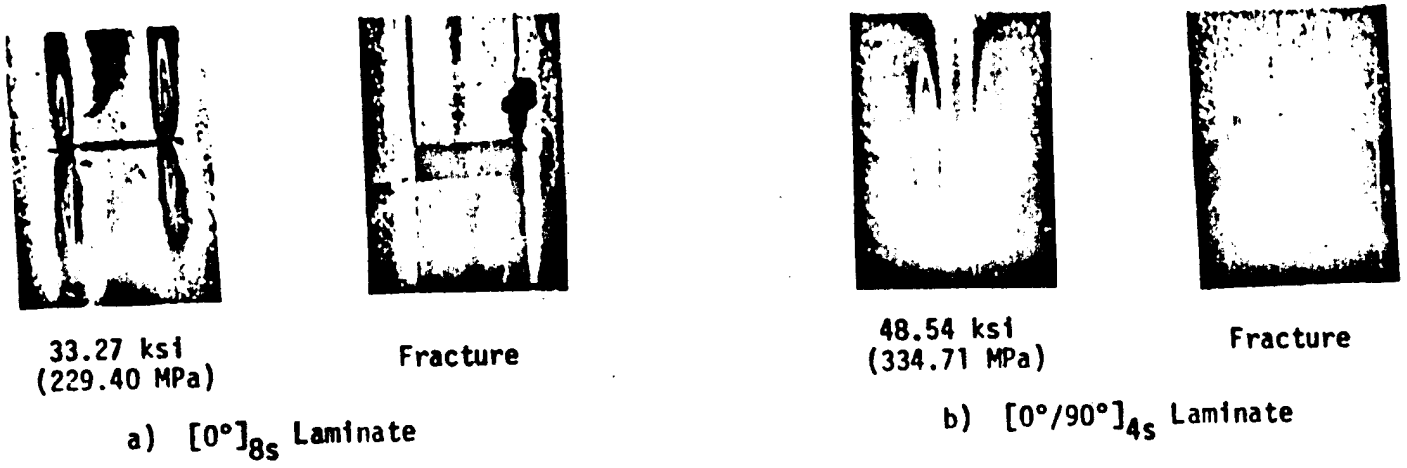

33.27 ksi
(229.40 MPa)

Fracture

a) $[0°]_{8s}$ Laminate

48.54 ksi
(334.71 MPa)

Fracture

b) $[0°/90°]_{4s}$ Laminate

13.10 ksi
(90.29 MPa)

Fracture

c) $[\pm 45°]_{4s}$ Laminate

39.28 ksi
(270.81 MPa)

Fracture

d) $[0°/\pm 45°/0°]_{2s}$ Laminate

Figure B-8. Photoelastic Coating Birefringence Photographs and Fracture Planes for Laminates Tested.

was observed for the $[0°/90°]_{4s}$ laminates. The intense shear stress regions for the $[\pm 45°]_{4s}$ laminates were adjacent to the notch tips and were in the 45° directions. Generally, the pattern was more dense in the +45° direction than the -45° direction. Since the outer laminae were in the +45° direction, this observation merely indicates that the inner -45° laminae were constrained by the outer laminae (+45° direction) to produce this effect. The fringe pattern was similar to the ones observed in isotropic materials in the case of the $[0°/\pm 45°/0°]_{2s}$ laminate; i.e., butterfly wing shaped patterns, Figure B-8d.

No attempts were made to quantify the birefringence results as the mismatch between the properties of the coating and the underlying material (Poisson's ratio and moduli) as well as anisotropy of the laminate made proper fringe interpretation difficult [86]. Further, the properties of the material were not constant and changed with stress level. Similar results have been reported by others [12]. Perhaps more importantly, the uncertainties relative to the nature and strength of the singular stress field for the slits and slots further compounded our fringe interpretation difficulties. That is, the nature of the singularity of the laminate was likely quite different than the nature of the singularity in either the continuous or perforated coating.

In-Situ and Post Failure Examinations

Stable crack growth was often observed during most of the tests. In all cases stable crack growth occurred by matrix fracture. In the

case of the $[0°]_{8s}$ laminates, stable axial crack growth always occurred at the notch tip and proceeded to the gripped sections of the specimen. Catastrophic transverse failure would occur only upon completion of the axial crack propagation.

The most interesting situations of stable crack growth was observed in the DEN $[90°/\pm60°/90°]_{2s}$ tests. A typical example of crack propagation for this notch geometry is shown in Figure B-9. Initially, the self-similar crack would originate at the notch tips and propagation would continue as the remote load was increased. At higher stress levels, micro-cracking was observed away from the plane of the implanted notch. Finally, separation of the specimen occurred at the region where the cross-sectional was minimum.

Post failure microscopic examination of all the unnotched and notched specimens of the first and second test series revealed a large number of micro-cracks on all the free edges. In the notched cases, microscopic examination clearly indicated more pronounced micro-cracks on the free surfaces of the implanted notch as opposed to the specimen boundary free surfaces.

A qualitative comparison of the boundary free edges for unnotched and notched specimen within each general laminate lay-up showed more pronounced cracks in the notched case than in the unnotched case. This was true even though the remote stress levels of the unnotched specimens were the higher of the two situations. This, perhaps, indicated that the notches had an adverse affect on the stress state at the specimen free edge.

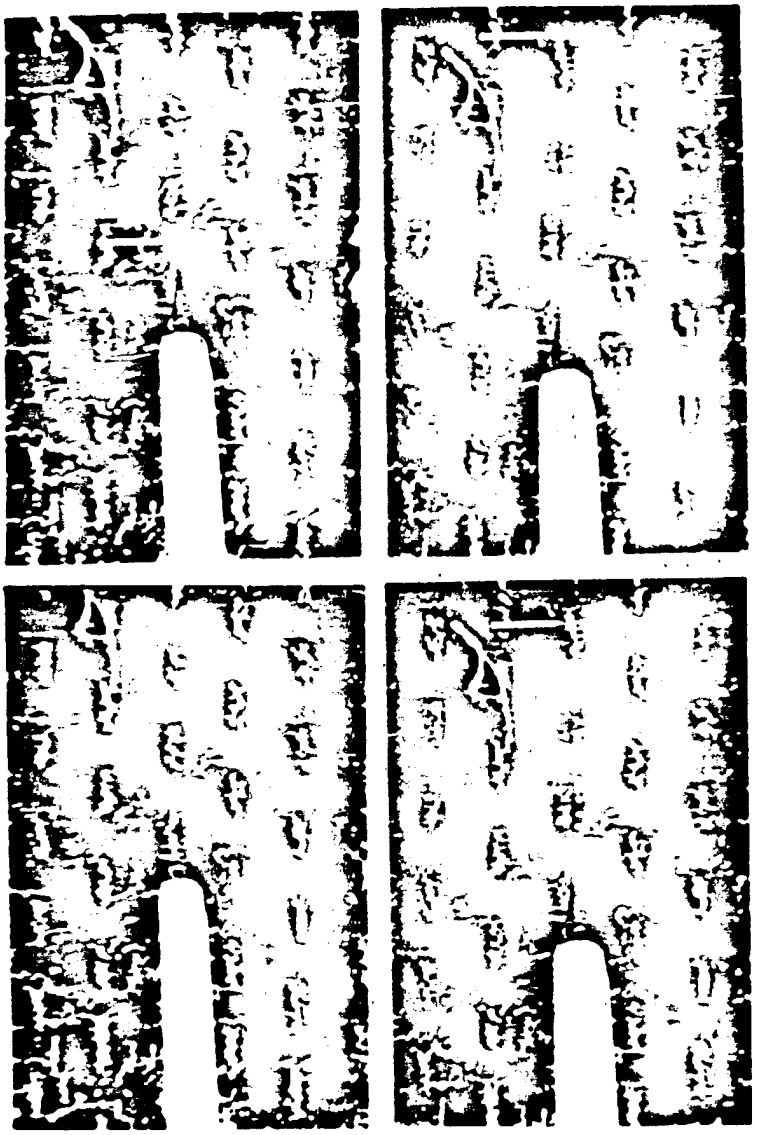

Figure B-9. Stable Crack Growth for $[90°/\pm60°/90°]_{2s}$ AS-3501 Graphite/Epoxy DEN Specimen. (Arrows indicate extent of crack growth.)

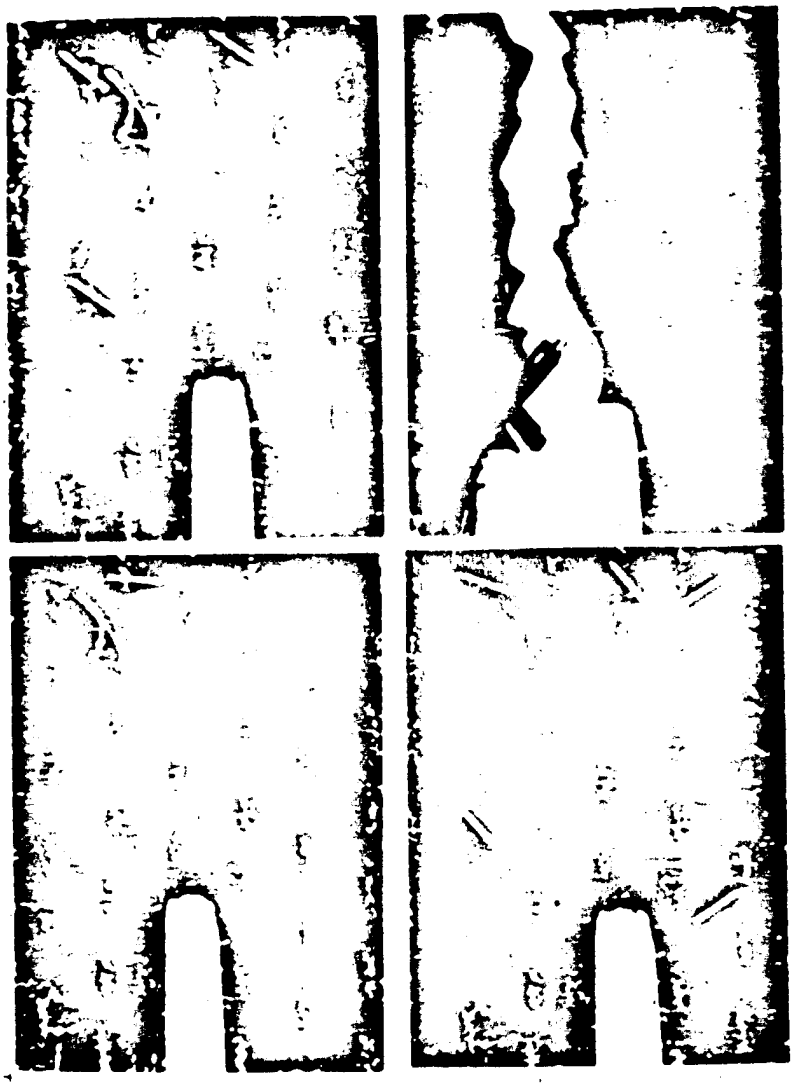

Figure B-9 (cont.). Stable Crack Growth for $[90°/\pm60°/90°]_{2s}$ AS-3501 Graphite/Epoxy DEN Specimen. (Arrows indicate extent of crack growth. Note additional cracks above and below the notch plane.)

Characteristic Lengths

In order to obtain favorable correlations between the two-parameter fracture models (inherent flaw, point stress and average stress) and experiments, the characteristic length or damage zone must be known. In fact, even to use these methods at all requires that this dimension must be established for a particular laminate. The originators of the inherent flaw and point stress criteria suggested a characteristic length of 0.04 inch (1.016 mm) for all aspect ratios would be a reasonable assumption while for the average stress criterion they suggested a characteristic length of 0.15 inch (3.810 mm). They further suggested that this quantity could be assumed to be constant for a type of composite; i.e., graphite/epoxy, glass/epoxy, etc. To validate the above suggested characteristic lengths for our materials (T300/934 graphite/epoxy), an attempt was made to calculate these parameters (Equations (B-4), (B-6) and (B-7)) from the experimental data generated in this investigation.

As shown in Figure B-10, the characteristic lengths determined from our experiments were higher than the ones suggested previously [66,72]. It should be noted that non-self-similar crack growth was observed in the cases shown in Figure B-10 and it is probably due to this fact that a decreasing characteristic length with increasing aspect ratio trend was observed. The proposed two-parameter fracture models do not allow for such a trend. In all fairness, however, the models were originally proposed for quasi-isotropic laminates and the laminate types shown in Figure B-10 are not quasi-isotropic.

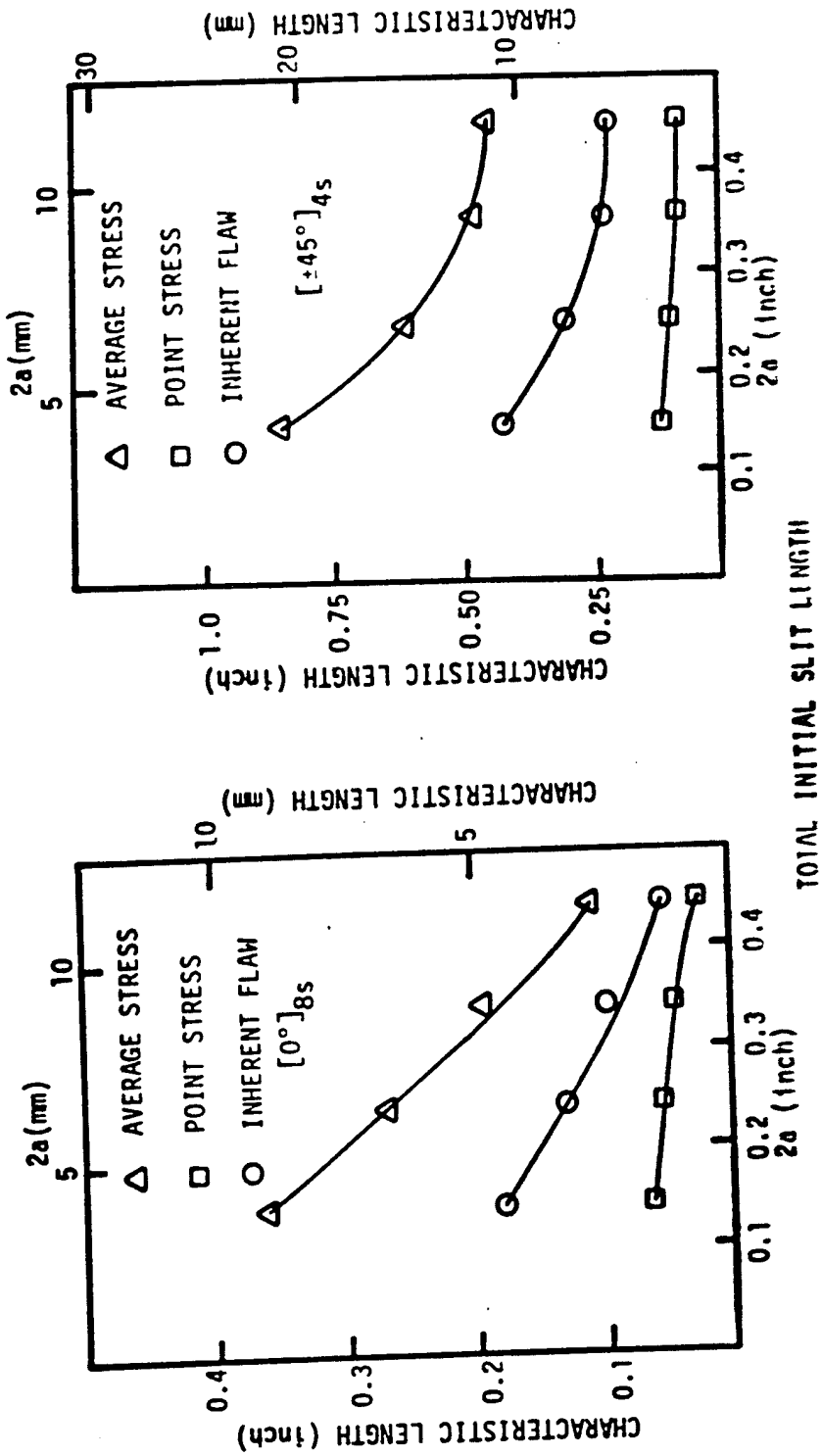

Figure 8-10. Characteristic Lengths for T300/934 Graphite/Epoxy Laminates with Implanted Cracks.

Quasi-self-similar crack growth was observed for the nearly quasi-isotropic laminates and the trends were similar to the ones suggested by the proposed models as evident by examination of Figure B-11. In this latter figure, the total crack extension prior to separation as determined by the load-COD method were consistent with the characteristic lengths of the inherent flaw model for the $[0°/\pm45°/0°]_{2s}$ laminate. In the case of the $[0°/90°]_{4s}$ laminate, this trend was opposite to the ones proposed by the three two-parameter models.

Notched Strength Predictions

The two two-parameter models of Nuismer and Whitney utilize the exact anisotropic infinite plate solution for centrally located cracks and holes. As a result, comparisons of these models with the inherent flaw model and BIE method can only be made for center notched (CN) laminates. Comparisons between experimental and predicted strengths of the CN specimens for different aspect ratios and laminate orientations are as shown in Figures B-12 to B-15 for our T300/934 graphite/epoxy materials. Equations (B-4), (B-6) and (B-7) of the two-parameter models were used to obtain the analytical curves representative of those models. The characteristic lengths used to generate these curves were assumed to be constant and specific values as suggested by the originators of the models were used as was discussed earlier. As may be noted in Figures B-12 to B-15, considerable differences were found between predictions based upon the three two-parameter models and the experimental results. While some of the variations may have been due to experimental error, it is felt that the fundamental reason

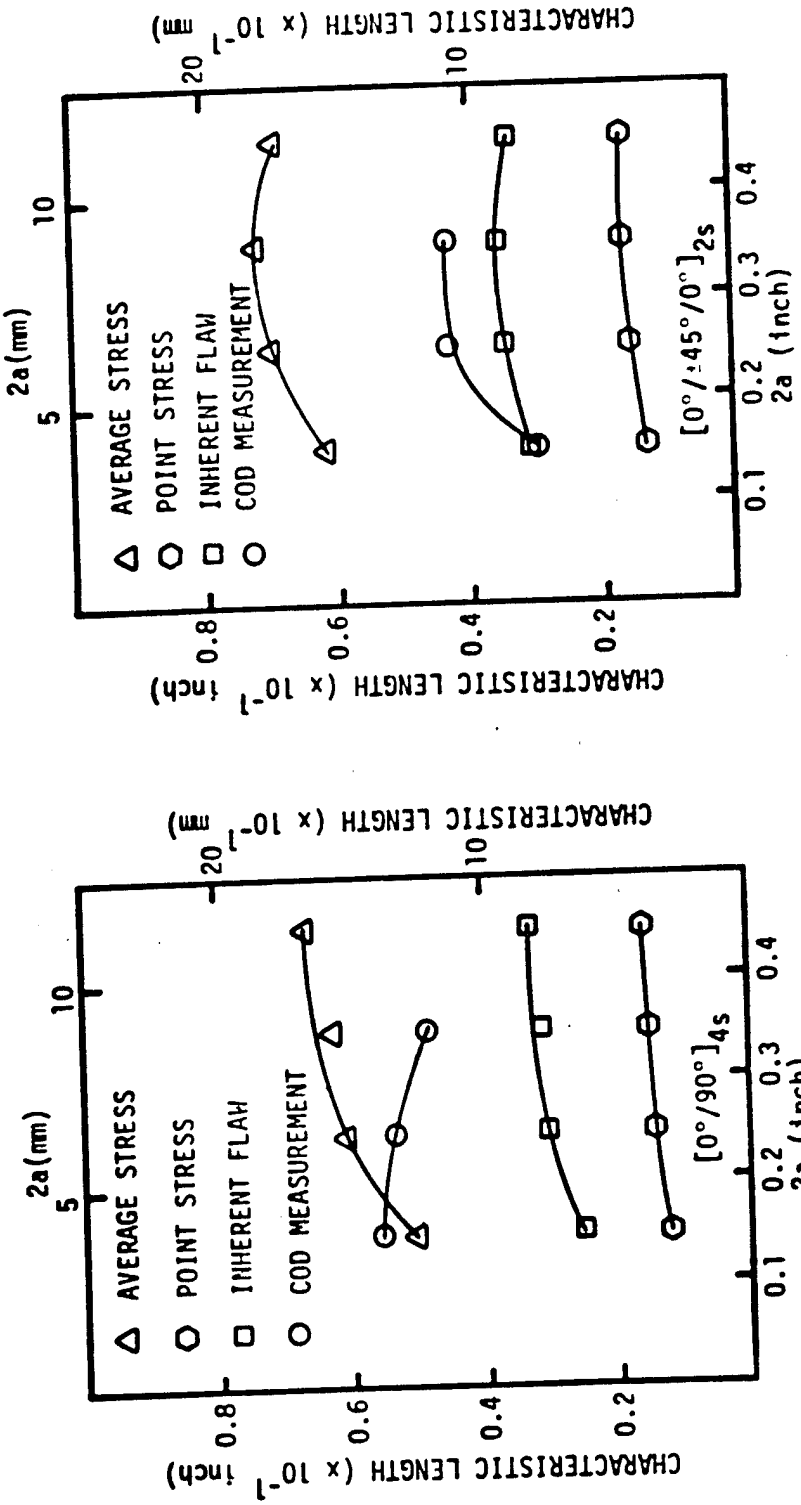

Figure B-11. Characteristic Lengths for T300/934 Graphite/Epoxy Laminates with Implanted Cracks.

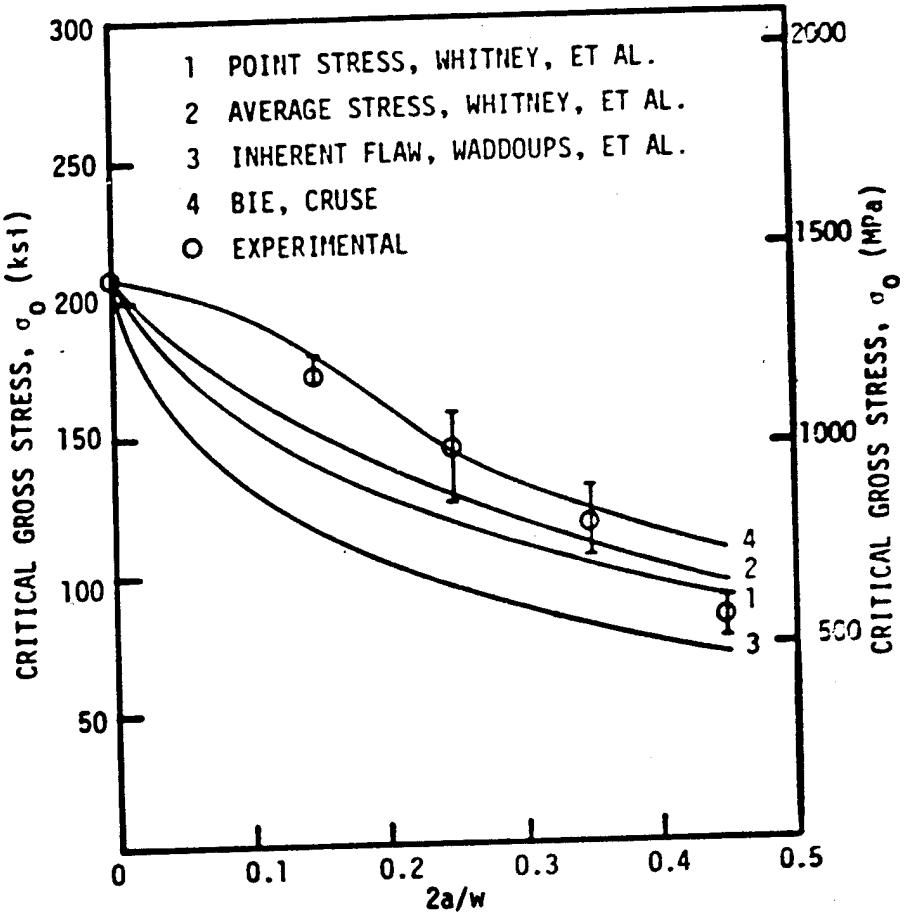

Figure B-12. Comparison Between Experimental and Analytical Critical Remote Stresses for CN $[0°]_{8s}$ Laminates.

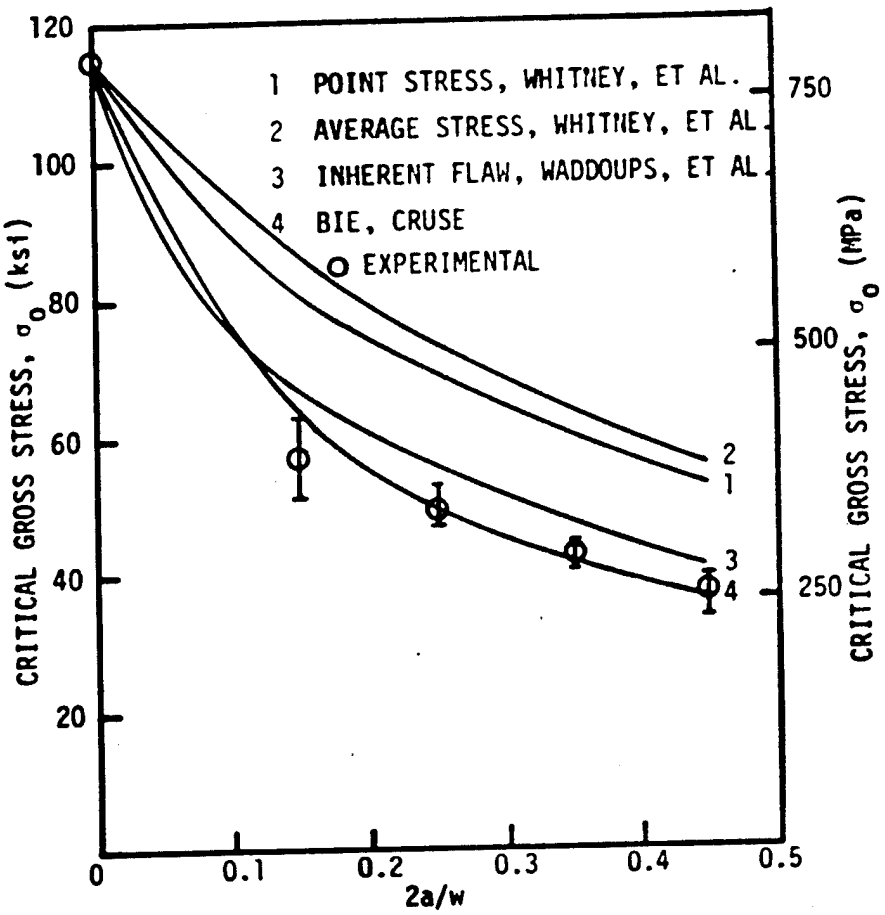

Figure B-13. Comparison Between Experimental and Analytical Critical Remote Stresses for CN $[0°/90°]_{4s}$ Laminates.

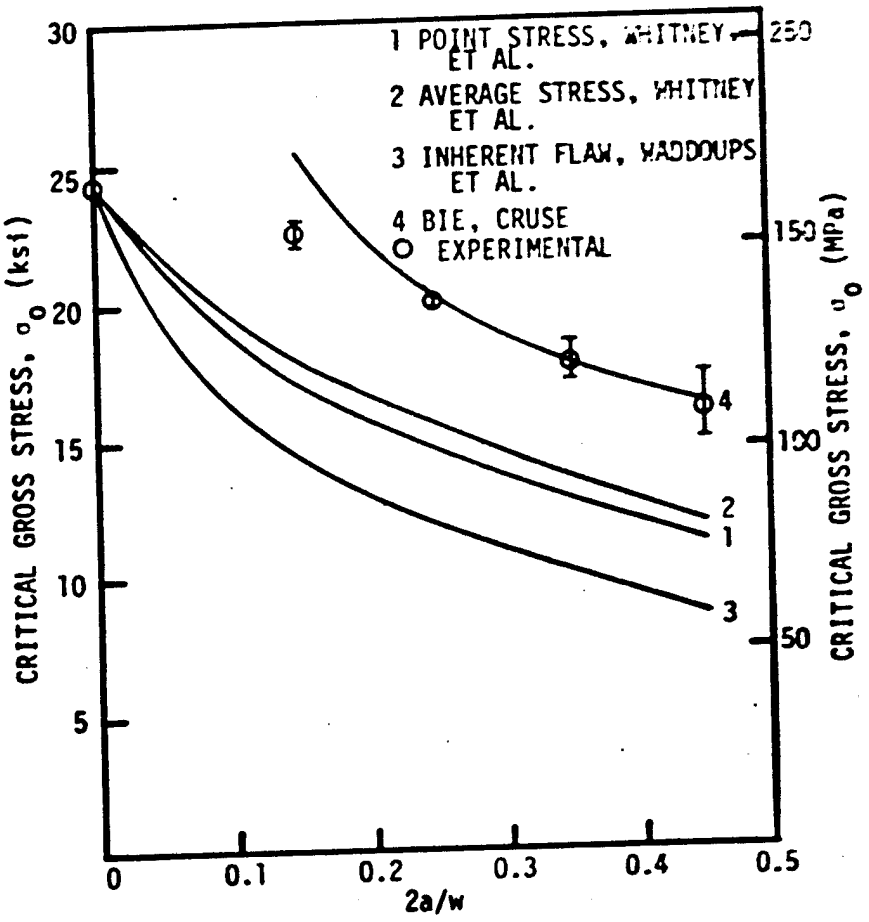

Figure B-14. Comparison Between Experimental and Analytical Critical Remote Stresses for CN $[\pm 45°]_{4s}$ Laminates.

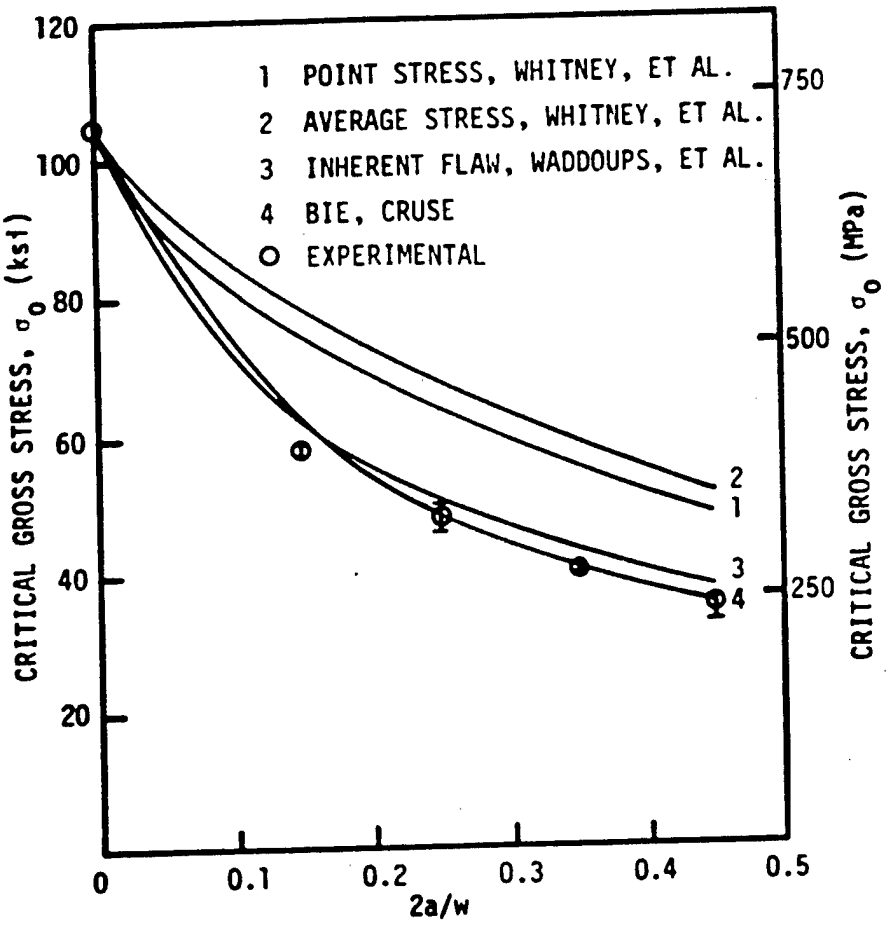

Figure B-15. Comparison Between Experimental and Analytical Critical Remote Stresses for CN $[0°/\pm45°/0°]_{2s}$ Laminates.

for the difference between the various methods of approach were likely due to the assumed constant characteristic lengths. Obviously, better comparison between analysis and experiment would have been obtained if a "best fit" characteristic length had been used. Such a procedure is nothing more than "curve fitting" and does not lead to a better understanding of the fracture behavior of composites.

The results labelled Cruse in Figures B-12 to B-15 were obtained by assuming that the fracture toughness calculated using the aspect ratio, $2a/w = 0.25$, represented the true value for the laminate. This value was chosen because in all cases the fracture toughness approached asymptotic values beyond $2a/w = 0.25$. In these figures, the best comparison between analysis and experiment was seen using the one-parameter BIE model of Snyder and Cruse.

The three two-parameter fracture models can be used for circular holes as well as for crack-like flaws. Thus, using the same constant characteristic lengths as discussed above for the AS-3501 graphite/epoxy specimens containing holes, comparisons between the predicted fracture strengths of the three two-parameter models and experiments are shown in Figures B-16 and B-17 for a variety of laminate orientations. Generally, the inherent flaw predictions correlated better with the experimental fracture strengths than the two approaches of Whitney and Nuismer. Again, a better correlation between analysis and experiment could have been obtained by adjusting the characteristic dimension which again would have represented a "curve fitting" process. This was not done for the same reasons discussed earlier.

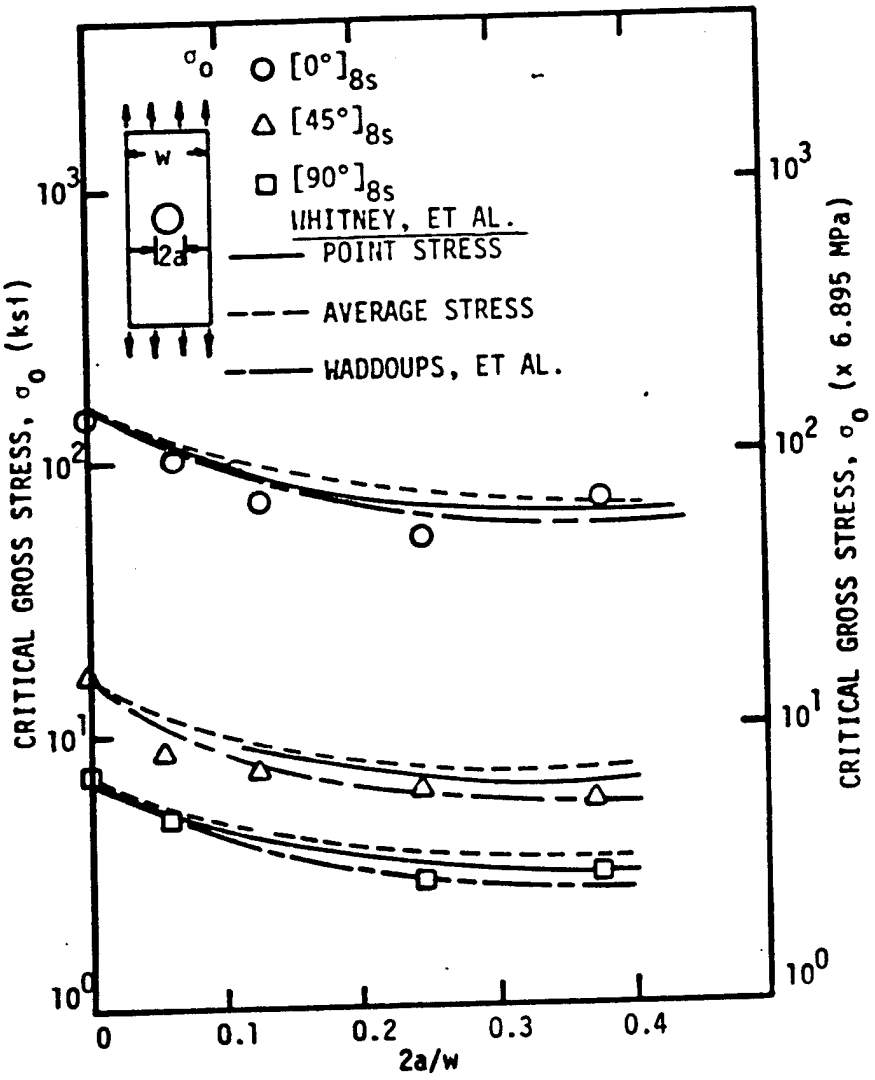

Figure B-16. Comparison of Experimental and Theoretical Fracture Strengths for AS-3501 Graphite/Epoxy Laminates Containing Centrally Located Holes. (Results corrected to infinite width using isotropic stress concentration factor.)

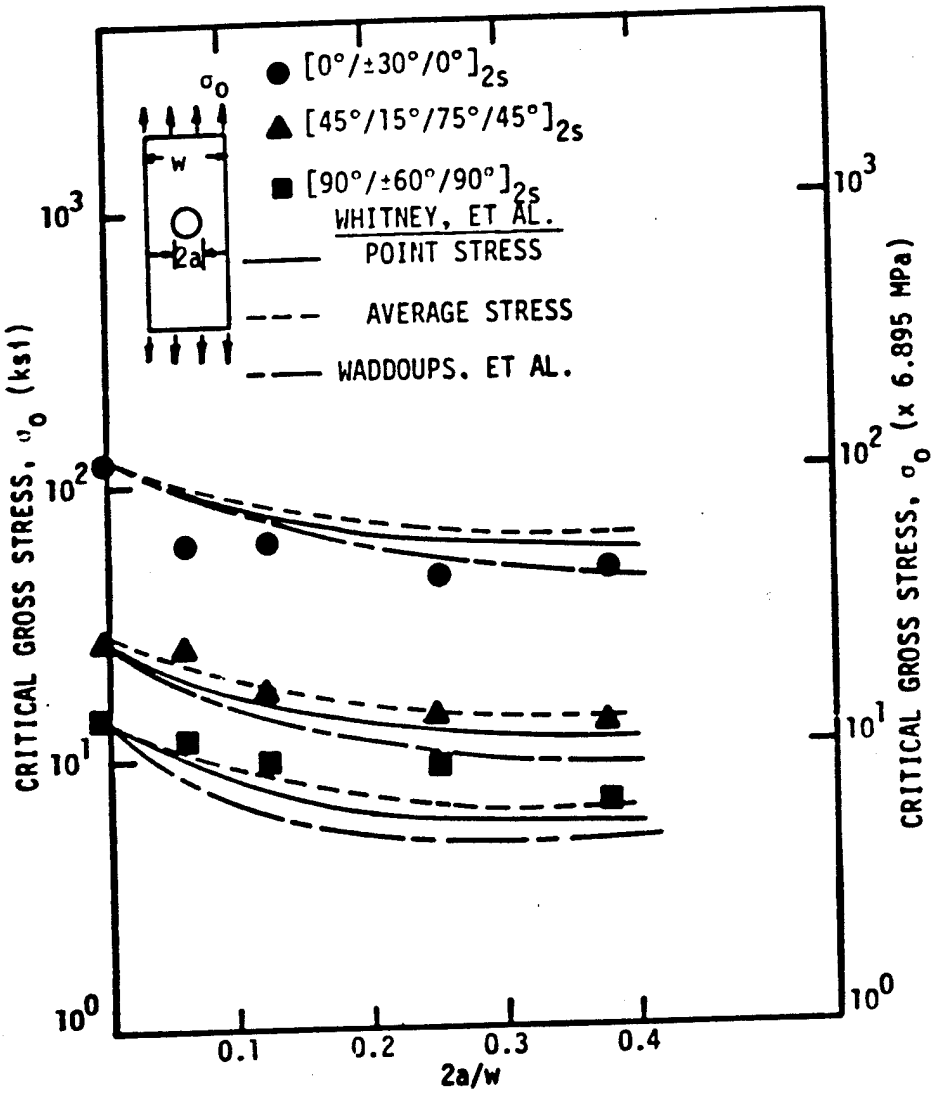

Figure B-17. Comparison of Experimental and Theoretical Fracture Strengths for AS-3501 Graphite/Epoxy Laminates Containing Centrally Located Holes. (Results corrected to infinite width using isotropic stress concentration factor.)

Finite Width Correction Factor

When correlating experimental results with analyses based on a body with infinite dimensions or vice-versa, finite width correction factors (FWCF) must be employed if the correlations are to be meaningful. To date, most of the FWCF's for isotropic materials are numerically obtained. In the case of composite materials, all the FWCF's are obtained numerically. Thus, a comparison of the isotropic FWCF and the anisotropic FWCF (obtained from the BIE method) for the notched specimens used in this investigation would be appropriate.

Since the BIE method is a numerical method and like other numerical methods, its convergence should be determined. The procedure adopted here was to determine the segment spacings first, followed by prescribing the boundary conditions. The results obtained were compared to the results reported in reference [80] for isotropic materials. For the three types of implanted notches used here, the difference between the BIE results and the ones in reference [80] was less than 0.3%. Upon completion of this preliminary work, the conversion to anisotropic cases was just a matter of defining the laminate orientation and principal material properties.

The variations between the isotropic FWCF (equation (B-11)) and the anisotropic values for the CN specimens are as shown in Figure B-18. Except for the $[\pm 45°]_{4s}$ laminate, the difference between the isotropic and anisotropic values are less than 5% for all aspect ratios. In the case of the $[\pm 45°]_{4s}$ laminate, the most anisotropic laminate investigated here, the maximum difference between the isotropic and anisotropic value was approximately 10% when $2a/w = 0.45$.

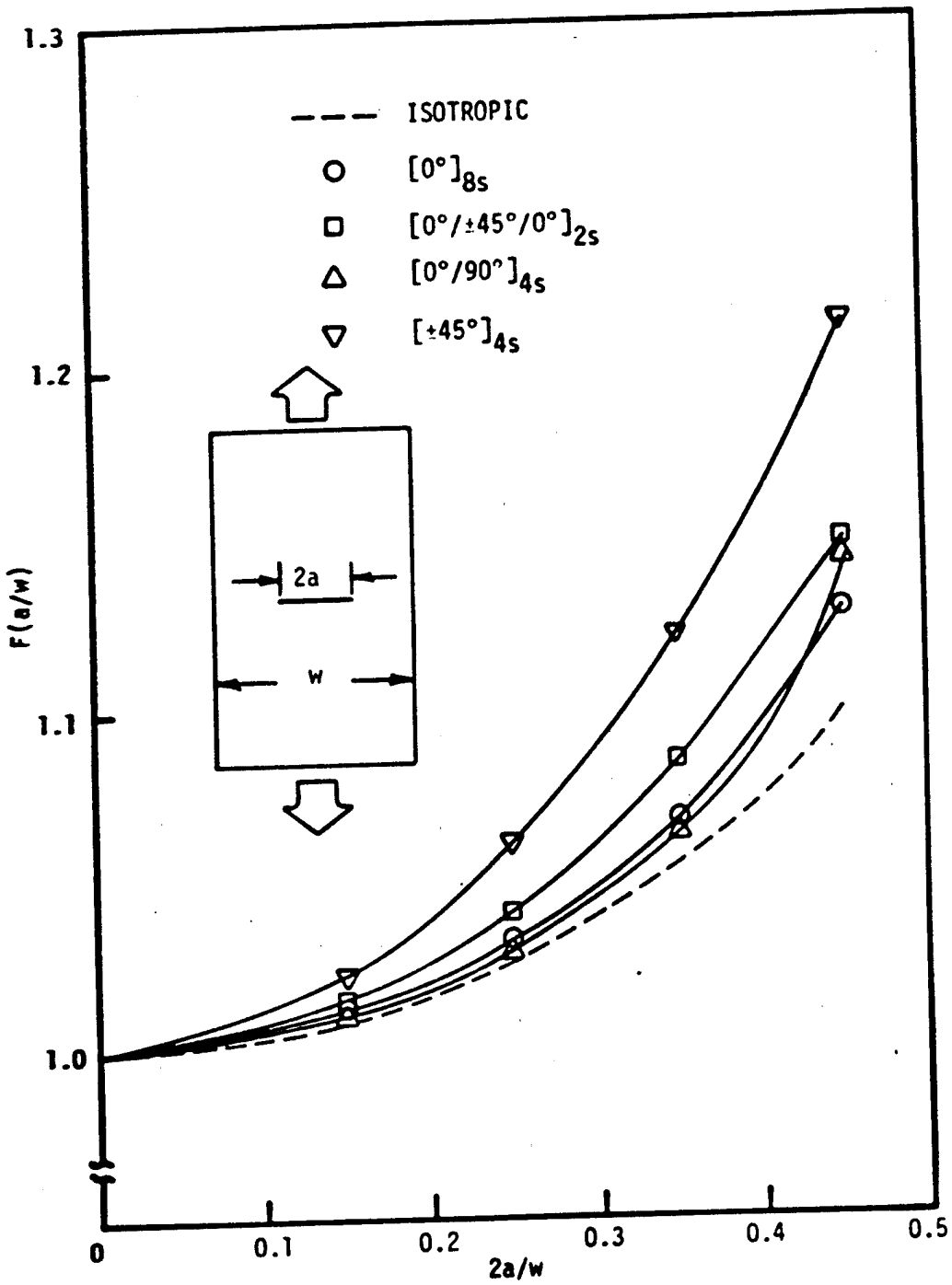

Figure B-18. Finite Width Correction Factors for CN T300/934 Graphite/Epoxy Laminates.

Comparisons between the isotropic FWCF [80] and the anisotropic FWCF of the DEN and SEN laminates are as shown in Figures B-19 and B-20, respectively. Variations in the FWCF's were noted, especially in the DEN cases. For these two notches, the largest variations between the isotropic and anisotropic FWCF's were seen for the $[45°]_{8s}$ laminate. Quantitatively, the maximum deviation was about 20% at the largest aspect ratio.

Thus, depending on the anisotropy, aspect ratio and type of implanted notch, the isotropic FWCF may or may not vary substantially from its anisotropic counterpart. However, it should be noted that the isotropic FWCF's, for the three types of implanted notches investigated here, were much easier and convenient to compute than the anisotropic FWCF's.

Conclusion and Future Considerations

From the results and discussion here on the fracture behavior of graphite epoxy laminates, the following observations can be made:

- The COD measurements of the CN specimen indicated that the compliance of square slots was always higher than narrow slits, for all laminates and aspect ratios. Consequently, the remote fracture stresses of square slots were the higher of the two cases.
- $[\pm 45°]_{4s}$ laminate containing circular holes had a slightly lower remote fracture stress than those containing narrow slits even though the compliance of the holes was higher. This conclusion was drawn from observations of the

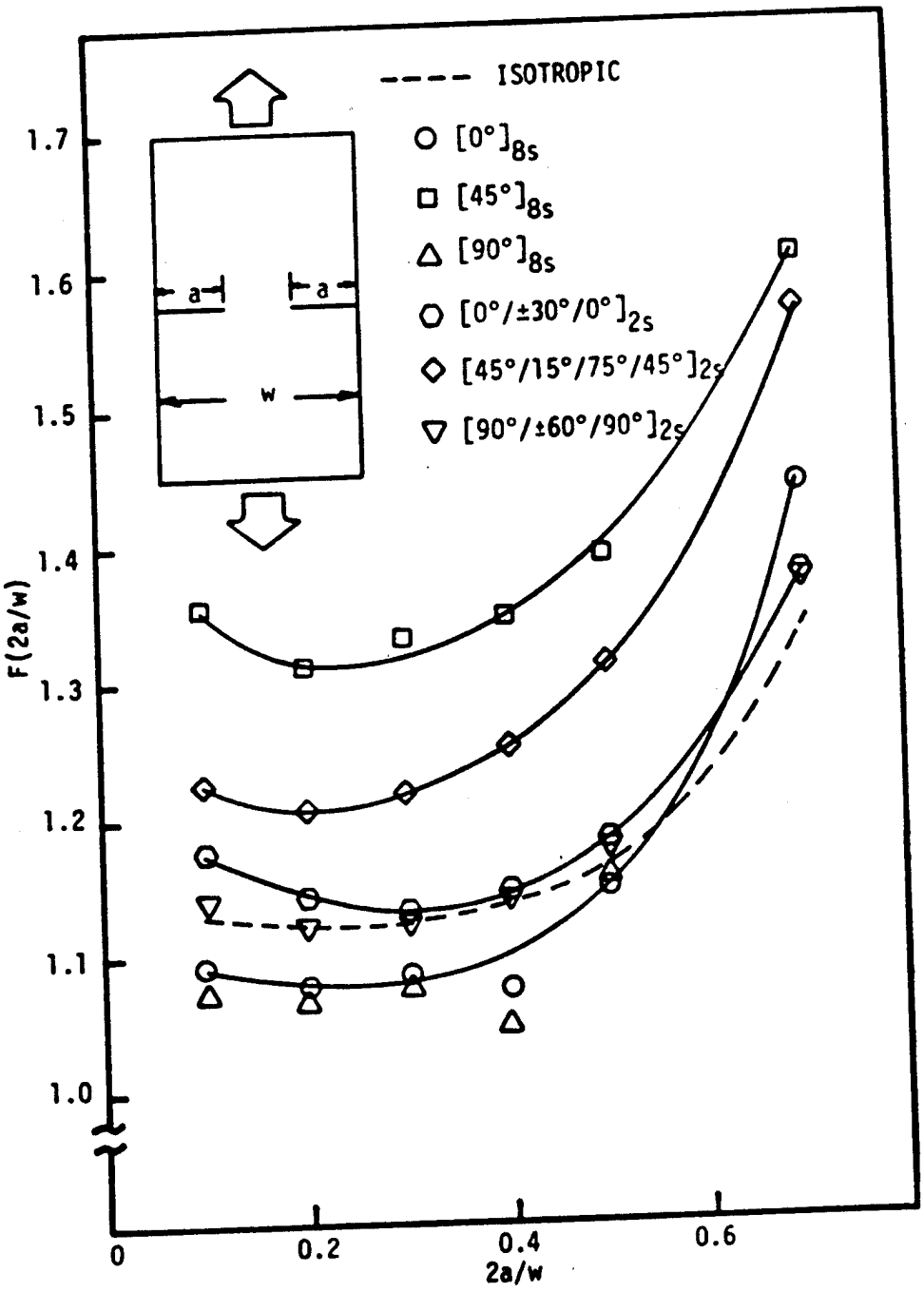

Figure B-19. Finite Width Correction Factors for DEN AS-3501 Graphite/Epoxy Laminates.

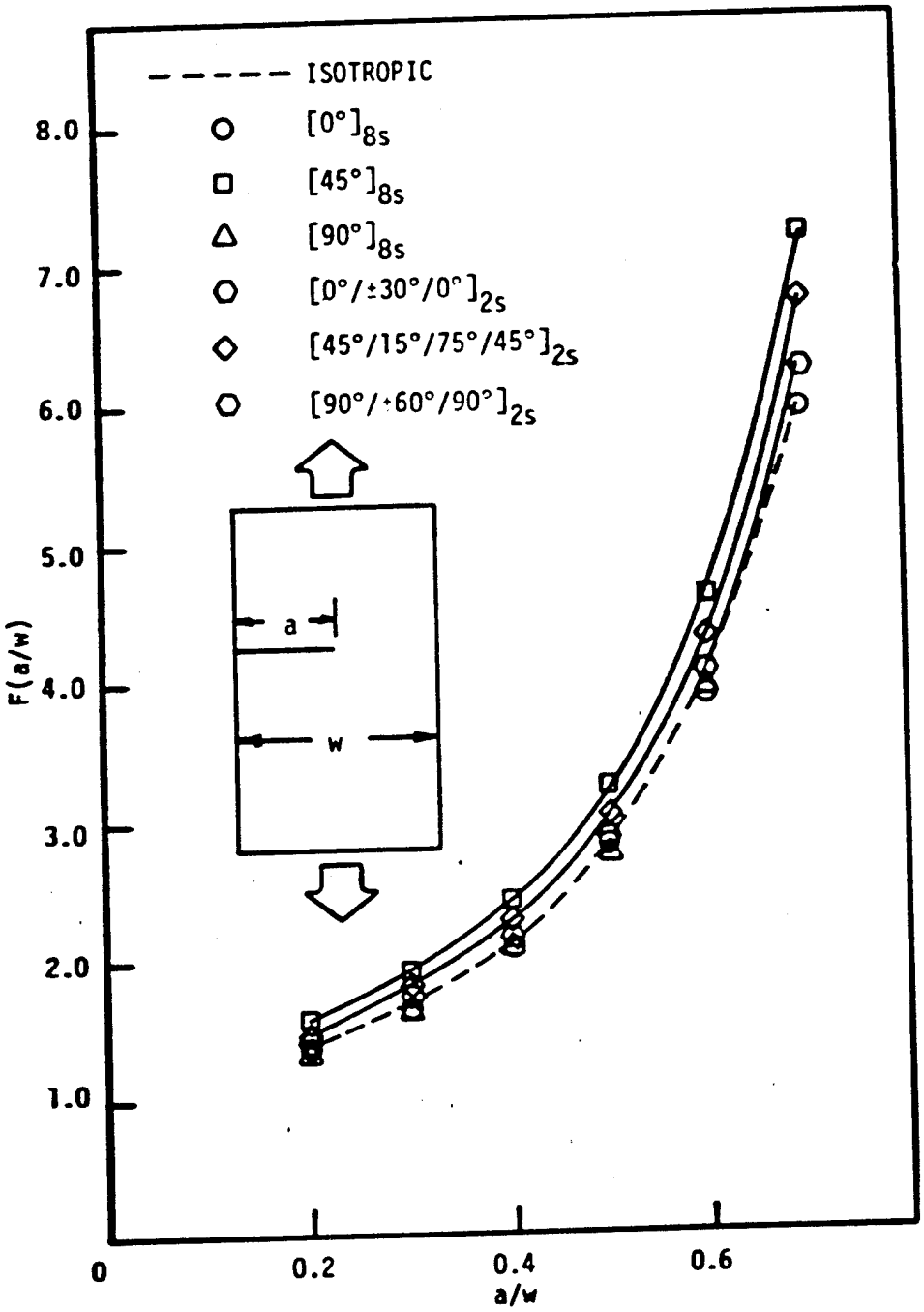

Figure B-20. Finite Width Correction Factors for SEN AS-3501 Graphite/ Epoxy Laminates.

photoelastic coatings which revealed that the intense regions were larger in the case of the holes. Thus, holes are more critical than slits for this laminate geometry.

- The effects of anisotropy on the stress field in the vicinity of the notch tips of the CN specimens were clearly illustrated by the birefringent coatings. By varying the anisotropy of the material from quasi-isotropic to highly anisotropic, the pattern of the fringes was varied. For $[\pm 45°]_{4s}$ laminates, the effects of interlamina constraints were detected.
- Stable crack growth was observed in most of the in-situ microscopic observations and was generally associated with matrix-dominated situations. Microcracks were always present in the notched and unnotched free surfaces of the failed general laminates.
- For CN laminates, when non-self-similar crack propagation occurred, characteristic lengths decreased as the aspect ratio increased. When self-similar crack propagation occurred, the characteristic lengths approached an asymptotic value as the aspect ratio increased, which was also seen in the results of the work of the originators of the two-parameter models.
- Using the suggested characteristic dimension of 0.04 inch (1.016 mm) for the point stress and inherent flaw models and 0.15 inch (3.810 mm) for the average stress model, a comparison of the predicted fracture strength with the experimental results of specimens containing CN and holes was made. For CN specimens the best correlation between analysis and

experiment was obtained using the BIE method. The inherent flaw model generally correlated better with experimental results than the other models used for circular hole geometries. No "curve-fitting" was attempted with the two-parameter models.

- The finite width correction factors used to correlate the experimental results with analysis varied according to the anisotropy of the laminate. The maximum deviation between the isotropic and anisotropic correction factors (obtained from the BIE method) was approximately 10% for the $[\pm 45°]_{4s}$ CN laminate at $2a/w = 0.45$ and approximately 20% for the $[45°]_{8s}$ SEN and DEN cases when $a/w = 0.7$ and $2a/w = 0.7$, respectively.

In conclusion, the BIE method is an excellent analytical tool for investigating the fracture behavior of composite materials. The two-parameter models and isotropic finite correction factors should only be used as a rule of thumb type judgment or design situation and primarily only for quasi-isotropic laminates.

Tentatively, future investigations on the time-dependent fracture behavior of notched composites should utilize the rationale of the BIE method. This is primarily because it is more convenient to use and has a better accuracy than other numerical methods such as finite elements and finite difference. The results and discussion presented here should be sufficient justification for the preliminary time-dependent analysis of notched composites using the BIE method.

VITA

The author was born in Pahang, West Malaysia in May, 1948. He received his basic education in the Methodist Boys' School, Kuala Lumpur and matriculated in December, 1968.

In September 1969, he went to Winnipeg, Manitoba, Canada to pursue his undergraduate studies. He obtained his Bachelor of Science degree in Mechanical Engineering from the University of Manitoba, Manitoba, Canada in April, 1973.

In September 1973, he came to the United States to pursue his graduate studies in Engineering Science and Mechanics at Virginia Polytechnic Institute and State University, where he was appointed as a Teaching and Research Assistant. Upon completion of his Master of Science requirements in March 1975, he was appointed as Research Associate in the Department of Engineering Science and Mechanics, V.P.I. & S.U. In September 1975, he started his Ph.D. program.

THE TIME-TEMPERATURE BEHAVIOR OF GRAPHITE/EPOXY LAMINATES

by

Yew Thye Yeow

(ABSTRACT)

An in-depth study on the time-temperature behavior of epoxy based continuous and elastic fiber reinforced composite materials and the feasibility of using the time-temperature analogy as an accelerated characterization method to predict the long-term behavior are presented. This is a two-pronged investigation as the material investigated (graphite/epoxy) is essentially quasi-elastic at room temperature and viscoelastic at elevated temperatures. Correlations between analysis and experiments are presented whenever possible.

At elevated temperatures, master curves of matrix dominated unidirectional laminates are obtained using the time-temperature superposition principle. Using the principal properties (E_{11}, $E_{22}(t)$, $G_{12}(t)$ and ν_{12}), master curves of other off-axis laminates reduced at any arbitrary ambient temperature are predicted. The results obtained from the short-term (16-minute) tests, medium term (25-hour) tests and predictions are shown to correlate reasonably well. In addition, the delayed failure prediction and experimental results are shown to correlate reasonably well. Both the experimental and predicted delayed failure results indicate that the creep strength master curves are dependent on the in-plane stress states and that failure modes vary

from ductile to quasi-brittle depending on the duration of the tests.

At room temperature, a summary of the unnotched and notched behavior is presented. In the unnotched case, total stress-strain responses of general symmetric laminates are predicted with a non-linear analysis and compared with experimental results. The analysis is used to validate intralamina shear test methods. In the notched case, test results for specimens containing variations in notch geometries and anisotropy are given. These results are correlated to three two-parameter and one one-parameter analytical fracture models.